International Atomic Energy Agency

INDC(NDS)-334
Distrib.: G+RP

INDC INTERNATIONAL NUCLEAR DATA COMMITTEE

"MEASUREMENT, CALCULATION AND EVALUATION OF PHOTON PRODUCTION DATA"

Texts of Papers presented at the
1st Research Co-ordination Meeting
organized by the International Atomic Energy Agency
in co-operation with ENEA, Bologna
and held at ENEA, Bologna, Italy,

14 to 17 November 1994

Compiled by

Pavel OBLOŽINSKÝ
IAEA Nuclear Data Section
Vienna, Austria

May 1995

IAEA NUCLEAR DATA SECTION, WAGRAMERSTRASSE 5, A-1400 VIENNA

INDC(NDS)-334
Distrib.: G+RP

"MEASUREMENT, CALCULATION AND EVALUATION OF PHOTON PRODUCTION DATA"

Texts of Papers presented at the
1st Research Co-ordination Meeting
organized by the International Atomic Energy Agency
in co-operation with ENEA, Bologna
and held at ENEA, Bologna, Italy,

14 to 17 November 1994

Compiled by

Pavel OBLOŽINSKÝ
IAEA Nuclear Data Section
Vienna, Austria

Abstract

Altogether 14 scientific and technical papers were presented at the IAEA 1st Research Co-ordination Meeting on "Measurement, Calculation and Evaluation of Photon Production Data" organized in co-operation with the Applied Physics Department, ENEA, Bologna, Italy. The papers, collected in the present report, are dealing with various aspects of photon production in neutron induced reactions in the incident energy range mostly below 20 MeV.

May 1995

Reproduced by the IAEA in Austria
May 1995

Contents

Compilations, Evaluations and Benchmarks

Foreword

The present report collects 14 scientific and technical papers presented at the 1st Research Co-ordination Meeting on "Measurements, Calculations and Evaluations of Photon Production Data" held in Bologna, Italy, 14–17 November 1994. The papers, dealing with various aspects of photon production data in low–energy neutron induced reactions, are subdivided into 3 categories as indicated in the title of the Meeting.

Initial 5 papers are devoted to measurements of basic photon production data in three incident neutron energy regions. In the 1–4 MeV region, a high-accuracy measurement of the discrete γ ray production on ^{56}Fe needed for improved reactor pressure vessel surveillance dosimetry is proposed (Oak Ridge). In the 14 MeV region, experimental database of discrete photon production cross sections in light nuclei is analyzed (Obninsk), and measurements of production of discrete gamma lines in light nuclei are reported (Bratislava). In the 10–200 MeV region, the measurement is described of discrete γ lines motivated by the need to test nuclear model calculations as a function of increasing neutron energy (Vienna/Los Alamos), complemented by a short overview on the current γ production measurements at the white neutron source (Los Alamos).

Next 5 papers are devoted to calculations. They are concerned with the modelling of high–energy ($>$ 10 MeV) γ rays, a missing step in achieving a complete picture of the physics underlying γ emission. Inclusion of the high–energy region is expected to be important for future evaluations in which the prediction of γ spectra over a broad range of incident–particle and γ energies is required. Recent significant improvements in the Direct Semidirect model (DSD) are reflected in 4 papers. Extension of the DSD model to transitions to unbound states (Livermore) is followed by papers on analogy of the coherence in the semidirect term to that of the Dicke superradiance (Ljubljana), phenomenological separation of the DSD and multistep parts of capture cross sections (Obninsk), and importance of angular distributions in interpreting cross sections for high–energy γ production (Ljubljana). The last theoretical paper is devoted to developments in the preequilibrium exciton model for γ emission and testing the spin–dependent code PEGAS (Bratislava).

Concluding 4 papers are devoted to compilation, evaluation and benchmarking activities. An update of the compilation of the gamma-ray strength functions (Petten/Vienna) is followed by an overview of evaluated photon production data in JENDL-3.2 (Tokai-mura), and benchmarking of neutron-induced photon production data for iron as measured at 14 MeV and compared with Monte Carlo transport calculations using the European Fusion File EFF-1 (Dresden). The last paper is devoted to benchmarking of photon production data in the evaluated files JENDL-3.2 and FENDL-1 with an important assessment of the quality of these files (Tokai-mura).

Vienna, 15 March 1995 Pavel Obložinský

PRECISION MEASUREMENT OF ^{56}FE CROSS SECTION FOR THE 846-keV GAMMA TRANSITION AND FOR E_n BETWEEN THRESHOLD AND 4 MeV*

J. K. Dickens
Oak Ridge National Laboratory
Oak Ridge, Tennessee 37830 USA

Abstract: An experimental system is described which is designed to provide accurate cross section measurements of the production of the 846-keV gamma ray due to inelastic neutron scattering by ^{56}Fe. Six aspects of the measurement are considered: (a) precision determination of the incident neutron flux; (b) gamma-ray detection resolution; (c) incident neutron energy determination; (d) interacting neutron-energy resolution; (e) counting rates; and (f) multiple scattering and attenuation corrections. For precision determination of the incident neutron flux, a simultaneous measurement of the 478-keV gamma ray from the ^{10}B(n,α)^{7}Li reaction is proposed, since this reaction cross section has been recently determined to a precision of 2-4% for incident neutrons up to 4 MeV. A large-volume intrinsic Ge detector is proposed for gamma-ray detection; the Oak Ridge Electron Linear Accelerator will provide a pulsed neutron beam. Measurements under actual operation will be necessary to optimize counting rates and incident neutron-energy resolution. Multiple scattering and attenuation corrections will be determined using a modification of the documented Monte Carlo code SCINFUL; needed cross sections will be taken from evaluation, or, in the case for the cross section for the ^{10}B monitor reaction, from recent experimental results.

*Research Sponsored by the Office of Energy Research, Division of Nuclear Physics, U. S. Department of Energy, under contract DE-AC05-84OR21400 with Martin Marietta Energy Systems, Incorporated.

Motivation: From Fu, et al.,[1] "The $^{56}Fe(n,n')$ cross section exciting the 0.847-keV level up to an incident neutron energy of 5 MeV is known to about 5% - 10%, but an accuracy of 2% is needed for reactor pressure vessel surveillance dosimetry."

Status: An indication of the problem is shown in figure 1, taken from a report by Smith.[2] At least part of the apparent substantial "discrepancies" exhibited in this figure is due to a very pronounced resonance-like structure in the inelastic scattering excitation function as indicated in figures 2 and 3. In these figures measurements by Voss[3] (shown by the shaded results) are compared with the evaluated[1] excitation function for the total cross section and for two different incident-neutron energy regions.

Proposed experiment: A tested intrinsic-Ge detector based system will be used. The detector size is "25%" with 1.7 keV resolution at 0.85 MeV gamma energy. The ratio of the detector efficiencies at gamma-ray energies of 0.48 and 0.85 MeV will be determined in situ with an expected uncertainty of 1% (or better). A pulsed white-source incident neutron spectrum will be used; incident neutron energy calibration will be checked using known resonances in Al and C. Incident neutron flux will be monitored by measuring the 0.48-MeV gamma ray from the $^{10}B(n,\alpha)^{7}Li$ reaction and using the recently reported cross sections of Schrack, et al.[4] Already prepared is a self-supporting sample of an iron-boron alloy, using iron of natural enrichment, but using boron enriched to 92.4% in the isotope ^{10}B. Corrections for multiple scattering and neutron attenuation will be calculated using a modification of the Monte Carlo program SCINFUL.[5]

Guidance from the CRP:

Problem: It appears that data for very high resolution in neutron energy cannot be obtained with a high accuracy for all data points within the time frame of the CRP.

Request: What resolution in neutron energy is needed, and are there regions of incident neutron energy deemed to be the more important regions.

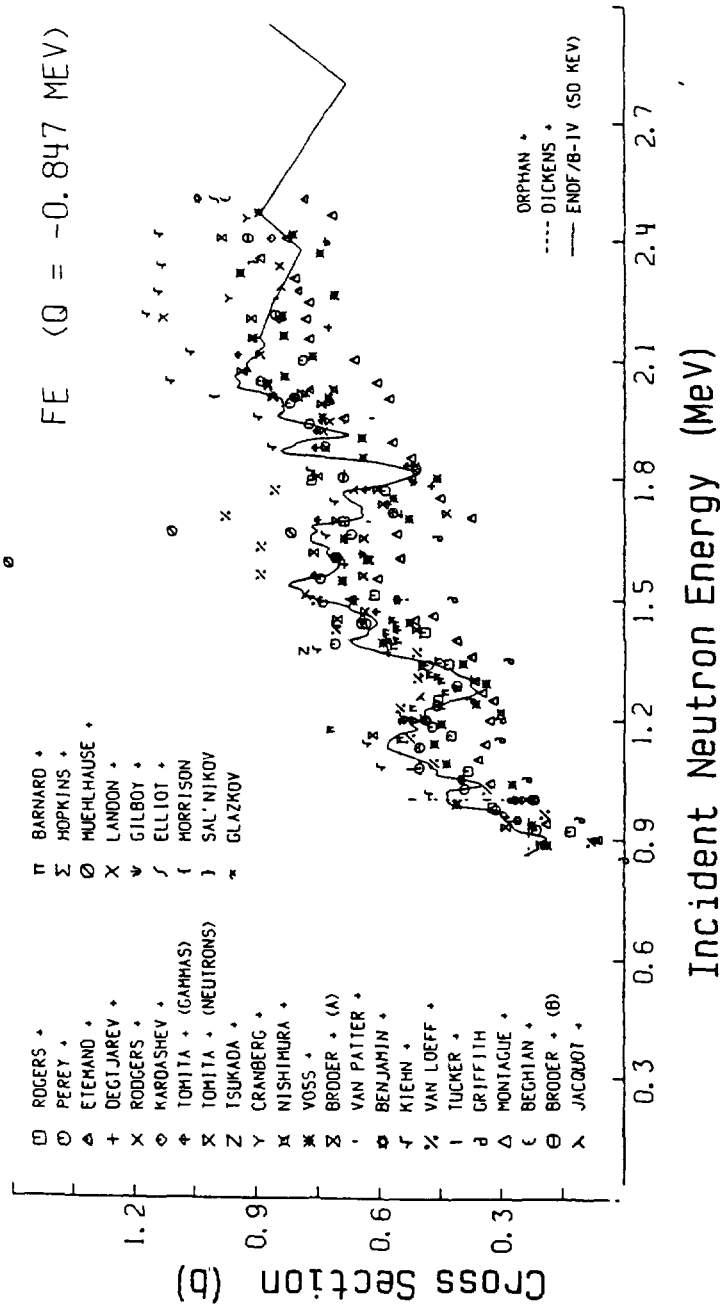

Figure 1. Compilation of measurements of the cross section for excitation of the 846-keV level in iron as of 1976 (Smith, ref. 2)

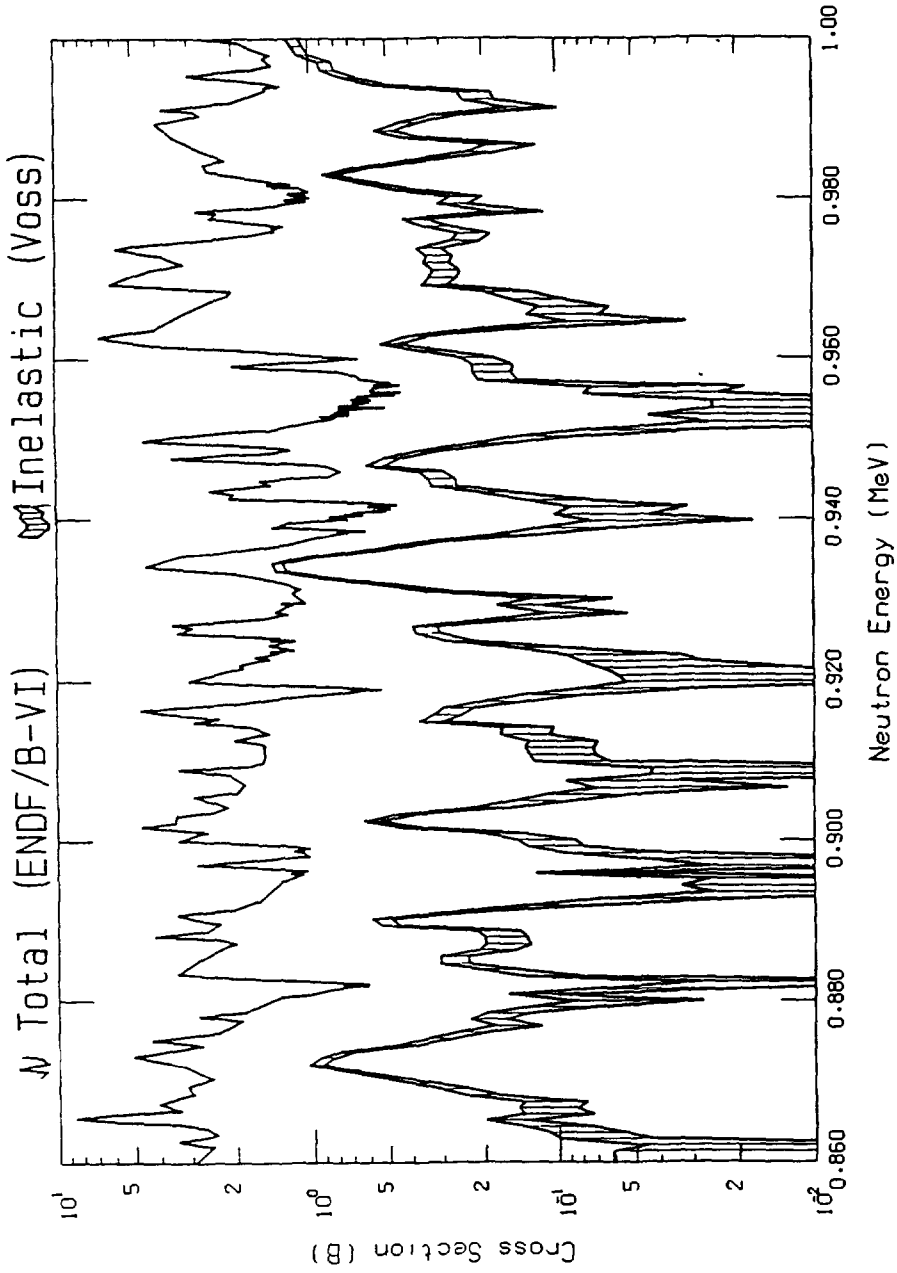

Figure 3. Measured excitation function (Voss, ref. 3) for the 846-keV gamma-ray compared with the ENDF/B-VI evaluation (ref. 1) for the TOTAL cross section.

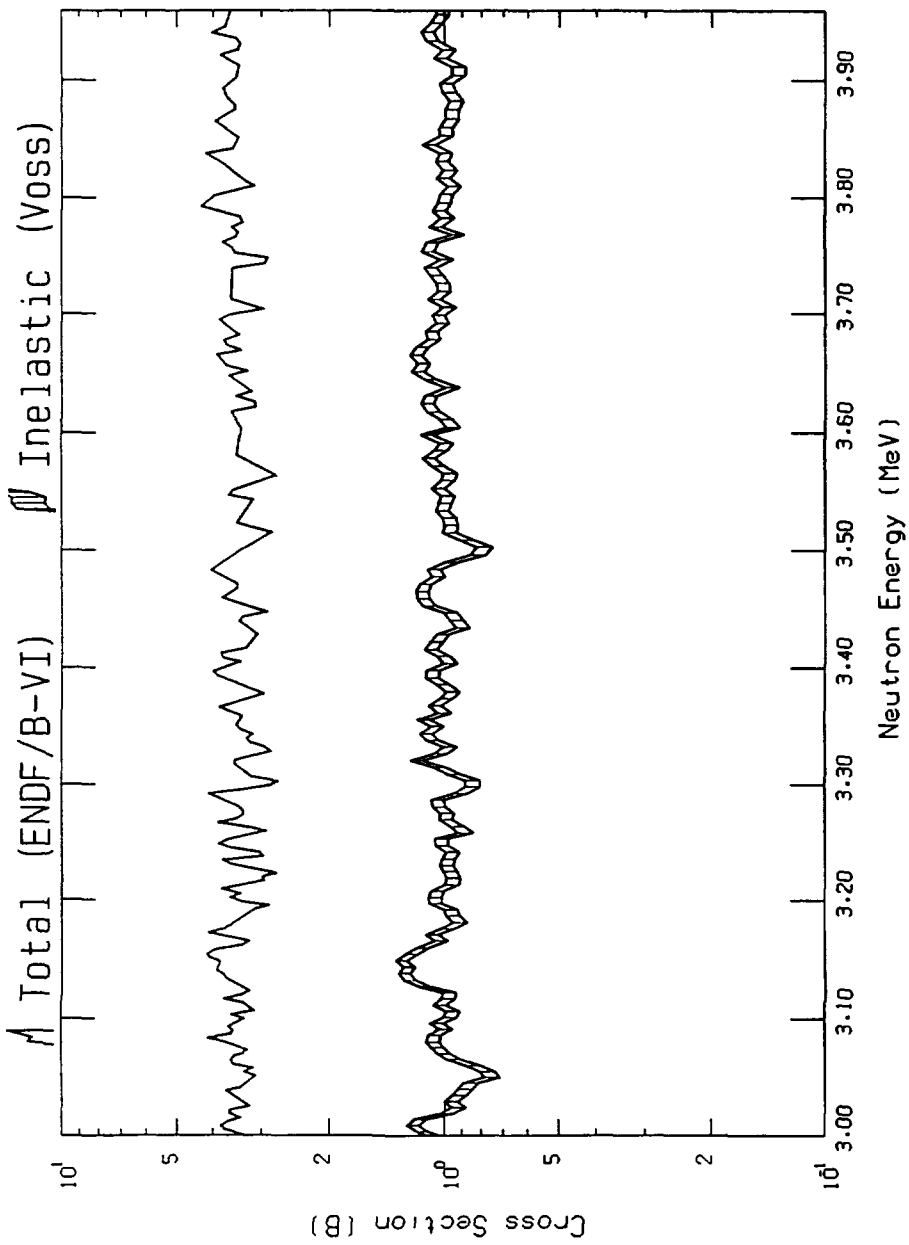

Figure 4. Same as figure 3 but for higher incident-energy neutrons.

References:

1. C. Y. Fu, D. M. Hetrick, C. M. Perey, F. G. Perey, N. M. Larson and D. C. Larson, "Description of Evaluations for ^{54,56,57,58}Fe Performed for ENDF/B-VI," in ENDF/B-VI Summary Documentation, comp. P. R. Rose, BNL-NCS-17541, 4th Edition [ENDF/B-VI] (1991).

2. D. L. Smith, "Fast-Neutron Gamma-Ray Production from Elemental Iron; $E_n \leq$ 2 MeV," ANL/NDM-20 (1976).

3. F. Voss, "Measurement and Fluctuations Analysis of Gamma-Ray Production Cross Sections After Inelastic Neutron Scattering on Fe^{56} and Al^{27} between 0.8 and 13 MeV., KFK-1611 (1971); Eng. trans. doc. no. EURFNR-1037 (1972).

4. R. A. Schrack, O. A. Wasson, D. C. Larson, J. K. Dickens, and J. H. Todd, *Nucl. Sci. Eng.* **114,** 352-362 (1993).

5. J. K. Dickens, "SCINFUL: a Monte Carlo Based Computer Program for a Scintillator Full Energy Response to Neutron Detection for E_n Between 0.1 and 80 MeV; User's Manual and FORTRAN Program Listing," ORNL-6462 (1988).

DISCRETE PHOTON PRODUCTION CROSS SECTIONS IN LIGHT NUCLEI AT 14MeV NEUTRON ENERGY.*

S.P.Simakov

Institute of Physics and Power Engineering
249020 Obninsk, Kaluga Region, Russia

Abstract

The aim of the paper is to examine the status of the experimental data on discrete gamma-ray production cross sections via (n.xγ) reaction for light nuclei (Z<20) at 14MeV incident neutron energy. From this point of view, the available experimental cross sections for most prominent gamma transitions measured by high resolution in-beam technique were summarized in the report. This experimental base was analyzed to estimate the actual uncertainty of experimental results, and to find out the nucleus and/or transitions for which the measurements are too scarce and controversial.

The ENDF/B6 library was checked as well to search whether the discrete photon production cross sections are presented there and how they agree with known experimental data.

The attempt was made to obtain the qualitative requirements arose from fusion reactor technology, geology, medicine and other needs.

As a final goal, the conclusions for what nuclei the further experiments and evaluations are of primary importance were made.

Frames of survey

Neutron induced gamma-ray production cross-sections are needed for design of nuclear plants, thermonuclear reactors, neutron therapy, geology and other applied neutronics works. Besides practical importance, they provide valuable information

---

*) This work is done under Research Contract No 7809/RB

base for understanding the nuclear structure and neutron reaction mechanisms.

Despite the last years trend in gamma-ray production researches toward the higher incident neutron energies, the 14MeV point is still continuing to be of high importance. This incident energy experimental data are a good "reference" point for experiment and theory, in which measuring techniques and model parameters can be checked and compared. This is why we restricted the present survey by the experiments made with neutrons in the vicinity of 14MeV energies (see Table 1). These measurements have been performed usually at neutron generates or sometimes at linacs which produce the white neutron spectrum. In the last case the experimental data were selected or interpolated from bins near 14MeV.

Table 1. The frames of the review.

Target nucleus charge	$1 \leq Z \leq 20$
Neutron incident energy	14.1 - 14.9 MeV
Gamma production processes	Prompt, Prompt+Delayed
Gamma-transitions	Resolved
Gamma-ray detectors	Ge(Li), HPGe, NaI(Tl)
Time Frames of Experiments	Sixties - Up today

The energy resolution of γ-ray detectors is not always adequate to extract cross sections for individual gamma-rays lines. This is why we restrict our survey by most intensive transitions to exclude the factor of large admixture of other lines. For the same reason we exclude experiments performed before 1960 year.

The measurement technique used for photon production measurements is in-beam spectroscopy. Sometimes it is supplemented by time of flight selection of gammas from fast neutrons in those experiments where pulsed 14MeV neutron source is available. In last case only prompt part (emitted in the time window usually of dozens nanoseconds) of total production cross section is detected. This is why we distinguish between prompt and prompt+delay data.

Photon production cross sections needs

The different branches of science and industry have its own specific request.

The fusion reactor technology needs different types of nuclear data, in particular, photon production reactions relevant to transport of radiation and heat generation in shielding, magnet and other structure elements. It was stated that for some nuclei these data have not yet adequate status [1,2]. The list of light nuclei, for which photon production cross section with definite accuracy are requested, are presented in the Table 2.

Table 2. Required accuracy of photon production cross-sections.

Field of Application	Elements	Accuracy needs	References
Fusion Technology	Li, Be, C, O, F, Al, Si	5-15%	[1,2]
Neutron Therapy	H, Be, C, N, O, Ca	4%	[1,3]
Geology and Mining	H, C, N, O, F, Na, Mg, Al, Si, P, Cl, K, Ca	Not adequate	[4,5]
Planetary γ-rays	O, Mg, Al, Si, Cl, Ca	Not adequate	[6]

Optimization of neutron therapy requires photon production cross sections for better solution next problems: 1) the selection of sources reaction for neutron production, 2) the design of collimators and shields, 3) the calculation of absorbed dose. The corresponding elements [3] are listed in the Table 2 as well.

Nuclear techniques are widely used for fast, nondestructive, multielemental analyses of geological samples. The most abundant elements, which constituent 95% of atomic elements in the vicinity of earth's crust are the atoms with $Z \leq 15$. The different nuclear techniques, used for elemental analysis, require the accurate knowledge of photon production cross sections induced by 14MeV neutrons [4,5].

The spectroscopy of cosmic γ-ray produced by interaction of neutrons with planetary objects is a perspective tool for determination the composition, origin, evolution and present state of those objects. Discrete gamma lines from neutron nonelastic-scattering reaction on most abundant elements

(H,O,Mg,Al,Si,Cl) has not yet adequate status for this applications [6].

Photon production experimental and evaluated data

The experimental data on production of most prominent γ-rays are collected in the Table 3. The data were collected either from original works or EXFOR Library (CINDA issues up to 1992 year was used as a guide). The gamma rays energies, producing reaction, decay scheme and speed of process (prompt, delayed or sum) are listed in the columns 1-4. The next ones show the experiment's parameters (incident neutron energy, range of angle, γ-ray detector), measured cross sections, first author of the work and year of publication. Table 3 shows that most of data were measured at one emission angle. In that case total production cross section, listed in the table, are those calculated by multiplying the measured one by 4π.

To estimate the achieved experimental accuracy, the average photon production cross section and mean square deviation of experimental results for every γ-ray transition are presented in the Table 4. For several transitions we have large enough statistical ensemble: number of experiments exceeds 5, thus the actual cross section and data scattering (mean square deviation) could be well estimated. But for many other γ-rays there are few or only one measurement. In the last case the cross section and uncertainty of this experiment are listed in Table 4.

It have to be noticed that for Phosphorus there are no experimental data on discrete gamma production cross sections.

Since gamma yield is angular dependent, the data measured at angles different from 55^{o} and 125^{o} were corrected to obtain accurate magnitude of integral cross section (corresponding cross sections are denoted by asterisk). The experimental information on γ-rays angular distribution was used for this procedure.

For some nuclei the difference of incident neutron energies (from 14 to 15MeV) could be additional source of discrepancy. This is illustrated in Fig.1, where production cross section of 4.44MeV gammas in C(n,n') reaction is shown. In contrary to ENDF/B6, which predict 25% decreasing, experimental data do not

clearly agree with this the tendency.

The different components of 1779keV γ-ray from Si(n,n'γ) reaction were independently measured: prompt one (387±30mb), delayed (32±16mb) and sum (614±25mb). It is seen that they contradict each other, even taking into account the uncertainty.

Evaluated data from ENDF/B6 library are shown in the Table 4 as well. It is seen that for some light elements No Discrete γ-ray Data (NDD) are presented there - continuous smooth photon energy spectra from all γ-rays producing reactions are only available from File MF=15 (photon spectrum), Section MT=3 (non-elastic scattering) for these nuclei. The extracting of discrete photon production cross section could result in to large error. For other nuclei or particular reactions No Data (ND) at all are presented or they are cut at low incident neutron energy.

Next column presents deviation (in percents) of ENDF/B6 prediction from average experimental results. Only for several γ-lines (4439keV from C(n,n'), 3684keV from O(n,α), 1809keV from Al(n,d), 1779keV and 2839keV from Si(n,n')) both the scattering of experimental results and deviation of ENDF/B6 are less then a few percent, that meet the needs stated by applications. For other nuclei the spread of experimental data and accuracy of ENDF/B6 prediction have order of dozens percents. It means that these data status is not adequate.

For illustration, the range of experimental uncertainty for selected γ-rays transitions in each nucleus is shown in Fig.2. Upper point means maximum uncertainty, low - minimum, which are listed in Table 4 for given element. Dashed curves show the typical range of requested uncertainties (4-15%). Fig.2 demonstrates that accuracy of about half of the experimental data exceeds the level of needed requirements.

Conclusions

The published works and experimental information on discrete γ-rays production in light nuclei by 14MeV neutrons were reviewed and collected. This data base has shown:

- 10% of compiled γ-ray transitions were measured in more than 5 independent experiments, 35% - only in one, for Phosphorus the

discrete photon production cross sections are unknown;
- The uncertainty ascribed by authors (order of a few percent) usually less then discrepancies between different experiments (dozens percents);
- Suggesting that spread of experimental data is the actual experimental uncertainty, one can conclude that requested uncertainty (4-15%) is achieved only for 4439keV transition in carbon, 1779keV - in silicon, 3736keV - in calcium and for some transitions in boron. Whereas for majority of γ-rays transitions and nuclei either the data were obtained only in one experiment or discrepancy between known experiments too large to meet the requested accuracy.

Comparison of ENDF/B6 evaluated data with experimental ones resulted to the next conclusions:
- For some nuclei/reactions the discrete γ-ray production cross sections are not presented in ENDF/B6 at all or included in the total gamma rays emission spectra. Extraction of cross section for particular transition sometimes may be incorrect procedure.
- The disagreement of ENDF/B6 evaluated data with measured ones usually has an order of dozens percents, which exceeds the needed requirements. Only for some γ-rays transition, ENDF/B6 library predicts with more then 10% accuracy the experimental cross sections, which were measured in several independent experiments: 478keV from Be(n,t), 4439keV - C(n,n'), 2742keV - O(n,n'), 3684keV - O(n,α), 844keV - Al(n,n'), 1809keV - Al(n,d), 1779keV and 2839keV - Si(n,n').

In the present work we analyzed the status of experimental and evaluated data for the most intensive γ-rays transitions in light nuclei at 14 MeV incident energy. To meet requirements, arising from different applications, further experimental researches and evaluations for many of these transitions are still needed.

Table 3. Photon production cross sections in light nuclei.

E, keV	Reaction	Transition	Speed	E, MeV	Angle	σ, mb	Detector	Author	Year
		3-Lithium (7 - 92.5%, 6 - 7.5%)							
478	$^{7}Li(n,n')^{7}Li$	478 → 0	p	14	0-180	19± 3	NaI(Tl)	Bezotosny	1976
3562	$^{6}Li(n,n')^{6}Li$	3562 → 0	p	14	0-180	.11±.05	NaI(Tl)	Bezotosny	1976
		4-Beryllium (9 - 100%)							
478	$^{9}Be(n,t)^{7}Li$	478 → 0	p	14	0-180	2±.5	NaI(Tl)	Bezotosny	1976
				14.2	90	9± 3	NaI(Tl)	Drake	1978
		5-Boron-10							
478	$^{10}B(n,\alpha)^{7}Li$	478 → 0	p	14.8	55	34± 3	NaI,Ge	Nellis	1970
718	$^{10}B(n,n')^{10}B$	718 → 0	p	14.2	125	28± 3	HPGe	Dickens	1988
				14.8	55	31± 2	NaI,Ge	Nellis	1970
1022	$^{10}B(n,n')^{10}B$	1740 → 718	p	14.2	125	3± 1	HPGe	Dickens	1988
				14.8	55	9±.5	NaI,Ge	Nellis	1970
3368	$^{10}B(n,p)^{10}Be$	3368 → 0	p	14.8	55	21± 1	NaI,Ge	Nellis	1970
		5-Boron-11							
478	$^{11}B(n,n\alpha)^{7}Li$	478 → 0	p	14.2	125	23± 5	HPGe	Dickens	1988
2125	$^{11}B(n,n')^{11}B$	2125 → 0	p	14.2	125	4.5± 1	HPGe	Dickens	1988
		6-Carbon (12 - 98.9%, 13 - 1.1%)							
4439	$^{12}C(n,n')^{12}C$	4439 → 0	p	14.1	30-150	180± 7	Ge	Murata	1988
				14.9	90	159±10	Ge(Li)	Hongyu	1986
				14.2	45-130	188± 3	NaI(Tl)	Drake	1978
				14	0-180	255±26	NaI(Tl)	Bezotosny	1976
				14.2	125	168±20	Ge(Li)	Rogers	1975
				14.8	90	152±20	Ge(Li)	Martin	1971
				14.1	90	121±20	Ge(Li)	Clayeux	1969
				14.7	90	165±17	NaI(Tl)	Engesser	1967
				14		133±17	NaI(Tl)	Bezotosny	1966
				14.1	30-160	232±18	NaI(Tl)	Stewart	1964
				≅14	30-150	249±28	NaI	Benveniste	1960

Table 3. (continuation).

E, keV	Reaction	Transition	Speed	E, MeV	Angle	σ, mb	Detector	Author	Year
		7-Nitrogen (14 - 99.63%, 15 - 0.37%)							
2313	$^{14}N(n,n')^{14}N$	2313 → 0	p	14.7	125	47± 6	Ge(Li)	Rogers	1975
				14.8	55	39± 5	NaI(Tl)	Tucker	1970
				14.8	90	34± 7	Anticoi	Morgan	1969
				14.7	90	59±11	NaI(Tl)	Engesser	1967
3684	$^{14}N(n,d)^{13}C$	3684 → 0	p	14.7	125	33± 5	Ge(Li)	Rogers	1975
				14.8	55	38± 5	NaI(Tl)	Tucker	1970
				14.8	90	25± 5	Anticoi	Morgan	1969
				14.7	90	34±11	NaI(Tl)	Engesser	1967
4445	$^{14}N(n,\alpha)^{11}B$	4445 → 0	p	14.7	125	37± 6	Ge(Li)	Rogers	1975
				14.8	55	64± 8	NaI(Tl)	Tucker	1970
				14.8	90	37± 7	Anticoi	Morgan	1969
				14.7	90	63±13	NaI(Tl)	Engesser	1967
7029	$^{14}N(n,n')^{14}N$	7029 → 0	p	14.7	125	26± 5	Ge(Li)	Rogers	1975
				14.8	55	30± 4	NaI(Tl)	Tucker	1970
				14.8	90	11± 2	Anticoi	Morgan	1969
				14.7	90	60±20	NaI(Tl)	Engesser	1967
		8-Oxigen (16 - 99.76%, 17 - 0.04%)							
2742	$^{16}O(n,n')^{16}O$	8872 → 6130	p	14.8	90	33± 7	Antico	Morgan	1971
				14.8	55	27± 3	NaI(Tl)	Tucker	1969
				14.0		142±25	NaI(Tl)	Bezotsny	1966
3684	$^{16}O(n,\alpha)^{13}C$	3684 → 0	p	14.8	90	53±11	Antico	Morgan	1971
				14.3	125	41±21	Ge(Li)	Orphan	1970
				14.8	55	84±10	NaI(Tl)	Tucker	1969
				14.7	90	69±14	NaI(Tl)	Engesser	1967
3854	$^{16}O(n,\alpha)^{13}C$	3854 → 0	p	14.8	125	60±44	Ge(Li)	Yamamoto	1978
				14.8	90	33± 7	Antico	Morgan	1971
				14-16	125	18± 9	Ge(Li)	Orphan	1970
				14.7	90	32± 6	NaI(Tl)	Engesser	1967
6130	$^{16}O(n,n')^{16}O$	6130 → 0	p	14.8	125	137±40	Ge(Li)	Yamamoto	1978
				14.8	90	116±23	Antico	Morgan	1971
				14-16	125	84±17	Ge(Li)	Orphan	1970
				14.8	55	97±12	NaI(Tl)	Tucker	1969
6130	$^{16}O(n,p)^{16}N(\beta^-)^{16}O$	6130 → 0	7s						
6130	$^{16}O(n,n'+p\beta^-)^{16}O$	6130 → 0	p+d	14.7	90	153±15	NaI(Tl)	Engesser	1967
				14		260±42	NaI(Tl)	Bezotosny	1966
7117	$^{16}O(n,n')^{16}O$	7117 → 0	p	14-16	125	33±10	Ge(Li)	Orphan	1970
				14.7	90	63±13	NaI(Tl)	Engesser	1967
				14.8	90	25± 5	Antico	Morgan	1971
		9-Fluorine (19 - 100%)							
197	$^{19}F(n,n')^{19}F$	197 → 0	89ns	14.9	55-140	137± 9	Ge(Li)	Hongyu	1994

Table 3. (continuation).

E, keV	Reaction	Transition	Speed	E, MeV	Angle	σ, mb	Detector	Author	Year
			11-Sodium (23 -100%)						
440	$^{23}Na(n,n')^{23}Na$	440 → 0	p	14.8	125	596±72	Ge(Li)	Yamamoto	1978
				14.6	30-150	329±25	Ge(Li)	Degtyarev	1977
				14.2	30-150	440±37	NaI(Tl)	Abbondano	1973
				14.7	90	496±50	NaI(Tl)	Engesser	1967
				14.1	30- 90	463±56	NaI(Tl)	Martin	1965
1275	$^{24}Na(n,d)^{22}Ne$	1275 → 0	p	14.8	125	175±29	Ge(Li)	Yamamoto	1978
				14.6	30-150	146±11	Ge(Li)	Degtyarev	1977
				14.2	30-150	198±23	NaI(Tl)	Abbondano	1973
				14.7	90	183±31	NaI(Tl)	Engesser	1967
1636	$^{23}Na(n,n')^{23}Na$	2076 → 440	p	14.8	125	303±43	Ge(Li)	Yamamoto	1978
				14.6	30-150	110±10	Ge(Li)	Degtyarev	1977
				14.2	30-150	166±23	NaI(Tl)	Abbondano	1973
1636	$^{23}Na(n,n'+p\beta^-)^{23}Na$	2076 → 440	p+d	14.7	90	236±24	NaI(Tl)	Engesser	1967
			12-Magnesium (24 - 79%, 25 - 10%, 26 - 11%)						
350	$^{24}Mg(n,\alpha)^{21}Ne$	350 → 0	p	14.1	90	146±48	NaI(Tl)	Engesser	1967
472	$^{24}Mg(n,p)^{24}Na$	472 → 0	20ms	14.7	90	131±26	NaI(Tl)	Engesser	1967
1369	$^{24}Mg(n,n')^{24}Mg$	1369 → 0	p	14.2	90-130	364±38	NaI(Tl)	Drake	1978
				14.2	30-150	628±66	NaI(Tl)	Abbondano	1973
				14.1	55, 90	387±15	Ge(Li)	Grenier	1973
				14.7	90	388±39	NaI(Tl)	Engesser	1967
				14.1	30-90	619±60	NaI(Tl)	Martin	1965
				14.1	50-160	619±32	NaI(Tl)	Stevart	1964
			13-Aluminium (27 -100%)						
472	$^{27}Al(n,\alpha)^{24}Na$	472 → 0	20ms	14.9	55-140	51± 3	Ge(Li)	Hongyu	1994
				14.8	125	88±11	Ge(Li)	Yamamoto	1978
844	$^{27}Al(n,n')^{27}Al$	844 → 0	p	14.7	125	35± 5	HPGe	Hlavac	1994
				14.9	55-140	23± 1	Ge(Li)	Hongyu	1994
				14.1	30-150	26± 2	Ge	Murata	1988
				14.1	125	57± 6	Ge(Li)	Clayeux	1969
844	$^{27}Al(n,p)^{27}Mg(\beta)^{27}Al$	844 → 0	10s	14.9	55-140	47± 2	Ge(Li)	Hongyu	1994
844	$^{27}Al(n,n'+p\beta^-)^{27}Al$	844 → 0	p+d	14.9	55-140	70± 2	Ge(Li)	Hongyu	1994
				14.8	125	97±15	Ge(Li)	Yamamoto	1978
				14.7	90	88±18	NaI(Tl)	Engesser	1967
				14		102±13	NaI(Tl)	Bezotosny	1966

Table 3. (continuation).

E, keV	Reaction	Transition	Speed	E, MeV	Angle	σ, mb	Detector	Author	Year
1014	$^{27}Al(n,n')^{27}Al$	1014 → 0	p	14.7	125	64± 6	HPGe	Hlavac	1994
				14.9	55-140	59± 2	Ge(Li)	Hongyu	1994
				14.1	30-150	160± 5	Ge	Murata	1988
				14.1	125	198±50	Ge(Li)	Clayeux	1969
1014	$^{27}Al(n,p)^{27}Mg(\beta)^{27}Al$	1014 → 0	10m	14.9	55-140	25± 2	Ge(Li)	Hongyu	1994
1014	$^{27}Al(n,n'+\beta^-)^{27}Al$	1014 → 0	p+d	14.9	55-140	84± 3	Ge(Li)	Hongyu	1994
				14.8	125	97±13	Ge(Li)	Yamamoto	1978
				14.7	90	132±14	NaI(Tl)	Engesser	1967
				14		92±12	NaI(Tl)	Bezotosny	1966
1809	$^{27}Al(n,d)^{26}Mg$	1809 → 0	p	14.7	125	167±15	HPGe	Hlavac	1994
				14.9	55-140	157± 5	Ge(Li)	Hongyu	1994
				14.1	30-150	142±12	Ge	Murata	1988
				14.8	125	238±26	Ge(Li)	Yamamoto	1978
				14.1	125	146±38	Ge(Li)	Clayeux	1969
				14.7	90	172±34	NaI(Tl)	Engesser	1967
3004	$^{27}Al(n,n')^{27}Al$	3004 → 0	p	14.7	125	99±11	HPGe	Hlavac	1994
				14.9	55-140	94± 6	Ge(Li)	Honqyu	1994
				14.0	90	102±13	NaI(Tl)	Drosg	1991
				14.1	30-150	188± 8	Ge	Murata	1988
				14.8	125	139±23	Ge(Li)	Yamamoto	1978
				14.2	90-130	96±11	NaI(Tl)	Drake	1978
				14.1	125	155±50	Ge(Li)	Clayeux	1969
				14.7	90	99±20	NaI(Tl)	Engesser	1967
				14		131±20	NaI(Tl)	Bezotosny	1966
	14-Silicon (28 - 92.2%, 29 -4.7%, 30 - 3.1%)								
585	$^{28}Si(n,\alpha)^{25}Mg$	585 → 0	p	14.1	70,90	17± 1	Ge(Li)	Lychagin	1992
				14.9	90	58± 3	Ge(Li)	Guoying	1991
				14.1	30-150	36± 3	Ge	Murata	1988
				14.7	90	59±20	NaI(Tl)	Engesser	1967
1779	$^{28}Si(n,n')^{28}Si$	1779 → 0	p	14.9	55-140	407±25	Ge(Li)	Hongyu	1994
				14.1	70,90	344±52	Ge(Li)	Lychagin	1992
				14.9	90	488±29	Ge(Li)	Guoying	1991
				14.0	90	412±35	NaI(Tl)	Drosg	1991
				14.1	30-150	310±25	Ge	Murata	1988
				14.2	90-130	388±46	NaI(Tl)	Drake	1978
				14.2	30-150	373±40	NaI(Tl)	Abbondano	1973
				14.1	55,90	293±28	Ge(Li)	Grenier	1973
				14.1	30-90	471±70	NaI(Tl)	Martin	1965
1779	$^{28}Si(n,p)^{28}Al(\beta)^{28}Si$	1779 → 0	2m	14.9	55-140	232±16	Ge(Li)	Hongyu	1994
1779	$^{28}Si(n,n'+p\beta^-)^{28}Si$	1779→ 0	p+d	14.9	55-140	639±30	Ge(Li)	Hongyu	1994
				14.7	90	589±59	NaI(Tl)	Engesser	1967
2839	$^{28}Si(n,n')^{28}Si$	4618 →1779	p	14.1	70,90	30± 5	Ge(Li)	Lychagin	1992
				14.9	90	66± 6	Ge(Li)	Guoying	1991
				14.1	30-150	48± 5	Ge	Murata	1988
				14.7	90	67± 8	NaI(Tl)	Engesser	1967

Table 3. (continuation).

E, keV	Reaction	Transition	Speed		E, MeV	Angle	σ, mb	Detector	Author	Year
					15-Phosphorus (31-100)					
					No discrete γ-rays experimental data					
					16-Sulphur (32 - 95%, 33 - 0.75%, 34 - 4.21%)					
1273	$^{32}S(n,\alpha)^{29}Si$	1273 →	0	p	14.2	30-150	179±21	NaI(Tl)	Abbondano	1973
					14.7	90	113±13	NaI(Tl)	Engesser	1967
2028	$^{32}S(n,\alpha)^{29}Si$	2028 →	0	p	14.2	30-150	115±26	NaI(Tl)	Abbondano	1973
2230	$^{32}S(n,n')^{32}S$	2230 →	0	p	14.2	30-150	278±43	NaI(Tl)	Abbondano	1973
					14.7	90	192±20	NaI(Tl)	Engesser	1967
					14.1	30-90	332±50	NaI(Tl)	Martin	1965
4460	$^{32}S(n,n')^{32}S$	4460 →	0	p	14.7	90	9[illegible] ±19	NaI(Tl)	Engesser	1967
					17-Clorine (35 - 75.8%, 37 - 24.2%)					
1219	$^{35}Cl(n,n')^{35}Cl$	1219 →	0	p	14.7	90	96±20	NaI(Tl)	Engesser	1967
1727	$^{37}Cl(n,n')^{37}Cl$	1727 →	0	p	14.8	125	289±89	Ge(Li)	Yamamoto	1987
1763	$^{35}Cl(n,n')^{35}Cl$	1763 →	0	p	14.8	125	158±43	Ge(Li)	Yamamoto	1987
					14.7	90	82±16	NaI(Tl)	Engesser	1967
2127	$^{35}Cl(n,d)^{34}S$	2127 →	0	p	14.8	125	332±79	Ge(Li)	Yamamoto	1987
					14.7	90	215±23	NaI(Tl)	Engesser	1967
					19-Potassium (39 - 93.3%, 41 - 6.7%)					
1677	$^{41}K(n,n')^{41}K$	1677 →	0	p	14.7	90	112±11	NaI(Tl)	Engesser	1967
2168	$^{39}K(n,d)^{38}Ar$	2168 →	0	p	14.7	90	243±20	NaI(Tl)	Engesser	1967
2814	$^{39}K(n,n')^{39}K$	2814 →	0	p	14.7	90	102±20	NaI(Tl)	Engesser	1967
					20-Calcium (40 - 96.9, 42 - 0.7%, 43 - 0.1%, 44 - 2.1%, 48 - 0.2%)					
770	$^{40}Ca(n,p)^{40}K$	800 →	30	p	14.7	90	70±15	NaI(Tl)	Engesser	1967
892	$^{40}Ca(n,p)^{40}K$	892 →	0	p	14.1	90	31±10	Ge(Li)	Grenier	1973
					14.7	90	60±13	NaI(Tl)	Engesser	1967
1614	$^{40}Ca(n,p)^{40}K$	1644 →	30	p	14.1	90	29±10	Ge(Li)	Grenier	1973
					14.7	90	68± 8	NaI(Tl)	Engesser	1967
3736	$^{40}Ca(n,n')^{40}Ca$	3736 →	0	p	14.1	90	109±28	Ge(Li)	Grenier	1973
					14.7	90	113±23	NaI(Tl)	Engesser	1967

Table 4. Average photon production cross sections at 14MeV.

Reaction.	E, keV	No Exps	σ, mb Experim	σ, mb ENDF/B6	B6-Exp / Exp, %	Request %	ENDF/B6 Status
Li(n,n')	478	1	19± 3 (16%)	62	+226	15	N
(n,n')	3562	1	.11±.05(45%)	.13	+18		
Be(n,t)	478	2	5.5±3.5(64%)	5.4	-2	4-15	Y
^{10}B(n,α)	478	1	34± 3 (9%)	ND			
(n,n')	718	2	28.5±1.5(5%)	32	+12	NR	
(n,n')	1022	2	6± 3 (5%)	6.3	+5		
(n,p)	3368	1	21± 1 (5%)	22	+5		
^{11}B(n,nα)	478	1	23± 5 (22%)	ND		NR	
(n,n')	2125	1	45± 1 (22%)	46	+2		
C(n,n')	4439	10	216±33(15%)*	210	-3	4-10	Y
N(n,n')	2313	4	45±11(24%)	51	+13	4	N
(n,d)	3684	4	33± 5(17%)	10	-70		
(n,α)	4445	4	50±15(31%)	23	-54		
(n,n')	7029	4	32±21(64%)	24	-25		
O(n,n')	2742	3	67±65(96%)	62	-7	4-10	N
(n,α)	3684	4	62±19(30%)	60	-3		
(n,α)	3854	4	36±18(49%)	33	-23		
(n,n')	6130	4	109±23(21%)	165	+51		
(n,n'+p)	6130	2	207±54(26%)				
(n,n')	7117	3	40±20(54%)	75	+88		
F(n,n')	197	1	139± 9(6%)	184	+32	15	N
Na(n,n')	440	5	463±96(21%)*	NDD		?	?
(n,d)	1275	4	184±31(17%)*	NDD			
(n,n')	1636	3	193±99(51%)	NDD			
(n,n'+p)	1636	1	236±24(10%)	NDD			
Mg(n,α)	350	1	146±48(33%)	ND		?	?
(n,p)	472	1	131±26(20%)	ND			
(n,n')	1369	6	530±122(23%)*	282	-47		
Al(n,α)	472	2	70±20(27%)	ND		15	?
(n,n')	844	4	35±15(44%)	38	+9		
(n,p)	844	1	47± 2(4%)				
(n,n'+p)	844	4	89±14(16%)				
(n,n')	1014	4	120±70(58%)	82	-31		
(n,p)	1014	1	25± 2(8%)				
(n,n'+p)	1014	4	101±21(21%)				
(n,d)	1809	6	170±35(21%)	159	-6		
(n,n')	3004	9	123±33(27%)	92	-25		
Si(n,α)	585	4	43±20(47%)	73	70	5-10	N
(n,n')	1779	9	392±72(18%)*	361	-8		
(n,p)	1779	1	32±16(50%)				
(n,n'+p)	1779	2	614±25(4%)				
(n,n')	2839	4	53±18(33%)	58	+9		

Table 4. (continuation)

Reaction.	E, keV	No Exps	σ, mb Experim	σ, mb ENDF/B6	B6-Exp / Exp, %	Request %	ENDF/B6 Status
P(n,n')	1266	0	ND	150		?	N
(n,n')	2234	0	ND	150			
S(n.α)	1273	2	144±36(25%)*	NDD		?	?
(n,α)	2028	1	115±26(23%)	NDD			
(n,n')	2230	3	276±57(21%)*	NDD			
(n,n')	4460	1	94±19(20%)	NDD			
Cl(n,n')	1219	1	96±20(21%)	0	-100	?	?
(n,n')	1727	1	289±89(31%)	0	-100		
(n,n')	1763	2	120±38(32%)	0	-100		
(n,d)	2127	2	274±59(22%)	ND			
K(n,n')	1677	1	112±11(10%)	NDD		?	N
(n,d)	2168	1	243±20(8%)	NDD			
(n,n')	2814	1	102±20(20%)	0	-100		
Ca(n,p)	770	1	70±15(21%)	45	-36	4	N
(n,p)	892	2	46±15(32%)	23	-50		
(n,p)	1614	2	49±20(40%)	9	-82		
(n,n')	3736	2	111± 2(2%)	161	-45		

Comments:

NDD - No Discrete Data

ND - No Data

N - No satisfactory status of data

Y - Satisfactory status of data

? - No quantitative assee

* - Cross section are corrected for angular dependence

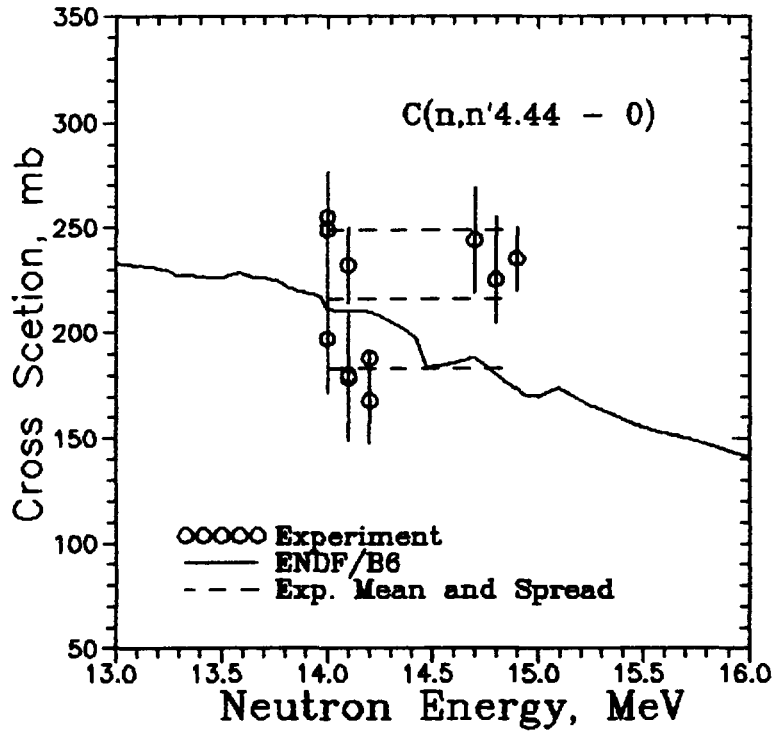

Fig.1. Production cross section of 4.44MeV γ-rays in C(n,n'γ).

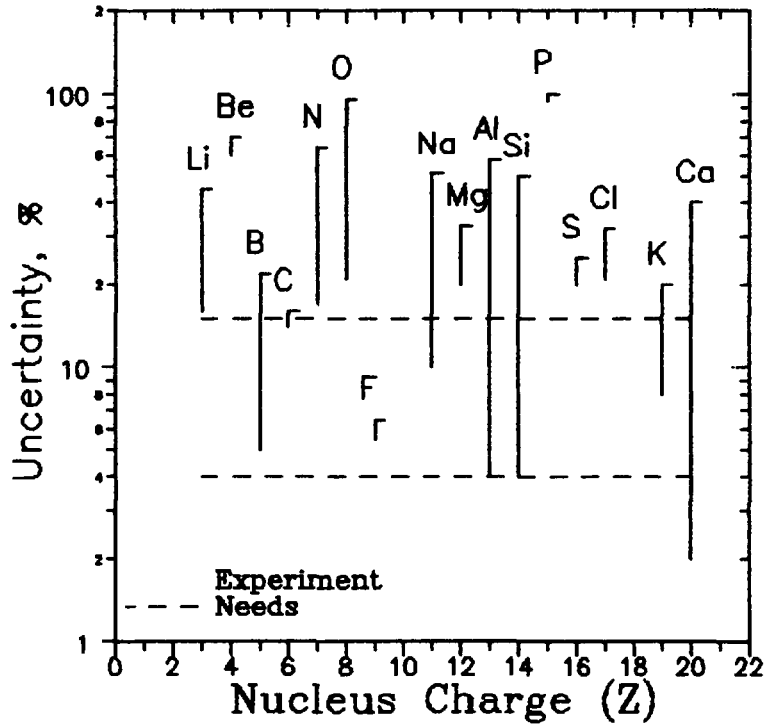

Fig.2. Uncertainty of experimental discrete photon production cross sections (vertical bars) and requested uncertainties corridor (dashed lines).

References

1. N. Kocherov, P. K. McLaughlin (Eds). WRENDA 93/94. Report INDC(SEC)-104, Vienna, 1993
2. E. T. Cheng, D. L. Smith. Proc. Intern. Conf on Nuclear Data for Science and Technology (May 1991, Julich), p. 273
3. A. Wambersie, V. Gregoire. Ibid 2, p. 579
4. J. Csikai. Ibid 2, p. 644
5. P. Oblozinsky and S. Hlavac. Nucl. Geophys., 1987, p. 263
6. R. C. Reedy. Proc. Int. Conf on Nucl. Data for Basic and Applied Science (May 1985, Santa Fe), p. 933

References for Table 3

Hongyu 1994: Z. Hongyu, H. Guangshun e. a. Proc. Int. Conf on Nucl. Data for Sci. and Tech. (Gatlinburg, May 1994)

Lychagin 1992: A. A. Lychagin, e. a. Report FEI-2281, Obninsk 1992

Drosg 1991: M. Drosg, D. M. Drake e. a. Proc. Int. Conf. on Nucl. Data for Sci. and Techn. (Julich, May 1991), p. 304

Guoyong 1991: F. Guoying, Z. Hongyu e. a. Proc. Int. Conf. on Nucl. Data for Sci. and Tech. (Julich, 13-17May 1991), p. 332

Dickens 1988: J. K. Dickens and D. C. Larson. Proc. Int. Conf. on Nucl. Data for Sci. and Tech. (Mito, May 1988), p. 213

Murata 1988: I. Murata, J. Yamamoto e. a. Proc. Int. Conf. on Nucl. Data for Sci. and Tech. (Mito, May 1988), p. 275

Hongyu 1986: Zhou Hongyu e. a. Report INDC(CRP)-010/L, Vienna 1986

Drake 1978: D. M. Drake e. a. Nucl. Sci. and Engi., 1978, v. 65, p. 49

Yamamoto 1978: T. Yamamoto e. a. J. of Nucl. Sci. Tech., 1978, v. 15, p. 797

Degtyarev 1977: A. P. Degtyrev e. a. "Neutron Physics", Moscow 1977, v. 2, p. 3, 57

Bezotosny 1976: V. M. Bezotosny e. a. "Neutron Physics", Moscow 1976, v. 4, p. 133

Rogers 1975: V. C. Rogers e. a. Nucl. Sci. Eng., 1975, v. 58, p. 298

Grenier 1974: G. Grenier "Neutron Physics" Obninsk, 1974, v. 3, p. 215

Abbondano 1973: U. Abbondano e. a. J. of Nucl. Ener., 1973, v. 27, p. 227

Martin 1971: T. C. Martin e. a. Report ORO-2791-32, 1971

Morgan 1971: I. L. Morgan e. a. Report ORO-2791-32, 1971

Nellis 1970: D. O. Nellis e. a. Phys. Rev., 1970, v. 1, p. 847

Orphan 1970: V. J. Orphan e. a. Nucl. Sci. Eng., 1970, v. 42, p. 352

Tucker 1970: W. E. Tucker e. a. Report ORO-2791-32, 1970

Clayeux 1969: G. Clayeux and G. Grenier. Report CEA-R-3807, 1969

Morgan 1969: I. L. Morgan e. a. Report ORO-2791-28, 1969

Tucker 1969: W. E. Tucker, D. O. Nellis e. a. Report ORO-2791-31, 1969

Engesser 1967: F. C. Engesser e. a. J. of Nucl. Ener., 1967, v. 21, p. 487

Bezotosny 1966: V. M. Bezotosny e. a. Sov. J. Nucl. Phys., 1966, v. 3, p. 861

Martin 1965: P. W. Martin e. a. J. of Nucl. Energy, 1965, v. 19, p. 447

Stewart 1964: D. T. Stewart, P. W. Martin. Nucl. Phys., 1964, v. 60, p. 352

Benveniste 1960: J. Benveniste e. a. Nuclear Physics, 1960, v. 19, p. 448

Production of discrete γ rays in light nuclei at 14 MeV

S. Hlaváč, I. Turzo and L. Dostál
Institute of Physics SAS, 84228 Bratislava, Slovakia

Abstract

Measurement of prompt discrete γ ray production in interaction of 14.7 MeV neutrons with light nuclei using associated α particle method is described. Measured γ production cross sections are used for reaction cross section determination, which are difficult to obtain using classical methods. This is demonstrated on reaction ^{16}O(n,$\alpha\gamma$)^{13}C, where the product nucleus ^{13}C is stable. Another example is the reaction ^{39}K(n,p)^{39}Ar, where the half-life of the product nucleus is 269 y. Both cross sections are important from different aspects for fusion technology. We determined experimentally 3 γ ray production cross sections in ^{16}O(n,$\alpha\gamma$) reaction and 8 cross sections in ^{39}K(n,xγ) reactions. The γ ray cross sections in ^{16}O(n,$\alpha\gamma$) are used to determine reaction cross section. Importance of theoretical calculations for reliable determination of the reaction cross section using our experimental method is stressed.

Introduction

Measurement of γ ray production in 14 MeV neutron induced reactions is important, especially when the data are needed for heating and energy balance calculations of fusion devices. Apart from such direct application, experimental information on discrete γ ray production is very useful for testing of physical ideas used in statistical compound as well as precompound model calculations. This is especially true when importance of spin variables in different models is discussed [1], because discrete level population is very sensitive to these variables. Moreover, experimental data of this kind are easily compared to the theoretical values, therefore they represent stringent test for models ideas.

It seems, that discrete γ ray production measurement may serve for still another useful purpose - in estimation of reaction cross sections which are difficult to measure by conventional means. Reaction cross sections are traditionally measured by activation method, which requires that the reaction product has a reasonable half-life and decay mode. The second mostly used method is spectrum method which may be used also in the case of stable reaction products, because the cross-section is determined counting particles emitted in the reaction. Here we must be able to uniquely determine the reaction channel, which is easy when only single channel is opened. The only possibility to determine cross section of reactions not fulfilling these conditions was opened only recently by accelerator mass spectroscopy. However, the necessary experimental equipment is rather expensive and up to now only very few cross sections were measured by this method.

On the other hand, most fast neutron induced reactions are accompanied by emission of discrete γ rays, independent on the properties of the reaction product. Moreover, discrete γ rays uniquely determine reaction channel. Therefore, measuring cross section for discrete γ ray gives us the opportunity to determine the reaction cross section. The inconvenience of this method is that we can measure only population of excited levels of the reaction product. To estimate the total reaction cross section, we have to add to this cross section a contribution representing direct particle population of the ground state. In some useful cases, this information is available from some other experiment, otherwise it must be obtained from a reasonable model calculation.

Here we demonstrate the ability of this method to provide reaction cross section in two cases, which are important for practical application in fusion technology. First reaction is $^{16}O(n,\alpha)^{13}C$ with stable reaction product ^{13}C. Cross section of this reaction is important for experiments on neutron multiplication in fusion reactor blanket, which are performed in a water bath. To obtain reaction cross section, we combine our γ ray production data with the result of spectrum method.

The second reaction is $^{39}K(n,n'p)^{38}Ar$, which is important for nuclear waste assessment [2]. Nucleus ^{38}Ar is also stable, but because there are two open channels (n,p) and (n,n'p) with Q-values 0.2 and -6.4 MeV, respectively, spectrum methods can neither provide required cross section. Because of this difficulty, to obtain the required reaction cross section we have to resort to theoretical methods and calculate the population of ground state.

Measurements were performed on recently developed system at Institute of Physics in Bratislava, which is optimized for γ ray production measurement in 14 MeV induced reactions. We used this setup earlier for discrete γ ray production measurements in reactions on ^{208}Pb [3] and recently also in ^{27}Al, which may be used as normalization measurements for experiments performed at white neutron source.

Experimental setup

The whole experimental setup is described in detail elsewhere [3],[4],[5], therefore only short description will be given here. It consists of a continuous 14 MeV neutron generator, associated α particle system for timing and a HPGe photon detector for discrete photon measurement. The setup is based on the time-correlated associated particle method and uses the advantage of strong spatial and time correlations between neutrons and alpha particles for background reduction.

A beam of magneticaly separated 150 keV D^+ ions bombarded a water cooled TiT target of 4.5 cm diameter. The beam itself was restricted to a diameter of 5 mm by a diaphragm placed close to the target to define the geometry of the setup. The beam current at the TiT target was about 50-80 μA. Neutrons were produced in the TiT target by the T(D,n)α reaction. Associated α particles were detected by a fast plastic scintillation counter placed at an angle of 135° with respect to the D^+ beam. We used fast plastic scintillator, similar to NE102, with thickness of 100 μm and a diameter of 2.0 cm. A movable diaphragm with dimensions of 1.5 $\times$ 1.5 cm^2 at the distance of 37.5 cm from the TiT target determined the solid angle of the α particle detector. Associated neutrons collimated electronically by α particles flew first through an iron and a concrete

shielding. This shielding fully separate the neutron source and the photon detector. The angle between deuteron beam and the axis of collimated neutron beam was 45° resulting in the mean neutron energy in the cone of 14.7 MeV and an energy spread of about 400 keV. Sample position was fixed at the distance of 270 cm from the TiT target. The size of the neutron cone at the sample spot was 14×14 cm^2, and the samples were always inside the cone, even taking into account possible shifts of the deuteron beam along the TiT target. Behind the sample, a NE213 (ϕ12 cm ×4 cm) scintillation detector was located to control the cone position by measuring the ratio of n×α coincidences to single neutrons.

Photons emitted from the sample were registered by a HPGe detector, which was placed at the distance of 18.7 cm from the sample and an angle of 125° with respect to the axis of the collimated neutron beam. This angle was chosen to set the second term in the Legendre polynomial to zero. The detector had a sensitive volume of 244 cm^3 and the FWHM energy resolution of 1.96 keV at the 1332 keV γ-ray energy. The intrinsic time resolution was rather poor, about 13 ns, due to rather large detector dimensions. The HPGe detector, with axis oriented perpendicularly to the detector - sample direction, was surrounded by a tungsten shielding in order to further reduce the background caused by scattered neutrons. The efficiency of the HPGe detector up to about 4000 keV was measured with calibrated ^{152}Eu, ^{24}Na sources and uncalibrated ^{56}Co source.

For cross section determination we used always relative method to avoid problems with absolute neutron flux and photon detection efficiency determination. For cross section measurements in ^{16}O(n,$\alpha\gamma$) reaction we used a powder sample of CrO_3 and measured cross section relative to the well known $2^+ \longrightarrow 0^+$ transition in ^{52}Cr(n,n'γ) channel. For cross section of this γ transition we have taken at 14.7 MeV a value of (695±28) mb [6].

For discrete γ ray production measurements in the ^{39}K(n,xγ) reaction we used mixed powdered sample of 100g KOH with 40g metallic Cr and again determined the cross sections relative to the known ^{52}Cr(n,n'γ) cross section.

Results and discussion

In the reaction ^{16}O(n,α) we determined cross sections of two strong discrete γ transitions with energies 3684.4 and 3853.6 keV to be (53.5±5.0) and (224.3±2.2) mb, respectively. The cross section of a very weak transition of 3053.2 keV was determined as (3.1±0.6) mb.

Comparison of our results with the literature data are shown in figs. 1 2 The γ production cross section of 3684.4 transition measured in this work is compared with known experimental data [8] in Fig.1 All these data are rather old and majority of them were obtained with low resolution NaI(Tl) detectors. Only 5 measurements were performed using high resolution Ge(Li) detectors. Of them four older measurements by Orphan, Clayeux, Nyberg and Yamamoto were handicapped by rather low efficiency of early semiconductor detectors with the active volume almost one order of magnitude lower than today available HPGe detectors. Only Nelson offer new data taken with a large Ge(Li), his data show in the 14 MeV region rather strong energy dependence and their uncertainties are also fairly large. Other literature data for production of this γ line show also large spread between 38 and 62 mb . Our value of 53.5±5.0 mb therefore represents an almost mean value of the older experimental data.

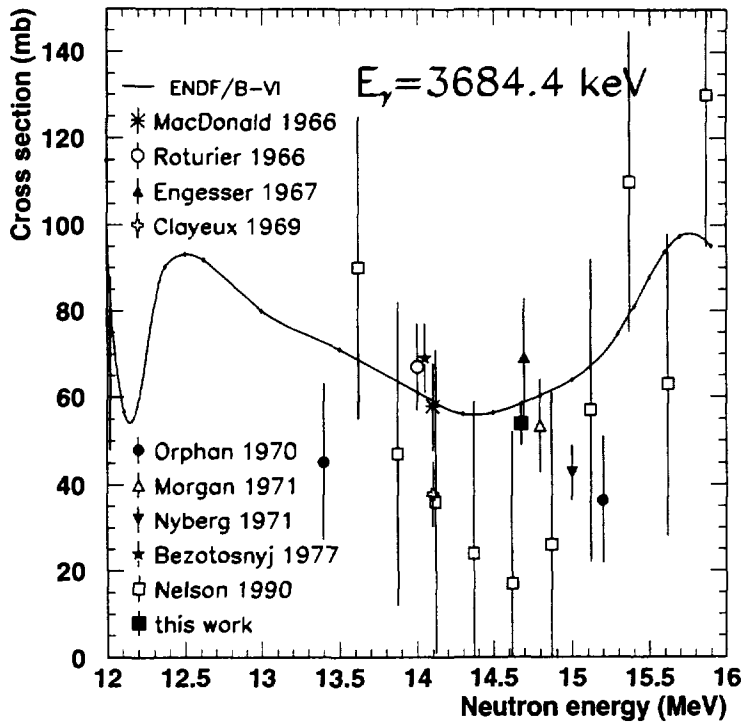

Figure 1: *Cross section for production of 3684.4 keV γ transition in the $^{16}O(n,\alpha\gamma)^{13}C$ reaction between 12 and 16 MeV incident neutron energy. Our result is compared with existing experimental data (see list in Ref.[8]). The smooth line is a spline polynomial connecting evaluated points from ENDF/B-VI.*

The origin of the differences is not completely understood. Part of the differences may be explained because of our improved experimental technique, large HPGe detector with very good energy resolution and setup with relatively low background. Relative cross section measurement also removed uncertainties usually connected with absolute neutron flux and detection efficiency determination. With respect to the evaluated data, our experimental point is slightly lower than the ENDF/B-VI value of 60.4 mb at 14.8 MeV.

The literature data [8] for the 3853.6 keV γ line production are summarized together with our result in Fig.2. The experimental data may be divided into two parts. The first group scattered around ~30 mb represent the part with less dispersion and lower values. Measurements by Scherrer and Yamamoto show rather large uncertainties and their values are substantially higher than the other group. Our measurement supports the former group with lower cross sections. Origin of the discrepancies is not known. However, the Scherrer measurement is rather old and was performed with very low resolution NaI(Tl) spectrometer. The result given by Yamamoto is relatively new, but its uncertainty is so high that it is even in accord with other measurements. Our experimental value (24.3±2.2) mb is here again somewhat lower than the ENDF/B-VI evaluation, which

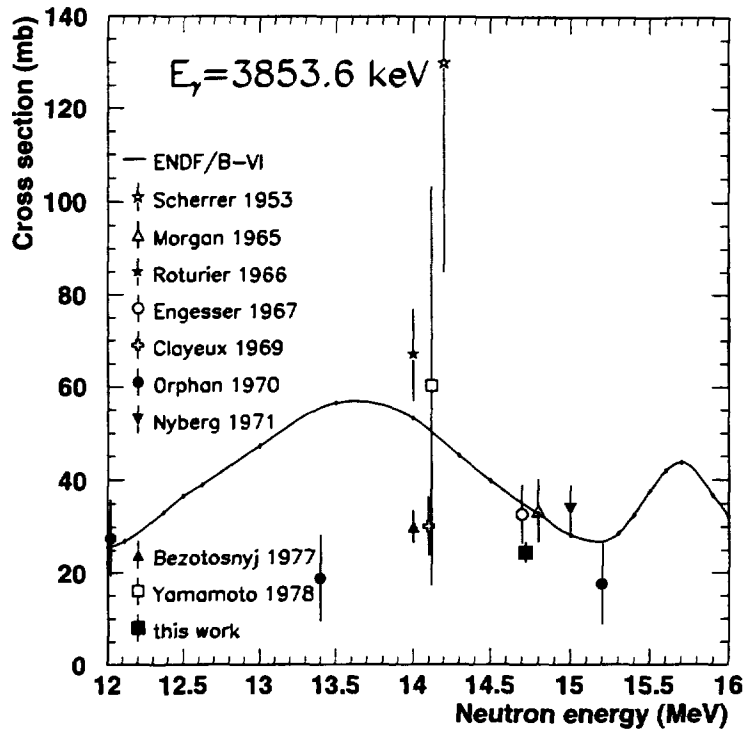

Figure 2: *Cross section for 3853.6 keV γ transition production in the $^{16}O(n,\alpha\gamma)^{13}C$ reaction. Our cross section is compared with other literature data [8] and ENDF/B-VI evaluation between 12 and 16 MeV incident neutron energy. The smooth line is a spline polynomial connecting points given by ENDF/B-VI.*

gives cross section of 32.7 mb at 14.7 MeV.

Total α particle production cross section is given by the sum of all partial level populations. Naturally, in our method we can not account for direct ground state population. For the total population of excited states in ^{13}C we get

$$\sigma_{\alpha'} = \sigma_{3684} + \sigma_{3853} + \sigma_{3088} = (53.5 \pm 5.0) + (24.3 \pm 2.2) + (3.1 \pm 0.6) = (80.9 \pm 5.4)\ mb. \quad (1)$$

However, using experimental cross section for the α_0 branch [7] of 17.3±3.4 mb for g.s. population, we can estimate from our γ production cross section the total α production cross section to be

$$\sigma_\alpha = \sigma_{\alpha_0} + \sigma_{\alpha'} = (80.9 \pm 5.4) + (17.3 \pm 3.4) = (98.8 \pm 6.4)\ mb \quad (2)$$

This value is lower than the cross section accepted in the ENDF/B-VI evaluation for the total α particle production, which is 131.7 mb. On the other hand, our value is in accord with the JENDL-3 evaluation which gives at 14.6 Mev cross section of 99.4 mb.

In the reaction $^{39}K(n,x\gamma)$ we determined production cross sections for 9 discrete transitions in reactions (n,n'γ), (n.pγ), (n,$\alpha\gamma$) and (n,n'pγ). Our preliminary results are summarized in the Tab. 1.

E_γ(keV)	Transition	Reaction	Cross section (mb)
788.4	$3^+ \rightarrow 2^+$	^{39}K(n,$\alpha\gamma$)^{36}Cl	20.9±2.2
1164.7	$1^+ \rightarrow 2^+$	^{39}K(n,$\alpha\gamma$)^{36}Cl	17.3±1.6
1267.2	$3/2^- \rightarrow 7/2^-$	^{39}K(n,pγ)^{39}Ar	19.3±2.2
1769.0	$2^+ \rightarrow 2^+$	^{39}K(n,n'pγ)^{38}Ar	6.7±1.4
1951.0	$2^- \rightarrow 2^+$	^{39}K(n,$\alpha\gamma$)^{36}Cl	9.7±1.6
2167.6	$2^+ \rightarrow 0^+$	^{39}K(n,n'pγ)^{38}Ar	193±14
2813.8	$7/2^- \rightarrow 3/2^+$	^{39}K(n,n'γ)^{39}K	74.4± 5.3
3597.6	$9/2^+ \rightarrow 3/2^+$	^{39}K(n,n'γ)^{39}K	23.2± 2.8
3680.0	$? \rightarrow 0^+$	^{39}K(n,n'pγ)^{38}Ar	98±10

Table 1: *Preliminary values of discrete γ ray production cross sections in the reactions ^{39}K(n,xγ) measured at 14.7 MeV incident neutron energy.*

Now we compare our experimental results with literature data. We can form from discrete γ ray production cross section a reaction cross section keeping in mind γ decay properties of product nucleus. It is for instance well known, that for vibrational medium heavy even-even nuclei the last $2^+ \rightarrow 0^+$ ground state transition collects almost the whole reaction cross section. It is therefore sufficient to measure only this single γ transition. In our experiment this situation arises in the reaction ^{39}K(n,n'p)^{38}Ar, where the transition $2^+ \rightarrow 0^+$ exhausts the whole reaction cross section. The other extreme represent odd-odd nuclei with many weak ground state transitions. To estimate reaction cross section in such a case, it is necessary to sum up cross sections of all those transitions. We can find similar situation in the reaction ^{39}K(n,α)^{36}Cl, where we observed 3 ground state transitions. In both cases we need to estimate the ground state population by an independent method, either be another experiment or by a reasonable model calculation. In the last case used model should well reproduce all partial discrete γ ray cross sections.

Our experimental value for (n,$\alpha\gamma$) cross section is sum of all partial cross sections which give value of (48±3) mb. In Fig. 3 we compare our data with literature data in the energy region around 14 MeV. Literature data show great discrepancies and are substantially higher than our data. The only known evaluation JENDL-3 is even higher than any experimental data. Our results seem to support lower values given by Borman, which measured α particle production in a KI(Tl) scintillation crystal, which served both as a target and the detector. The population of ground state can't be very high, because the Q-value of the (n,α) reaction is positive +1.4 MeV and there is no strong energy limitation. This is further supported by our data, which show that the population of excited levels at energies 0.788 MeV and 1.95 MeV differ only by a factor of 2. Because also spins of the low lying excited levels and ground state are similar, we expect that the g.s. population is of the same order as the population of excited states . It seems therefore, that the experimental value given by Bass and also the JENDL-3 evaluation around 14 MeV are too high.

Experimental cross section of ^{39}K(n,xpγ) reaction given in Fig. 4 show greater discrepancies. We found 4 independent cross section values, 3 of them obtained by charged

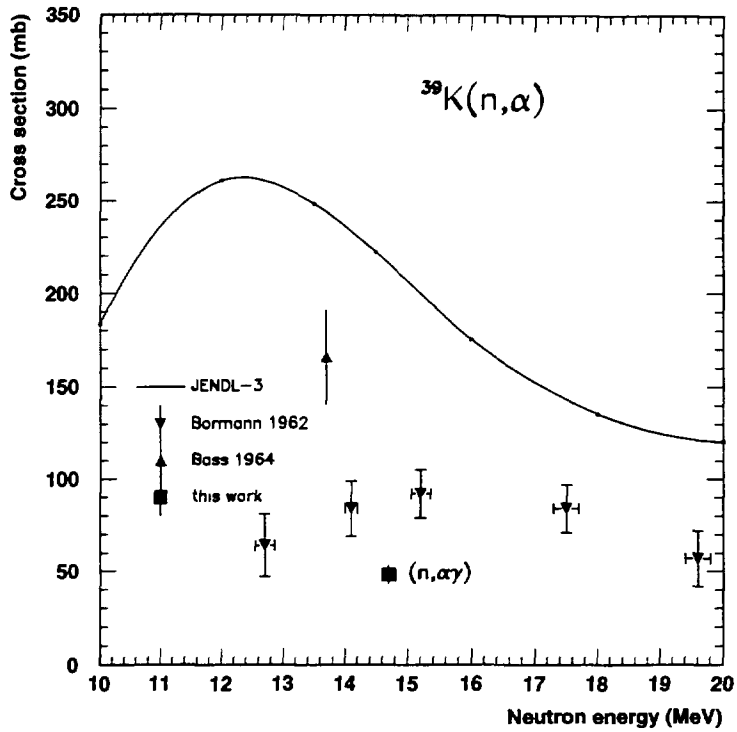

Figure 3: *Cross section of the $^{39}K(n,\alpha\gamma)^{36}Cl$ reaction compared with other available experimental data (see list in Ref. [9]) and JENDL - 3 evaluation.*

particle measurement and a single activation value (half-life of ^{39}Ar is 269 y). By measuring emitted protons only as was done in all in-beam experiments it is very difficult to distinguish between (n,p) and (n,n'p) channels, therefore it seems that these experiments measured rather the sum of both channels than the (n,p) cross section alone. Our method, where we can uniquely determine the reaction channel shows, that (n,n'p) channel is dominant. Literature data show rather strong discrepancies. Although older data of Borman and Alexandrov are in good agreement, they are by a factor of ≈ 3 higher than the last value of Foland. The sum of our (n,pγ) and (n,n'pγ) cross sections is within the quite large error bars of Borman and Alexandrov. In view of these arguments, the (n,p) activation cross section of Schantl seems to be very high.

In the (n,n'p) channel we determined cross section of the $2^+ \rightarrow 0^+$ transition in the even-even product nucleus ^{38}Ar. It is well known, that this transition in (n,n') reactions on medium nuclei exhaust approximately 90 % of the reaction cross section. If this is also the case in our reaction, than our (n,n'pγ) cross sections is very close to the (n,n'p) cross sections. Our experimental value is in rather good accord with JENDL-3 evaluation of (n,n'p) channel.

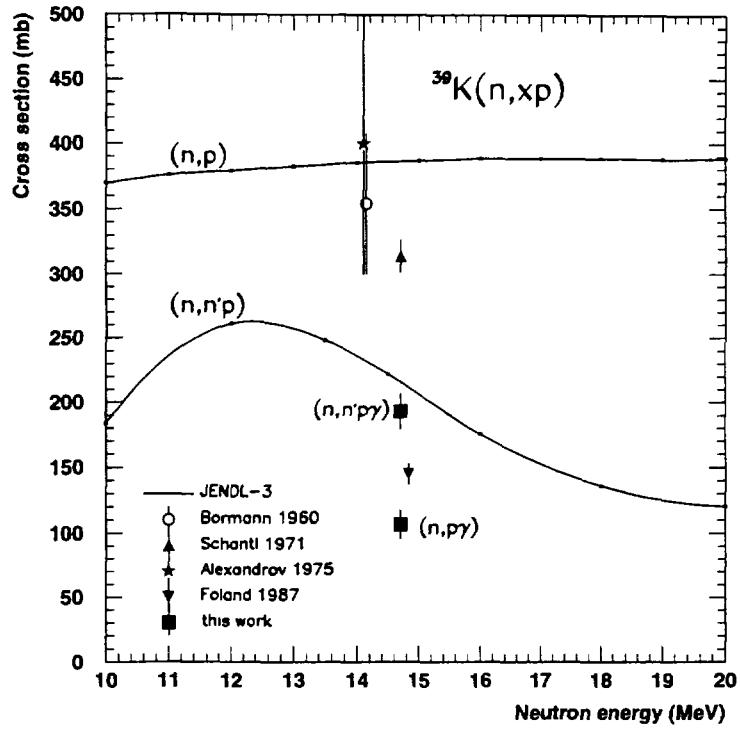

Figure 4: *Measured cross sections of (n,pγ) and (n,n'pγ) reactions on ^{39}K compared with other available data [9] and JENDL – 3 evaluation. Experimental data of Borman and Alexandrov represent most probably a sum of both cross sections. The result of Schantl was obtained by activation method and should refer to the (n,p) cross section.*

Conclusions

To summarize, using prompt in-beam γ ray technique, we measured discrete γ ray production cross section in neutron induced reactions on light nuclei ^{16}O and ^{39}K. Our data for γ production ^{16}O(n,α) reaction are in good agreement with overall mean experimental values from older experiments. There are no available experimental data on γ production in reactions on ^{39}K, where we determined 8 different cross sections.

We used our γ ray cross sections to determine also the whole ^{16}O(n,α)^{13}C reaction cross section. In addition to our γ ray production cross section of (80.9±5.4) mb we used a published value for g.s. population which gave us the reaction cross section of (98.9±6.4)mb. This value is lower than ENDF/B-VI evaluation, but is in good accord with JENDL-3. In the literature there are no simmilar data for reactions on ^{39}K, therefore we are not able to compare reaction cross sections. To do this, we need a reliable theoretical data on discrete level population. We are prepared to perform these calculations in the near future using well established statistical model codes like STAPRE or GNASH. We are in favorable position, because we measured cross sections of several discrete transitions in 4 different reaction channels. This data are sufficient to adjust parameters used in model calculations.

We have shown, that from measurement of discrete γ ray production cross sections also the reaction cross section can be determined. This is useful mainly in cases, where the reaction product is stable or very long-lived nucleus. Using discrete γ ray technique, which uniquely determine the reaction product may be even used with advantage in circumstances, where also the spectrum method is not enough conclusive. There are still several recommendations from activation community [2] for new cross section measurements, where our technique may be used.

References

[1] M. B. Chadwick, P. G. Young, P. Obložinský and A. Marcinkowski, Phys. Rev. C49 (1994) R2885.

[2] A. B. Paschenko, Report INDC(NDS)-301, (IAEA Vienna, July 1994).

[3] S. Hlaváč, P. Obložinský, I. Turzo, L. Dostál, H. Vonach, A. Pavlik and S. Simakov, accepted for publication in Nucl. Sci. Eng.

[4] J. Pivarč and S. Hlaváč, Nucl. Sci. Eng. 106 (1990) 266.

[5] S. Hlaváč, P. Obložinský, I. Turzo, L. Dostál and J. Kliman, Report INDC(SLK)-002, IAEA Vienna 1994.

[6] H. Vonach, S. Tagesen, M. Wagner and A. Pavlik, Physics Data 13-6, (Fachinformationszentrum Karlsruhe 1991).

[7] M. Borman, Z. Physik 258 (1973) 285.

[8] Literature data for production of 3684.3 and 3853.6 keV γ rays in ^{16}O(n,$\alpha\gamma$) reaction:

- **Scherrer 1953**—V. E. Scherrer, R. B. Theus and W. R. Faust, Phys. Rev. 91 (1953) 1476, EXFOR 11306.
- **McDonald 1966**—W. J. McDonald, J. M. Robson and R. Malcolm, Nucl. Phys. 75 (1966) 353, EXFOR 11383.
- **Roturier 1966**— J. Roturier, Compt. Rendu 262 (1966) 1736, EXFOR 20599.
- **Engesser 1967**— F. Engesser and W. Thompson, J. Nucl. Energy 21 (1967) 487, EXFOR 11531.
- **Clayeux 1969**— J. Clayeux, Report CEA-R-3807, EXFOR 21677.
- **Morgan 1969**— I. L. Morgan, J. B. Ashe and D. O. Nellis, Oak Ridge Report ORO-2791-32, 1971, EXFOR 12695.
- **Orphan 1970**— V. J. Orphan, C. G. Hoot and J. John, Nucl. Sci. Eng. 42 (1970) 352, EXFOR 10097.
- **Nyberg 1971**— K. Nyberg-Ponnert, B. Jönsson and I. Bergqvist, Phys. Scripta 4 (1971) 165, EXFOR 20245.

- **Bezotosnyj 1978**— V. M. Bezotosnyj, V. M. Gorbachev, M. A. Efimova, L M. Surov and M. S. Shevcov, Yad. Konst. 30 (1978) 21, EXFOR 40516.
- **Yamamoto 1987**—T. Yamamoto, Y. Hino, S. Itagaki and K. Sugiyama, J. Nucl. Sci. Techn. 15 (1978) 797, EXFOR 21304.
- **Nelson 1990**— R. Nelson, Proc. Washington Conf. Nucl. Data 1990.
- **ENDF/B-VI**— G. Hale, Z. Chen and P. Young, Evaluation of ^{16}O for ENDF/B-VI, LANL 1990.

[9] Literature data on $^{39}K(n,x\gamma)$ reactions cross section:

- **Borman 1960**—M. Borman, H. Jarmie, G. Andersson-Lindström, H. Neuert, H. Pollehn, Z. Naturforschung 15 (1960) 200, EXFOR 21668
- **Schantl 1971**—W. Schantl, IRK Vienna 1971, unpublished thesis, EXFOR 21846
- **Alexandrov 1975**—D. V. Alexandrov, L. I. Klochkova, B. S. Kovrigin , Yad. Energia, 39 (1975) 137, EXFOR 40433
- **Foland 1987**—K. A. Foland, R. J. Borg, M. G. Mustafa, Nucl. Sci. Eng. 95 (1987) 128, EXFOR 13109

^{208}Pb(n,pxnγ) Reactions for Neutron Energies up to 200 MeV

A Pavlik and H. Vonach
Institut fur Radiumforschung und Kernphysik, Universitat Wien
A-1090 Wien, Austria

and

R. O Nelson, R C. Haight, S A. Wender, P. G. Young, and M. B. Chadwick*
Los Alamos National Laboratory, Los Alamos, NM 87545, U.S.A.

ABSTRACT

The prompt gamma-radiation from the interaction of fast neutrons with enriched samples of ^{208}Pb was measured using the white neutron beam of the WNR facility at Los Alamos National Laboratory The samples were positioned at about 40 m distance from the neutron production target The spectra of the emitted gamma-rays were measured with a high-resolution HPGe detector. The incident neutron energy was determined by the time-of-flight method and the neutron fluence was measured with a ^{238}U fission chamber. In addition to the primary purpose of this experiment, the study of (n,xnγ) reactions leading to various lead isotopes, gamma transitions in the residual nuclei ^{207,205,203,201}Tl were analyzed. From these data gamma-production cross sections in the neutron energy range from the effective thresholds to 200 MeV were derived The lines for the analysis had to be chosen carefully as the (n,pnxγ) cross sections are rather small and the interference with unresolved lead lines (even weak ones) would cause significant errors The effect due to isomers with half-lives exceeding a few nanoseconds was taken into account and corrected for, if necessary. The measured cross sections were compared with the results of nuclear model calculations based on the exciton model for preequilibrium particle emission and the Hauser-Feshbach theory for compound nucleus decay Unlike the case of (n,xnγ) reactions the calculated results in general did not give a good description of the measured cross sections

1. Introduction

One method to measure photon-production cross sections in neutron induced reactions is the use of a "white" neutron spallation source and high-resolution gamma-ray spectroscopy. The incident neutron energy is determined by the time-of-flight method and gamma-ray production cross sections can be measured simultaneously for a wide neutron energy range. Recently such measurements have been performed at the Weapons Neutron Research facility (WNR) at the Los Alamos National Laboratory in an energy range covering several hundreds of MeV.[1] One of the recent experiments was a study of (n,xnγ) reactions on ^{207,208}Pb in the neutron energy range from 3 to 200 MeV [2,3] The (n,xnγ) reactions were analyzed first, as neutron emission is the dominant reaction channel. Good agreement was found between the experimental results and model calculations performed with the code GNASH.[4] These calculations are based on the Hauser-Feshbach formalism for compound nucleus decay and the exciton model for preequilibrium particle emission. Multiple preequilibrium particle

* *Present address Lawrence Livermore National Laboratory, Livermore, CA 94551, U.S.A*

emission was taken into account and the level density formula given by Ignatyuk[5] was used More details on these calculations can be found in Ref. 2.

The objective of the present work was to identify gamma-rays related to less intense reaction channels in the already measured spectra. We analyzed ^{208}Pb(n,pxnγ) reactions leading to various isotopes of Tl As our nuclear model calculations can reproduce (n,xnγ) cross sections very satisfactorily, it was the goal of this work to check these calculations for a weaker channel

2. Experiment

The experiment was performed on the 30° left flight path of the WNR facility and is described in detail in Ref 2 A schematic diagram of the flight path collimation and shielding is shown in Fig 1 The isotopically enriched Pb sample (99 56% ^{208}Pb) was mounted at a distance of 41.48 m from the neutron production target on a thin plastic frame Two high-purity coaxial Ge detectors with active volumes of approximately 70 cm^3 and 140 cm^3 were used at γ-ray emission angles of 90° and 125°. The collimators were steel tubes filled with tungsten powder, because the usual lead shielding emits the same gamma rays as the isotopic lead targets when excited by scattered neutrons. The detector position of 125° was chosen because the value of the P_2 Legendre polynomial function is zero at that angle The angle integrated cross section can then be approximated as 4π times the measured cross section at θ = 125°, provided the coefficients of the higher-order polynomials are small Gamma rays from Tl isotopes were analyzed in the spectra measured with the 125° detector only.

The neutron energy range from 3 to 200 MeV was divided into 53 groups with increasing widths according to the energy resolution of the experiment. The neutron flux was measured with a fission chamber containing a ^{238}U fission foil centered on the beam at a distance of 37.30 m from the production target The neutron fluence for each energy group was determined from the two-dimensional (neutron TOF versus fission pulse height) fission chamber spectra using ^{238}U(n,f) cross sections given by Lisowski et al.[6]

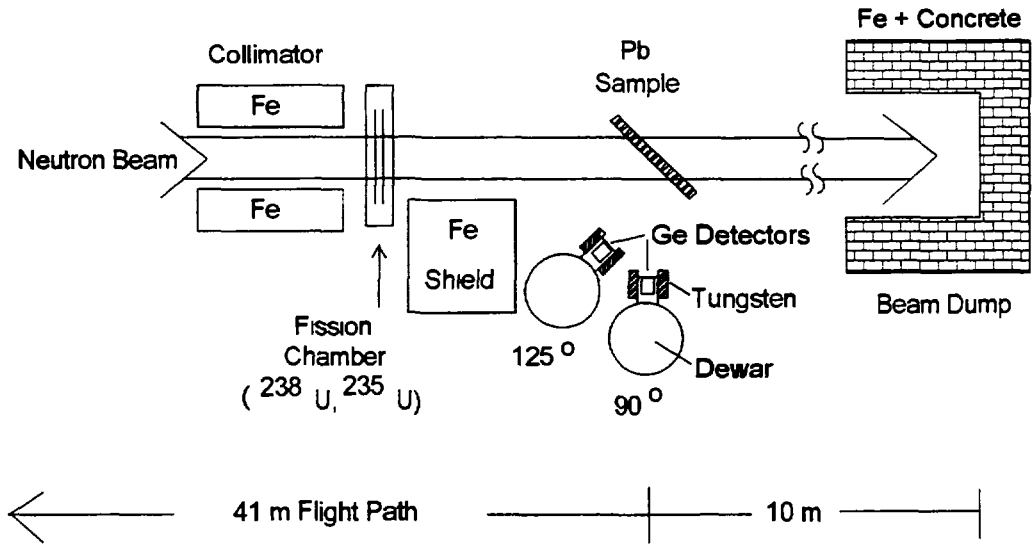

Figure 1: Experimental setup

Two-dimensional spectra, neutron TOF versus gamma pulse-height, were recorded for the Ge detector. The time resolution, determined from the γ–ray flash from the neutron-production target, varied from 10 ns FWHM for E_γ = 200 keV to 5 ns FWHM for E_γ = 3 MeV. The γ-ray energy resolution obtained during the experiments was 2.8 keV FWHM at a γ-ray energy of 803 keV.

3. Data Reduction

Gamma-ray transitions considered for the analysis were those with rather large cross sections (more then about 10 mb in the maximum as predicted by the code GNASH). As even weak gamma-lines from ^{208}Pb(n,xnγ) reactions reach such cross section values, it was essential to select only such Tl-lines which could clearly be separated from the Pb lines in the gamma-ray spectra. Finally there must also be no interfering background lines, especially from the tungsten collimator

A major problem in such white source experiments is the presence of isomers with half-lives exceeding a few nanoseconds in the residual nuclei. When isomers are present in the cascade preceding the gamma-transitions investigated, the measured gamma-radiation is not emitted promptly. Such delayed transitions may be detected in this type of experiment but they cannot be properly correlated with the neutron energy because the measured TOF includes the decay delay Therefore correction procedures have to be applied to ensure that the derived cross sections relate only to the prompt emission of gamma rays. Due to the pulse structure of the WNR-facility, the actual correction procedure depends on the half-life of the isomer If the lifetime of the isomer is large compared to the duration of a macropulse (typically 800 μs), most of the delayed γ-rays (about 98%) would be emitted between the macropulses when the detector electronics is gated off, and thus will not be counted. If the half-life of an isomer in the cascade is comparable to the duration of a macropulse, the delayed γ-rays are observed in the measured spectrum with a uniform distribution in time and can be subtracted as a constant background. The background rate then can be determined from the measured intensities below the effective reaction threshold. For isomers with shorter half-lives the delayed contribution to the measured transition can be determined from the time distributions of the decay of the corresponding isomers. (See Ref. 2 for details). The applicability of this last method depends on the decay scheme, γ-ray intensities and energies of transitions related to the decay of the isomers. It was not possible to use this method in any of the Tl-nuclei studied in this work. If the lifetime of the isomer is smaller than the time resolution of the experiment the delay can be neglected.

According to the decay schemes[7] and the γ-ray intensities, the transitions listed in Table I were chosen for analysis Table I also shows the isomers which might cause delayed emission of the γ-rays.

As seen from Table I long-lived isomers have to be considered for the γ-transitions in ^{205}Tl and ^{201}Tl. The isotope ^{203}Tl does not have any known isomers, from ^{207}Tl a prompt transition was chosen for analysis No correction was necessary for the 203.8-keV isomer in ^{205}Tl with a half-live of 1.46 ns. The average lifetime of this isomer is well below the time resolution of our experiment and can therefore be neglected. To get a coarse estimate of the effect of the 1484.0-keV isomer ($t_{1/2}$ = 4.5 ns) in ^{205}Tl, the data analysis was redone under the assumption that the 203.7-keV and 720.1-keV γ-rays were partially delayed by a constant delay time equal to the mean lifetime of this isomer. The fraction of the γ-ray intensity delayed was estimated using the results of model calculations. This procedure resulted in

somewhat different cross sections. On the average the differences were about 4%, much smaller than the statistical uncertainties of about 15% to 30%. Because correction factors could be estimated with large uncertainties only (due to the poor statistics), we neglected also this correction for the delay caused by this 4.5-ns isomer.

If significant intensity of the 203 7-keV and 720 1-keV lines in ^{205}Tl is delayed by the 3290 6-keV level ($t_{1/2}$ = 2 6 μs), this would result in significant intensity below the effective thresholds of the relevant excitation functions As this intensity is not observed, the measured cross sections for the 203 7-keV and 720 1-keV transitions can be considered a good approximation to the total γ-ray production cross sections for these lines.

Table I: Nuclear reactions and gamma transitions investigated

Reaction investigated	γ Transition (Level energies in keV)	γ Energy	Isomers in γ cascade Jπ	E[keV]	$t_{1/2}$
^{208}Pb(n,pnγ)^{207}Tl	1682.7 → 351.0	1331.7		none	
^{208}Pb(n,p3nγ)^{205}Tl	203.7 → gs	203.7	$3/2^+$	203 7	1.46 ns
			$11/2^-$	1484.0	4 5 ns
			$25/2^+$	3290.6	2.6 μs
^{208}Pb(n,p3nγ)^{205}Tl	923.8 → 203 7	720.1	$11/2^-$	1484.0	4 5 ns
			$25/2^+$	3290 6	2 6 μs
^{208}Pb(n,p5nγ)^{203}Tl	680.5 → 279 2	401.3		none	
^{208}Pb(n,p7nγ)^{201}Tl	331.2 → gs	331 2[a]	$(9/2^-)$	919 5	2 035 ms
			$(13/2^-)$	2015 0	2 9 ns
^{208}Pb(n,p7nγ)^{201}Tl	1571.7 →1238.8	332.9[a]	$(13/2^-)$	2015 0	2.9 ns

[a] The 331 2-keV and 332 9-keV γ lines in ^{201}Tl were not resolved

In the residual nucleus ^{201}Tl there are two gamma-transitions with 331.2 and 332.9 keV γ-ray energy. These two lines cannot be resolved by our experiment The delay from the 2015 0-keV isomer can be neglected due to the short half-life of 2.9 ns The half-life of the 919.5-keV level (2.035 ms) is long enough that more than 98% of the delayed intensity is emitted outside the time range (corresponding to the neutron energy range between reaction threshold and 200 MeV) which was actually analyzed There is in addition also no significant intensity (within the uncertainty limits) observed in the neutron energy range below the threshold Therefore corrections need not be performed and the measured cross section for the residual nucleus ^{201}Tl is the sum of the γ-ray production cross sections for the 332.9-kev transition and the prompt part of the 331.2-keV transition.

To derive γ-ray production cross sections, a one-dimensional γ pulse-height spectrum was derived from the two-dimensional spectrum, neutron TOF versus γ pulse-height, for each neutron energy group. Fig. 2 shows an example of a spectrum for the neutron energy range 90 to 100 MeV. Four of the lines actually analyzed are marked in the figure. The number of counts in the γ-peak areas were obtained by adding the channel contents within the peak and subtracting a smooth (linear) background As the choice of the peak limits and the

background region is somewhat subjective, an additional uncertainty component was added quadratically to the statistical uncertainties An estimate of this uncertainty was obtained by comparing the peak areas determined by different summing limits and background regions Corrections were applied for the attenuation of the γ rays within the samples.

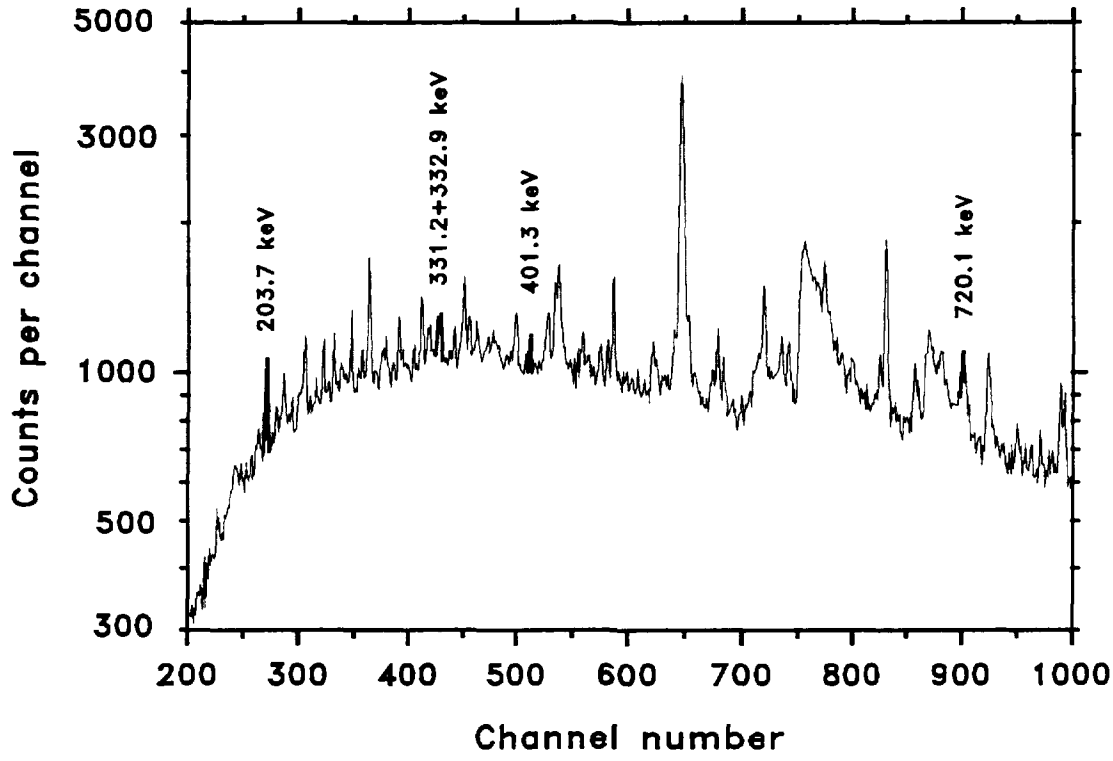

Figure 2: Part of the gamma-ray spectrum for the neutron energy group 90 - 100 MeV The marked γ-lines were analyzed

From the peak areas, the neutron fluence, and the γ detector efficiency, relative excitation functions were derived for each γ transition analyzed. The differential cross sections at θ =125° were converted to total γ-production cross sections by multiplying them by 4π

Because of uncertainty in our knowledge of the Ge detector dead time and the absolute flux intercepted by the irregular shaped samples, the results were normalized to data obtained in a separate 14-MeV experiment performed at the Institute of Physics of the Slovak Academy of Sciences.[8] Normalization factors were derived from the cross sections of prominent transitions in ^{208}Pb(n,n'γ) and ^{208}Pb(n,2nγ) reactions.

The total uncertainties were obtained by adding statistical and estimated systematic uncertainties in quadrature. Uncertainties in the range from 35% to 50% were estimated for γ-ray production cross sections of the 1331.7-keV and 401.3-keV transitions in ^{207}Tl and ^{203}Tl, respectively. For the measured γ-ray production cross sections in the residual nuclei ^{205}Tl and ^{201}Tl the total uncertainties were in the range from 15% to 35%.

4. Results and Discussion

Extensive calculations of the γ-ray production cross sections in ^{208}Pb(n,xγ) reactions were performed by means of the code GNASH[4] in the course of the investigation of ^{208}Pb(n,xnγ) reactions (see Ref. 2). Three extensions in the modeling of preequilibrium reactions were installed in GNASH to improve the physics for calculations at higher energies Until now it was assumed that after the first preequilibrium particle is emitted, the remaining particle-hole states proceed to equilibrium via a series of nucleon-nucleon collisions before decaying. This assumption was modified to allow the particle-hole states left after primary preequilibrium emission to decay by "multiple preequilibrium" emission The second modeling improvement was to calculate spin distributions for the residual states formed in preequilibrium reactions using angular momentum distributions based on the exciton model. And finally, we have incorporated the excitation-energy dependence of the Ignatyuk level-density formula[5] into the particle-hole state densities used in the exciton model calculations Cross-section calculations were performed with this *a priori* "best choice" parameter set (see Ref 2 for details) For the nuclear level densities, the Ignatyuk model was chosen instead of the simpler Gilbert-Cameron[9] and other Fermi-gas models. The energy-dependent level density parameter of the Ignatyuk model accounts for the theoretically expected disappearance of shell effects in the nuclear level densities at higher excitation energies Within this model the nuclear moment of inertia was given the value of the full rigid body moment of inertia

The same "best choice" parameter set, which gave good agreement with the experimental cross sections in ^{208}Pb(n,xnγ) reactions leading to various lead nuclei was used in the calculations of γ-ray production cross sections in Tl nuclei from ^{208}Pb(n,pxnγ) reactions. The results for transitions in ^{207,205,203,201}Tl are given in Figs. 3 to 7 In Fig. 7, from the sum of the calculated γ-ray production cross sections for the 331 3-keV and 332 9-keV transitions, the production cross section for the 919 5-keV level ($t_{1/2}$ = 2 035 ms) was subtracted to correct for the fact that only the promptly emitted 331 2-keV γ-rays are observed in the experiment.

There are rather large uncertainties, and also some approximations are made regarding the effect of long-lived isomers on our experimental results Because model calculations without special parameter adjustments can predict experimental results in general not better than within about 20% to 30%, the experimental results are suitable quantities for comparison with calculations.

Other than in the case of reactions with neutron emission only (see Refs. 2 and 3), there is no agreement between experimental results and model calculations for the majority of the transitions analyzed. For the analyzed transitions in ^{207}Tl (Fig 3) and ^{205}Tl (Figs 4 and 5) the model calculation overestimates the measured cross section for neutron energies above about 70 MeV The calculations result in cross sections about a factor of 3 to 4 higher than the experimental ones There is rather good agreement for the 401.3-keV transition in ^{203}Tl. Finally the calculated cross sections are smaller than the experimental results for γ-ray transitions in ^{201}Tl for high neutron energies. It seems that our calculation gives a too hard spectrum of the emitted protons. Proton emission is important for the preequilibrium stage of the reaction only, as proton emission from compound nucleus decay is strongly suppressed by the Coulomb barrier. An average energy of the emitted protons from the preequilibrium stage that is too high results in higher cross sections for reactions with the subsequent emission of only a few neutrons, and in lower cross sections for reactions with multiparticle emission as less energy is available after emission of the proton As seen from Figs. 3 to 7 this effect is observed in the present study It should be mentioned that the experimental information on

discrete levels and γ-ray branching in Tl nuclei is not as good as for Pb As the information on discrete levels and γ-ray branching is essential for the calculation of γ-ray production cross sections for individual transitions, incomplete level scheme information might also contribute to some of the observed discrepancies

Neutron emission is such a dominant reaction channel that the results of the previous investigations[2,3] of ^{208}Pb(n,xnγ) reactions are virtually independent of the description of protons in the exit channel The present study of ^{208}Pb(n,pxnγ) reactions gives us experimental information, that may help to improve the modeling of (n,pxn) reactions for lead

Acknowledgments

This work was supported by the Fonds zur Förderung der wissenschaftlichen Forschung in Österreich (Project P 7908-TEC), and the U.S Department of Energy under contracts W-7405-ENG-36 and W-7405-ENG-48

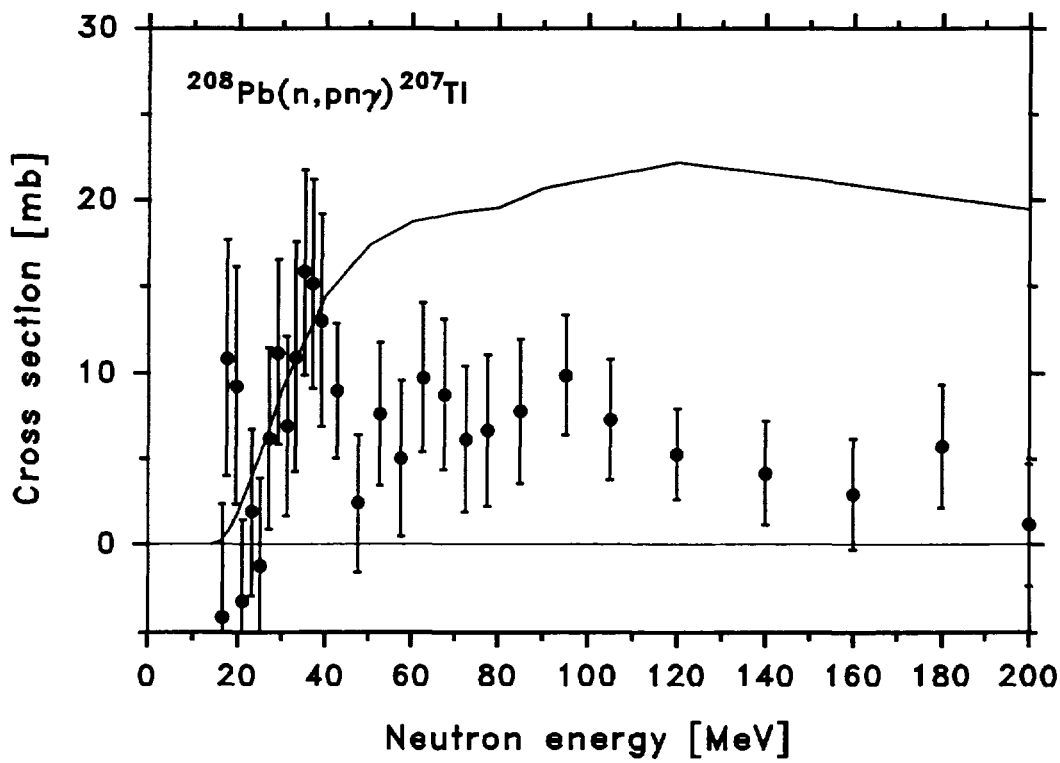

Figure 3: ^{208}Pb(n,pnγ)^{207}Tl cross section for the 5/2$^+$ (1682.7 keV) → 3/2$^+$ (351.0 keV) transition (E_γ = 1331.7 keV) in ^{207}Tl. Symbols Present experiment. Solid line GNASH calculation

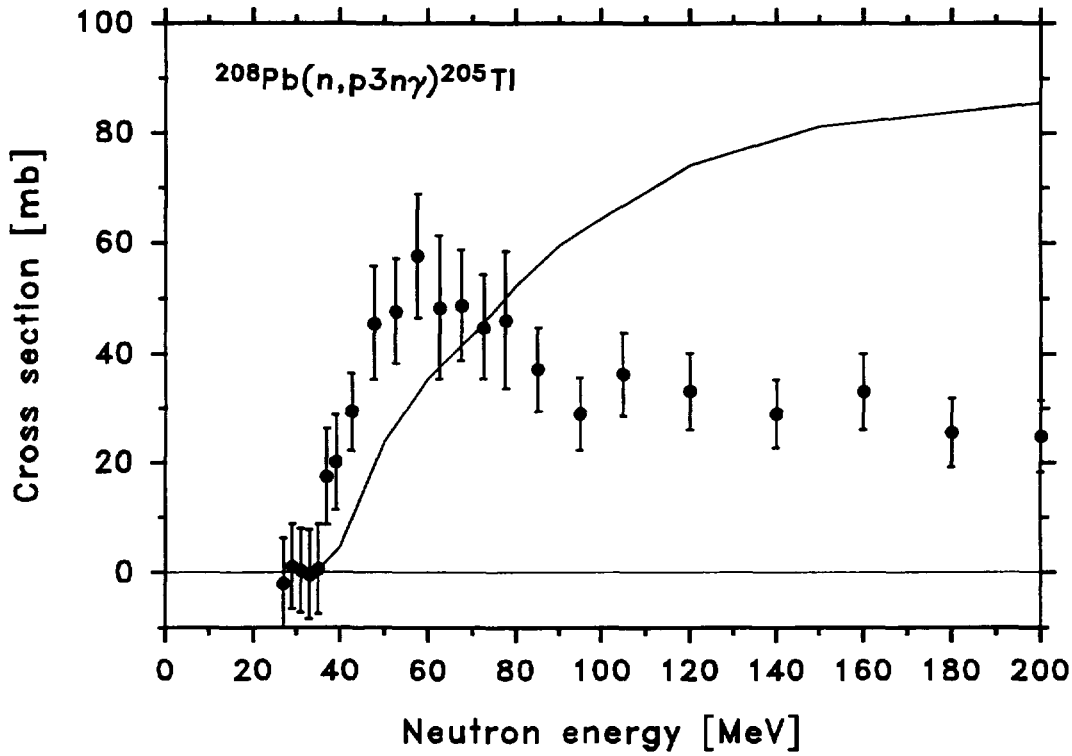

Figure 4: $^{208}Pb(n,p3n\gamma)^{205}Tl$ cross section for the $3/2^+$ (203 7 keV) → gs transition (E_γ = 203 7 keV) in ^{205}Tl Symbols Present experiment Solid line GNASH calculation

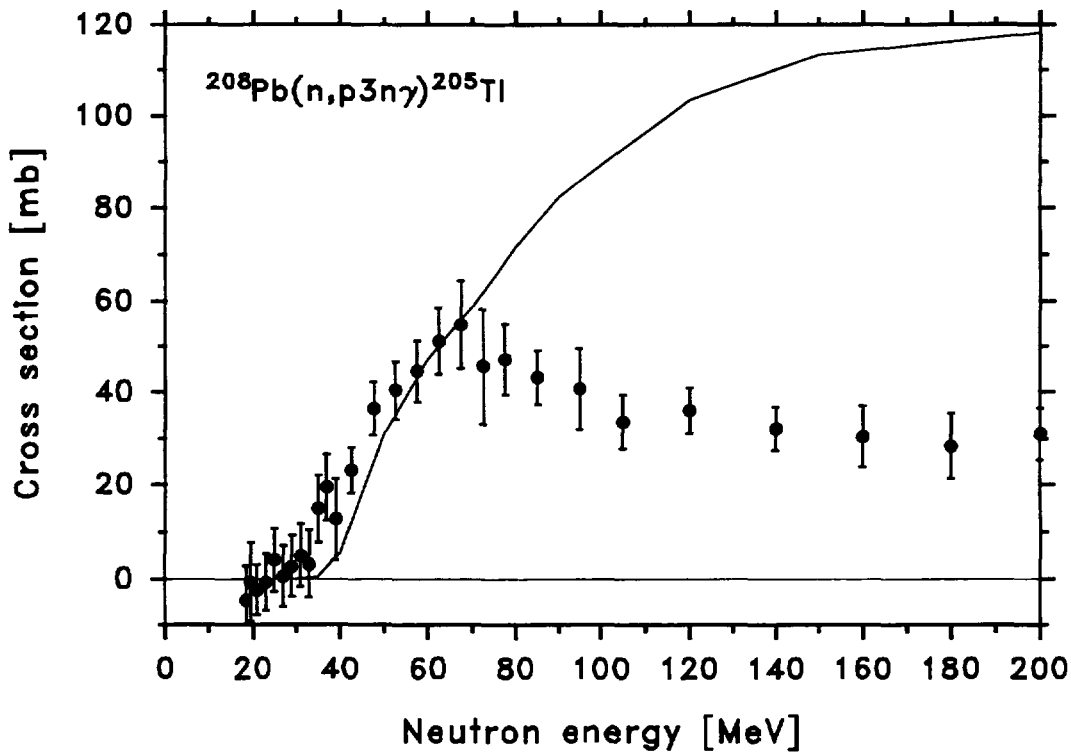

Figure 5: $^{208}Pb(n,p3n\gamma)^{205}Tl$ cross section for the $7/2^+$ (923 8 keV) → $3/2^+$ (203 7 keV) transition (E_γ = 720 1 keV) in ^{205}Tl Symbols Present experiment Solid line GNASH calculation

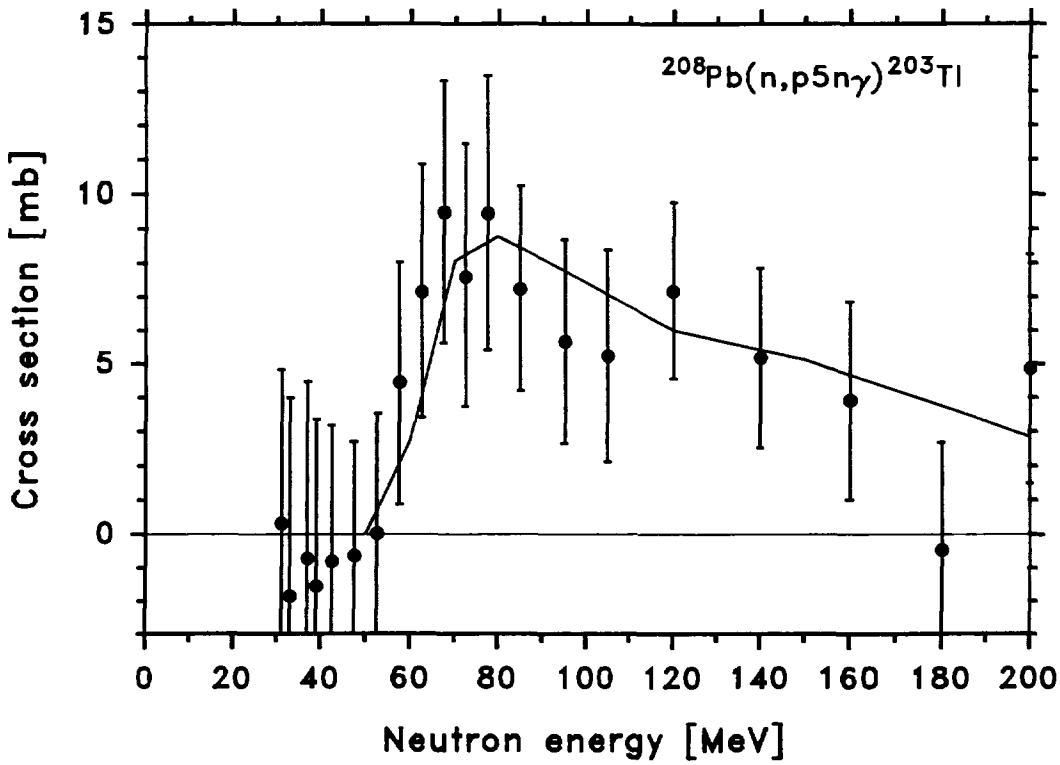

Figure 6: ^{208}Pb(n,p5nγ)^{203}Tl cross section for the $5/2^+$ (680 5 keV) → $3/2^+$ (279.2 keV) transition (E_γ = 401.3 keV) in ^{203}Tl Symbols Present experiment Solid line GNASH calculation

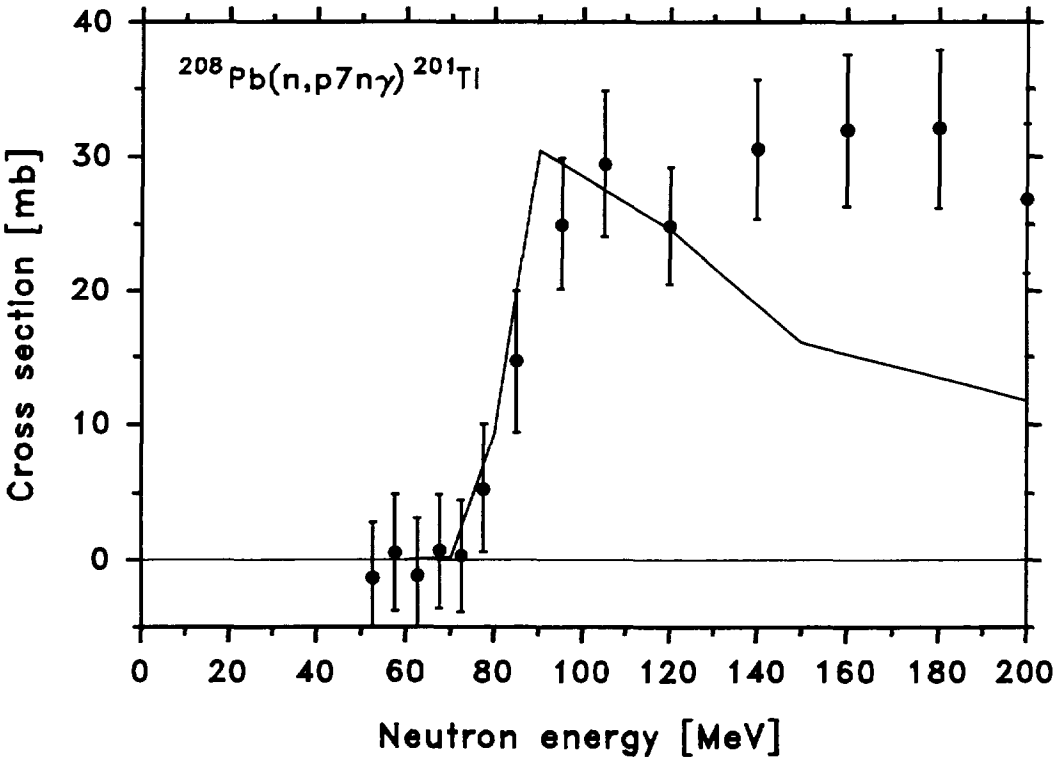

Figure 7: ^{208}Pb(n,p7nγ)^{201}Tl cross section Sum of the cross sections for the $13/2^-$ (1571 7 keV) → $11/2^-$ (1238 8 keV) transition (E_γ = 332 9 keV) and for the prompt part of the $3/2^+$ (331 2 keV) → gs transition (E_γ = 331 2 keV) in ^{201}Tl. Symbols Present experiment Solid line GNASH calculation

References

1 R O Nelson, S A Wender, and D. R. Mayo, "Gamma-Ray Measurements at the WNR White Neutron Source," *Proc. NEA Specialists' Meeting on Measurement, Calculation and Evaluation of Photon Production Data, Bologna, Italy, 9 - 11 November 1994* (to be published by OECD Nuclear Energy Agency) and contribution to this conference

2 H Vonach, A Pavlik, M. B Chadwick, R C Haight, R O Nelson, S A Wender, and P G Young, *Phys. Rev. C* **50** (1994) 1952.

3. H Vonach, A Pavlik, H. Hitzenberger, R. O. Nelson, R C Haight, S A. Wender, P. G Young, and M B Chadwick, "Measurement of Gamma-ray Production Cross Sections in Neutron-induced Reactions for Al and Pb," *Proc. NEA Specialists' Meeting on Measurement, Calculation and Evaluation of Photon Production Data, Bologna, Italy, 9 - 11 November 1994* (to be published by OECD Nuclear Energy Agency)

4 P G Young, E. D Arthur, and M B Chadwick, *Comprehensive Nuclear Model Calculations: Introduction to the Theory and Use of the GNASH Code* (Los Alamos National Laboratory report LA-12343-MS, Los Alamos, 1992).

5 A. V Ignatyuk, G. N. Smirenkin, and A S Tishin, *Sov. J. Nucl. Phys.* **21** (1975) 255

6 P W Lisowski *et al.*, "Fission Cross Sections in the Intermediate Energy Region," in *Proc. Specialists' Meeting on Neutron Cross Section Standards for the Energy Region above 20 MeV, Uppsala, Sweden, 21 - 23 May 1991*, (Nuclear Energy Agency Nuclear Data Committee report NEANDC-305 'U', Paris, 1991), p 177.

7 ENSDF, *The Evaluated Nuclear Structure Data File*, Data received from National Nuclear Data Center, Brookhaven National Laboratory (1993)

8 S Hlaváč, P. Obložinský, L Dostál, I. Turzo, H. Vonach, A Pavlik, and S Simakov, "Study of γ-Radiation from Interaction of 14.7 MeV Neutrons with ^{208}Pb," *Nucl. Sci. Eng.* (in press)

9 A Gilbert and A G W Cameron, *Can. J. Phys.* **43** (1965) 1446.

Contributed paper presented at the IAEA First Research Coordination Meeting on Measurement, Calculation and Evaluation of Photon Production Data, Bologna, Italy, November 14 - 17, 1994

GAMMA-RAY PRODUCTION EXPERIMENTS AT THE WNR WHITE NEUTRON SOURCE

R.O. Nelson and S.A. Wender
P-23, M.S. H803, Los Alamos National Laboratory, Los Alamos, NM 87545, U.S.A.

ABSTRACT

Using the WNR white neutron source, photon production data have been acquired in the incident neutron energy range, $3 < E_n < 400$ MeV, for a number of target nuclei using BGO detectors and high-resolution Ge detectors. The gamma-ray energy range covered is $0.1 < E_\gamma < 10$ MeV for the Ge detectors and $1.0 < E_\gamma < 20$ MeV for the BGO detectors. The Ge detector measurements allow identification of reactions from the known energies of the gamma-ray transitions between low-lying states in the final nucleus. The lower resolution BGO data were also for discrete transitions. The data are useful both for testing nuclear reaction models at intermediate energies and for numerous applied purposes. We list the target nuclei studied to date and the status of the data.

1. Introduction

Gamma-ray production data have been acquired for a variety of targets at the WNR spallation neutron source at Los Alamos. Most of the recent measurements used Ge detectors, although earlier experiments were performed with BGO detectors. The data provide continuous coverage of the neutron energy range, typically, from 3 to 400 MeV. The γ-ray energy range measured is from approximately 100 keV to 3 MeV for heavier targets, and from a few hundred keV to 10 MeV for lighter mass targets. These energy ranges were chosen because relatively intense, higher energy gamma rays are expected from the lighter nuclei. This is due to the larger level spacings of the low lying states of light nuclei, as compared to heavier nuclei. The WNR facility is described by Lisowski et al.[1] A description of some of the Ge detector experiments is given in Ref. 2.

The data were acquired with two main goals in mind. First, the data provide information that can be used in evaluations and applications. Second, by extending the data to higher energies we can validate extensions and improvements in nuclear reaction model calculations.

Here we present an overview of the data that have been acquired to date. In many cases the data reduction task is still in progress. The data are acquired as both 2 parameter arrays (neutron time-of-flight versus gamma-ray pulse height) and as event data, which allows resorting of the data with maximal dispersion in the spectra as needed. The amounts of data to be handled are large and hence require automated data reduction procedures to expedite the process.

2. Data

Some common features of the measurements are listed here: The data were measured relative to the ^{235,238}U(n,f) cross sections using a fission ionization chamber.[3] Almost all of the Ge detector data were taken on a 41 m flight path. The BGO data were taken on an 18 m flight path.

Several experimental factors determine the energy range over which reliable cross section values can be extracted from our data. Because our flux decreases exponentially, and due to the fact that cross sections tend to be smaller at higher energies, the number of counts available limits the maximum energy at which we obtain useful data. One must also consider the production of γ rays by secondary particles produced in the sample. In order to correct for this contribution, we must make measurements with two or more different sample thicknesses. The magnitude of the correction depends upon the reaction threshold energy as well as the magnitude of the cross section at a given energy. Inelastic scattering to the first excited state of the target nucleus is an example of a reaction which, at high energies, can have a very large correction due to its small cross section, and the larger cross section for excitation of the same state by charged particles and lower-energy scattered neutrons. A reaction with a higher energy threshold, such as (n,3n), will require less of a correction because the same residual nucleus is unlikely to be created by secondary charged particles, and the mean free path of neutrons with sufficient energy to initiate the reaction is much larger than for lower energy neutrons.

Additionally one must consider the angular distribution of the γ rays. It is usually desired to obtain the angle integrated cross section for a reaction from the γ-ray data. For γ rays that are emitted isotropically a measurement at any one angle is sufficient. For dipole transitions a single measurement at 125° is sufficient. But for γ rays of higher multipolarity, it is necessary to make measurements at several angles to determine the angular distribution. The variation from isotropy is observed to be large in some cases, especially in the resonance region of light nuclei. White sources are well suited for making such measurements because the energy dependence of the cross section is obtained in one experiment. The ^{16}O(n,n'$_2\gamma$) reaction is an example of a reaction for which the octupole γ-decay exhibits striking anisotropy of the angular distribution. The resonance structure persists to energies near 20 MeV, with the angular distributions varying rapidly with incident neutron energy.

Our data can be divided into two categories. In the first category are data which have been acquired with relatively fewer counts and for only one target thickness. These data, listed in Table 1, can be used reliably for incident neutron energies less than approximately 20 MeV for reactions with low thresholds, and may be useful for reactions with high thresholds at higher energies if the cross sections are large. The second category, listed in Table 2, contains data that were taken with two or more sample thicknesses and with more counts. From these data, we expect that reliable cross sections may be extracted for many reactions even at higher energies. Data on C, N, and B were

taken with lower resolution BGO detectors, but with an extended γ-ray energy range up to 20 MeV. These data are indicated in the column with the number of angles. The number of angles at which data were obtained, the status of the data reduction, and one or more applications are also listed in the tables.

Table 1. Samples for which limited data are available.

Sample	# of angles	Data Reduction Status	Application
B	2 +BGO	In progress	planetary exploration
Na	4	In progress	fusion, (n,2n) discrepancies
Si	2	In progress	planetary exploration
S	2	In progress	planetary exploration
Ca	2	In progress	planetary exploration
Ti	2	In progress	planetary exploration, structural material
Ni	2	In progress	structural material, planetary exploration
Mn	2	In progress	planetary exploration

Table 2. Samples for which more complete data are available.

Sample	# of angles	Data Reduction Status	Application
C	4 +BGO	Near completion preliminary results available	"standard", explosives detection, medical radiotherapy
N	4 +BGO	In progress, preliminary results	explosives detection, medical radiotherapy
O	7	In progress, preliminary results	medical radiotherapy, fusion experiment background, explosives detection
Al	2	Completed	model development
^{nat,56}Fe	4	In progress, preliminary results	compare with ORELA data, structural material, reaction model development
^{207,208}Pb	2	Completed	reaction model development, accelerator driven transmutation

3. Acknowledgments

The authors should like to thank M.B. Chadwick, D.M. Drake, R.C. Haight, P.G. Young, M. Drosg, H. Hitzenberger, A. Pavlik, H. Vonach, G. Bobias, and P. Englert for their support. This work was supported by the US DOE under contract W-7405-ENG-36.

References

1. P. W. Lisowski, C. D. Bowman, G. J. Russell, and S. A. Wender, *Nucl. Sci. Eng.* **106** (1990) 208.
2. R. O. Nelson, C. M. Laymon, and S. A. Wender, *Nucl. Instrum. and Meth. in Phys. Res.* **B56** (1991) 451.
3. S. A. Wender *et al.*, *Nucl. Instrum. and Meth. in Phys. Res.* **A336** (1993) 226.

OVERVIEW OF REACTION MECHANISMS FOR CALCULATING THE HIGH ENERGY COMPONENT OF FAST-NUCLEON INDUCED GAMMA SPECTRA

FRANK S. DIETRICH
Lawrence Livermore National Laboratory
P. O. Box 808, Livermore, CA 94550, USA

ABSTRACT

This presentation reviews the current status of quantum mechanical models for understanding the high-energy component of gamma spectra resulting from radiative capture of fast nucleons; i e., the part of the spectrum that is not amenable to standard statistical model (Hauser-Feshbach) treatments. These models are based on the direct-semidirect (DSD) model and its variants. Included are recent results on the extension of the DSD model to unbound final states, a discussion of problems and improvements in understanding the form factors in this model, and a brief discussion of a model closely related to the DSD, the pure-resonance model.

1. Introduction

In radiative capture of nucleons above a few MeV incident energy, the most energetic gammas are well understood as arising from direct reaction processes. Since its introduction 30 years ago, the direct-semidirect (DSD) model[1,2] has been the principal theoretical tool for interpreting this component of the gamma spectrum. In this model, direct radiative capture is supplemented by additional coherent amplitudes in which the incident nucleon excites giant resonances that subsequently decay by gamma emission. While both types of amplitudes are required for a full description of the capture process, semidirect excitation of the giant-dipole resonance (GDR) is dominant over a wide energy region about the position of the GDR. In addition to the dominant E1 multipolarity, higher multipolarities (M1, E2, E3) have also been included in DSD calculations.

An important feature of the semidirect terms is the form factors that contain the physics of the coupling of the incident nucleon to the giant resonances. These form factors are derived from models for the transition densities of the giant resonances[3], and contain input from the strength of the isovector or isoscalar nucleon-nucleon interaction, as well as the fraction of an appropriate sum rule exhausted by the giant resonances; form factors for both isovector (E1, E2) and isoscalar (E2) resonances have been implemented However, the details of the radial shape and strength of the form factors are poorly known. In particular, an imaginary component[4] in the form factor is required to achieve a phasing between the direct and semidirect terms that agrees with experiment, but its origin is not well understood. Section 3 below reviews an attempt to shed light on the real part of the form factor by employing a microscopic folding model which has proven successful

for calculating inelastic-scattering form factors as well as optical potentials. The importance of Coulomb excitation in calculating the form factors for proton capture is illustrated New insights into the imaginary component of the form factors are contained in the contribution of A Likar[5] to this meeting

Up to the present, DSD calculations have been limited to capture to bound final states, and consequently only the portion of the gamma spectrum between the incident nucleon energy and the endpoint (approximately 8 MeV higher) has been available for this model Consequently, the portion of the spectrum above the region where Hauser-Feshbach calculations apply (less than approximately 10-12 MeV) and below the region of bound final states has been calculated only with semiclassical pre-equilibrium models[6], or with multistep compound models that yield conflicting results[7,8] A recent extension of the DSD model to unbound final states[9] that significantly expands the region of applicability of this model is reviewed in Section 2 This extended model is also applicable to a portion of the bound final-state region where conventional DSD calculations are of limited usefulness because of fragmentation of the final single-particle orbitals among a dense background of complicated neighboring states.

Difficulties in applying the DSD model to certain transitions in heavy nuclei (particularly neutron and proton capture on ^{208}Pb) led to the development of a closely related model, the pure-resonance model (PRM). This model[10,11], which is an approximation to DSD, was developed in the course of an examination of the consistency of the DSD model. A current view of this model and recent results using it are presented in Section 4.

2. The Extended DSD Model for Capture to Unstable Final States

The direct-semidirect model has recently been extended to allow calculation of radiative capture to unstable final states Two types of unstable final states are included. 1) states in which the single-particle configuration following capture are unbound and may therefore decay into the continuum, and 2) single-particle states that are bound, but subsequently damp into the compound nucleus. In both cases, the correct treatment of the compound-nuclear damping is critical for the success of the model The model has been tested by performing an experiment on radiative capture of 19 6-MeV polarized protons on ^{89}Y, and is described in a paper recently submitted for publication[9].

The principal difference between the extended treatment and the standard DSD model is in the handling of the final state. In the standard DSD model, the final state of the captured particle is described by a bound-state wave function, usually obtained by solution of the Schrödinger equation for a Woods-Saxon well. In the extension of the model, all necessary information on the final state is determined by a complex (i.e., optical) potential, which is defined for both unbound and bound final-state single-particle configurations For unbound final states, the imaginary potential describes damping of the simple single-particle state following capture into the compound nucleus. Similarly, for bound final states, the imaginary potential represents the spreading of the single-particle configuration into a dense spectrum of complicated states in the neighborhood of the final-state energy

The extended model reduces to the standard DSD calculation in the limit of vanishing final-state imaginary potential.

In the extended model for capture to unbound final-state configurations, the double-differential inclusive cross section (i.e., in which only the outgoing gamma is measured) is

$$\frac{d\sigma}{dE_\gamma d\Omega_\gamma} = \sigma_1 + \sigma_2 \ , \tag{1}$$

in which the first term on the right-hand side is

$$\sigma_1 = -\frac{1}{\phi_{inc}}\frac{2}{\hbar}\left(\frac{1}{\hbar c}\right)^3 E_\gamma^2 \left\langle \overline{\Psi}_i^{(+)} \middle| H_\gamma G^{(+)\dagger} W G^{(+)} H_\gamma \middle| \overline{\Psi}_i^{(+)} \right\rangle, \tag{2}$$

and the second is

$$\sigma_2 = \frac{1}{\phi_{inc}}\frac{2\pi}{\hbar}\left(\frac{1}{\hbar c}\right)^3 E_\gamma^2 \sum_{\mathbf{p}} \left| \left\langle \tilde{\chi}_{\mathbf{p}}^{(-)} \middle| H_\gamma \middle| \overline{\Psi}_i^{(+)} \right\rangle \right|^2 \delta(E - E_p). \tag{3}$$

For bound final-state configurations, the corresponding expression is

$$\frac{d\sigma}{dE_\gamma d\Omega_\gamma} = -\frac{1}{\phi_{inc}}\frac{2}{\hbar}\left(\frac{1}{\hbar c}\right)^3 E_\gamma^2 \ \mathrm{Im}\left\langle \overline{\Psi}_i^{(+)} \middle| H_\gamma G^{(+)} H_\gamma \middle| \overline{\Psi}_i^{(+)} \right\rangle . \tag{4}$$

In these expressions, $\overline{\Psi}_i^{(+)}$ is the energy-averaged incident wave function at energy E_i, it is the optical-model wave function, plus resonant terms representing coupling to giant resonances that give rise to the semidirect amplitude. E_f and E_γ are the energies of the final nuclear state and gamma ray, respectively, while E is $E_i - E_\gamma$. H_γ is the electromagnetic operator ϕ_{inc} is the flux of incident particles. $G^{(+)}$ is a Green's function (with appropriate boundary conditions) for the interaction of the captured nucleon with the target via a complex optical potential. W is the imaginary part of the optical potential, defined for both continuum and bound final states, and $\tilde{\chi}_{\mathbf{p}}^{(-)}$ is an optical-model wave function for continuum final states For the unbound case, Eq. (3) is the straightforward extension of the conventional DSD calculation. The additional term, Eq. (2), represents damping of the final-state configuration following capture, and in fact is the dominant term[9]

Calculations using the extended DSD model are shown in Figs. 1 and 2 and are compared to the results of the ^{89}Y(p,γ) experiment with 19.6-MeV polarized protons. Direct E1, E2, and E3 radiation as well as semidirect E1 were included.

Fig. 1 shows the measured 90° differential cross section, together with the extended DSD calculations and with Hauser-Feshbach calculations using the GNASH code[12] of the equilibrium statistical emission using two different prescriptions for the gamma-ray transmission coefficient[13,14]. The peak at 15.11 MeV is due to inelastic scattering on a carbon impurity in the target. The combination of DSD and Hauser-Feshbach calculations reproduces the data reasonably well, and additional multistep reaction mechanisms are not required. The DSD calculation were made with Eqs. (2) and (3) in the unbound region below 19.6 MeV gamma energy, and with Eq. (4) in the bound-state region above that energy. There is no discontinuity between these two regions. The DSD calculations were

carried out to only 26 MeV, since the ground-state peak near 28 MeV is more appropriately treated by a conventional DSD calculation. The calculations show a transition between compound and direct processes in the region near 16 MeV.

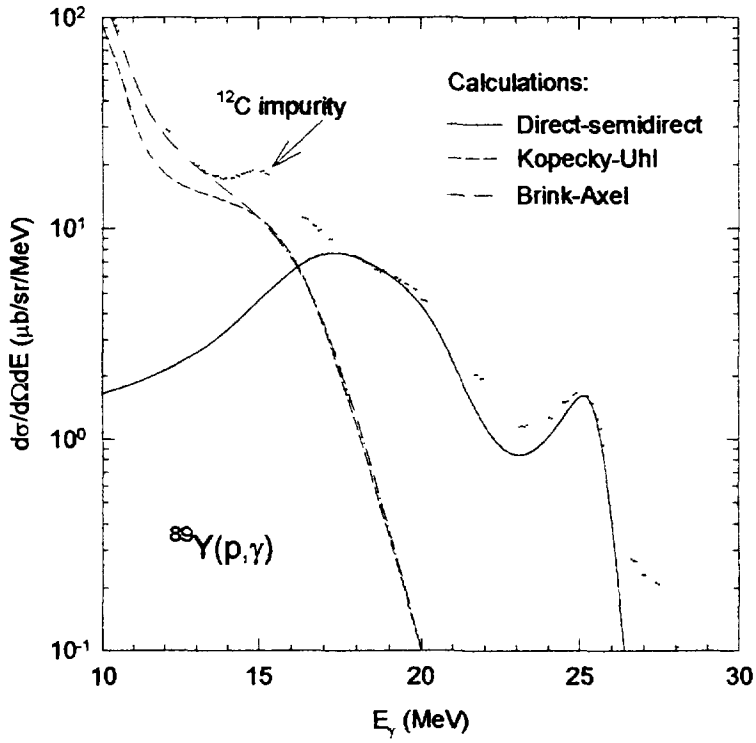

Figure 1 Unpolarized differential cross section at 90° The data (dots) are shown together with the extended DSD model calculation (solid line), and with Hauser-Feshbach calculations using Kopecky-Uhl (dashed line) and Brink-Axel (dot-dashed line) gamma transmission coefficients. The calculations were folded with experimentally determined lineshapes before presentation with the data.

In Fig 2 the extended DSD calculations are compared with the measured analyzing powers at the five angles for which data were taken. The data are well reproduced by the calculations, including the reversal in the sign of the asymmetries between the forward and backward hemispheres.

The calculations shown here suggest that multistep contributions may not be important at energies up to approximately 20 MeV. To further investigate this issue, the model is currently being applied to a set of gamma-production data taken with 34 MeV protons[15] If the higher-energy data show that multistep contributions are required, the extended model will be incorporated as the final step in a multistep-direct theory based on the FKK reaction theory[16]

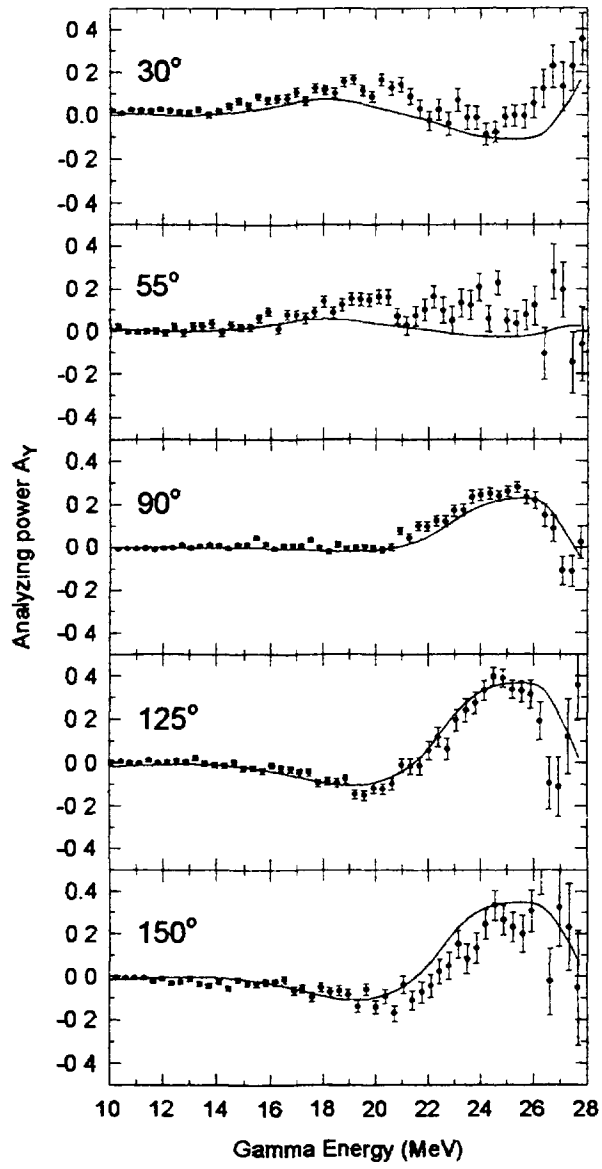

Figure 2. Measured analyzing powers compared with the extended DSD calculations. The calculations have been folded with the experimentally-determined lineshapes.

3. The Form Factor Used in Direct-Semidirect Calculations

As noted in the introduction, a correct description of the complex form factors for coupling to the giant resonances remains an important outstanding problem in the DSD model. There is an issue of consistency in the DSD model (noted below in Section 4) that may be best addressed through an improved treatment of the form factors The form factors are similar to those used in the DBWA description of nucleon inelastic scattering. However, radiative capture in the DSD picture contains an ingredient that is not present in inelastic scattering the direct-capture amplitude interferes with the semidirect amplitude, and this places additional demands on the form factor to assure the correct phasing. The imaginary component of the form factor, introduced phenomenologically[4], has been adjusted to fit experiments, but its origin is not well understood. A new approach to the imaginary form factor has been introduced elsewhere at this meeting[5] There is also a great deal of variation in the prescriptions used for the real part of the form factor. Most treatments of the real part are based on hydrodynamic models; however, a microscopic approach based on a particle-hole description of the giant resonances is also possible

This section reviews an early attempt[11] to calculate the real part of the form factor using a simple microscopic model for the giant dipole resonance. The shape of this form factor is significantly different from those obtained from hydrodynamic models The results are similar to those presented in another microscopic treatment by Shubin at this meeting[17] The contribution of Coulomb excitation to the form factor is easily calculated in a microscopic model, and the importance of this effect for proton capture is shown below.

The microscopic description of the form factor requires a description of the transition density for the giant resonance, which is convoluted with an effective interaction In the calculation shown in Fig. 3, the transition density for the giant dipole resonance in ^{208}Pb was obtained from the random phase approximation (RPA) form of the Brown-Bolsterli schematic model, and is shown in the lower part of the figure The effective interaction used to obtain the form factors shown in the upper part of the figure was taken from the isovector part of the microscopic optical potential of Jeukenne, Lejeune, and Mahaux[18] (JLM). This interaction is complex, and is energy and density dependent. Only the real part of the interaction was used, since the strong energy dependence of the imaginary part leads to an ambiguity in the calculation of the imaginary form factor (i.e , the energy at which the interaction should be evaluated for capture from the continuum to a bound state is ill defined). The strength of the JLM isovector interaction has been normalized upward by a factor of 2.5, which is in accord with the normalization required to reproduce the (p,n) reaction to isobaric analog states[19] For proton capture, the Coulomb excitation contribution was calculated by convoluting the transition density with an electromagnetic interaction of the form $1/r^2$

The resulting form factors for proton and neutron capture shown in Fig. 3 peak at significantly larger radii than those for hydrodynamic models. The curve labeled B-G is a typical volume-type hydrodynamic form factor using the isovector strength and geometry

of the Becchetti-Greenlees[20] optical potential The approximately 25% difference between the proton and neutron microscopic calculations is due almost entirely to the effect of Coulomb excitation. Coulomb excitation thus contributes significantly to the proton form factor, since the capture cross section near the peak of the giant resonance is nearly proportional to the square of the strength of the form factor. It should be noted that the microscopic form factor peaks at a larger radius than the transition density; this is a consequence of the density dependence of the effective interaction. It would be desirable to carry out a systematic comparison of DSD calculations with data using a microscopic form factor for the real part of the GDR coupling, supplemented by a phenomenological form for the imaginary part.

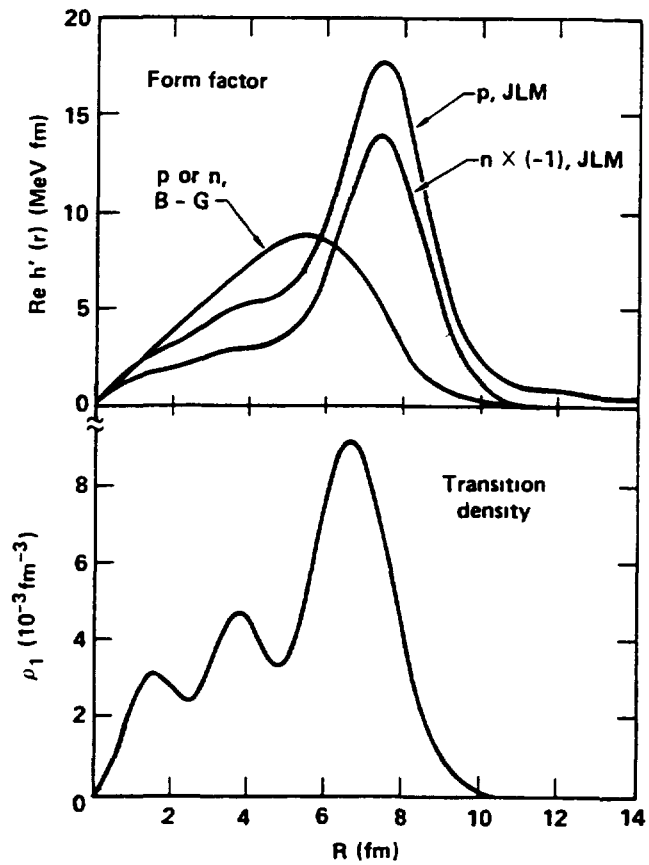

Figure 3. Folding-model calculation of the real part of the GDR form factor for ^{208}Pb, based on a schematic-model description of the transition density and the JLM effective interaction. The curve labeled B-G is a hydronamic form factor shown for comparison. The difference between proton and neutron microscopic form factors is due to Coulomb excitation.

4. The Pure-Resonance Model

The pure-resonance model[10,11] (PRM) was developed to address questions of consistency between the two terms in the direct-semidirect model It was based on the two observations that 1) in the photoejection reaction (which is inverse to radiative capture) experimental data show symmetric resonant peaks without an obvious nonresonant contribution; and that 2) the direct amplitude in DSD contains a giant-resonance contribution, since the incident optical-model wave function is not orthogonal to the giant resonance

The PRM results from reformulating the capture model so that the continuum wave function appearing in its matrix elements no longer contains giant-resonance components This is accomplished by using projection operator techniques as developed for the photonuclear problem by Wang and Shakin[21] Using these techniques, the direct-semidirect amplitude

$$c_1 + \frac{c_2}{E_\gamma - E_{GDR} + \frac{1}{2} i\Gamma_{GDR}} \tag{5}$$

may be formally rearranged (neglecting an unimportant small term) as

$$\frac{c_3 - c_4}{E_\gamma - E_{SP} + \frac{1}{2} i\Gamma_{SP}} + \frac{c_5}{E_\gamma - E_{GDR} + \frac{1}{2} i\Gamma_{GDR}} \tag{6}$$

in which c_1 through c_5 are matrix elements calculated with ordinary optical wave functions in the DSD case (Eq. (5)), or projected wave functions for the PRM (Eq. (6)) E_{SP} and Γ_{SP} are the position and width of a single-particle resonance in the entrance channel, and are computed from the optical potential. The single particle resonance lies in the region of approximately 8 to 10 MeV E_{GDR} and Γ_{GDR} are the position and width of the giant dipole resonance.

In Eq. (6), c_3 and c_4 are both large and nearly cancel. Thus, a potential instability that is implicit in the DSD model is exhibited explicitly in the PRM formulation. In the pure-resonance model this instability is eliminated by assuming that this cancellation is exact, leaving only the giant resonance term.

A recent experiment[22] on the ^{40}Ca(n,γ_0) reaction, which was performed to search for the isovector quadrupole giant resonance, shows the usefulness of the PRM. Fig 4 shows the data for this reaction, together with two calculations that included E1 and E2 radiation The right-hand panel shows the 90° differential cross section, while the left-hand shows the fore-aft asymmetry A(55°), defined as $[\sigma(55°)- \sigma(125°)]/[\sigma(55°)+\sigma(125°)]$, where σ is the differential cross section. The solid curves used DSD for both E1 and E2, whereas the dashed curves were calculated using PRM for E1 and DSD for E2

In the case shown in Fig. 4, it is apparent that the PRM yields a better reproduction of the experiment than the DSD. However, it should be noted that the approximation of neglecting the first term in Eq (6) may be extreme, and that this approximation may not be necessary if the consistency between the direct and semidirect terms in the DSD model is better understood than at present. Further work should be done in this direction.

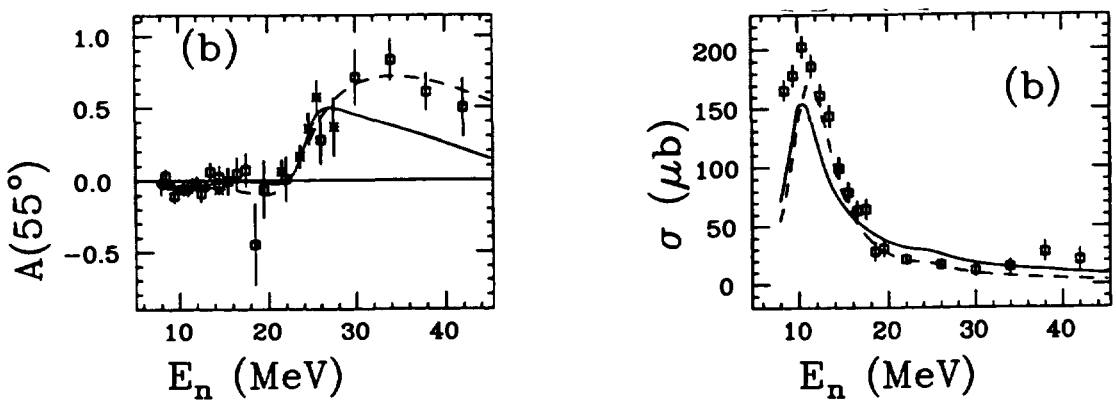

Figure 4 Fore-aft asymmetry (left panel) and 90° differential cross section (right panel) in the $^{40}Ca(n,\gamma_0)$ reaction[22]. Calculations were made with DSD for E1 and E2 amplitudes (solid curves), and with PRM for E1 and DSD for E2 (dashed curves).

5. Acknowledgment

The work required for the preparation of this review was supported by the Lawrence Livermore National Laboratory under United States Department of Energy contract W-7405-ENG-48.

6. References

1 G. E. Brown, Nucl Phys. **57**, 339 (1964).
2. C F. Clement, A. M. Lane, and J. R. Rook, Nucl. Phys. **66**, 273,293 (1965).
3. G. R. Satchler, Nucl. Phys. **A195**, 1 (1972).
4. M. Potokar, Phys. Lett. **46B**, 346 (1973).
5 A. Likar, contribution to this meeting.
6. E. Betak, contribution to this meeting and references therein
7 P. Oblozinsky and M. Chadwick, Phys. Rev. **C42**, 1652 (1990).
8. M. Herman, A. Höring, and G. Reffo, Phys Rev. **C46**, 2493 (1992)
9. W. E. Parker *et al.*, submitted to Physical Review **C**
10. F. S. Dietrich and A. K. Kerman, Phys. Rev. Lett. **43**, 114 (1979).
11. F. S. Dietrich, in AIP Conference Proceedings No. 125, Capture Gamma-Ray Spectroscopy, Knoxville, TN, 1984, p. 445.
12. P. G. Young, E. D. Arthur, and M. B. Chadwick, Los Alamos National Laboratory Report LA-12343-MS (1992).

13 D M. Brink, Ph D. thesis, Oxford University (1955); P Axel, Phys Rev **126**, 671 (1962)
14 J. Kopecky and M. Uhl, Phys. Rev **C41**, 1941 (1990).
15 S J. Luke, Ph.D. thesis, University of Washington, 1992.
16 H Feshbach, A. K. Kerman, and S Koonin, Ann. Phys. (New York) **125**, 429 (1980)
17. Yu Shubin, contribution to this meeting.
18 J P. Jeukenne, A. Lejeune, and C Mahaux, Phys. Rev. **C16**, 80 (1977), and references therein.
19. F S Dietrich and F. Petrovich, in AIP Conference Proceedings No 124, Neutron-Nucleus Collisions -- A Probe of Nuclear Structure, Burr Oak State Park, Ohio, 1984, p 90
20. F. D Becchetti and G. W Greenlees, Phys. Rev. **182**, 1190 (1969).
21 W L. Wang and C M Shakin, Phys Rev **C5**, 1898 (1972)
22. C M. Laymon, R O. Nelson, S. A. Wender, and L. R Nilsson, Phys. Rev. **C46**, 1880 (1992)

Nuclear Dicke States in the Direct-Semidirect Model

A. Likar
Institute J.Stefan and Department of Physics
University of Ljubljana, Ljubljana, Slovenia

Abstract

The structure of the doorway state assumed in the direct-semidirect (DSD) model was addressed by Sokolov and Zelevinsky. Modification of the model due to nuclear Dicke states in presence of two open channels has been done. The results of calculations for capture to the single particle states in Pb are presented.

1 Introduction

Sokolov and Zelevinsky [6] discovered a new type of collectivity in the regime of strongly overlapping compound states interacting with open decay channels. They showed that a Dicke type state may be formed if a complex system interacts with one open decay channel: a specific state is formed with large decay width, all other states remain quasi-stationary with negligible decay widths.

In the DSD model the giant resonance state is considered as collective state which exhaust most of the dipole sum rule and, as well, is strongly coupled to the neutron channel. The giant resonance was therefore considered to be also the Dicke state. This may not be generally the case. In the modified DSD model the form factor and semi-direct part of transition amplitude must be changed in order to adequately represent the giant dipole resonance. The modified model requires new parameter, measuring the overlap between giant resonance state and nuclear Dicke state. We firstly give short description of the DSD model and sketch derivation of the form factor for inelastic scattering of nucleon to the bound state. Then we propose the modification of the model due to Dicke states and show that modified model better reproduces the measured cross sections in heavy nuclei.

2 The DSD model

The T matrix for nucleon radiative capture in the first order perturbation theory is:

$$T = \langle 0|H_\gamma|\psi^+\rangle\,, \tag{2.1}$$

where $|0\rangle$ is ground state of the target nucleus with captured nucleon in a single particle state and $|\psi^+\rangle$ is exact continuum state with incoming nucleon. The electromagnetic interaction is denoted with H_γ. The time independent state $|\psi^+\rangle$ is solution of Schrödinger equation:

$$(E - H)|\psi^+\rangle = 0\,, \tag{2.2}$$

The nuclear Hamiltonian is H and the energy of the nucleus plus incoming nucleon is E.

In the Feshbach's [7] projection-operator formalism the state $|\psi^+\rangle$ is divided in elastic channel state (P), doorway state (D) and the rest of the states (Q):

$$|\psi^+\rangle = (P + D + Q)|\psi^+\rangle, \tag{2.3}$$

The projection operators P,D, and Q satisfy relations: $P + D + Q = 1$ and $P^2 = P, D^2 = D, Q^2 = Q$. The projection operators P, D and Q also modify the Hamiltonians and for DHQ we write H_{DQ}.

The transition matrix T in the DSD model is:

$$T_{DSD} = \langle 0|H_\gamma|\psi_0^+\rangle + \langle 0|H_\gamma \frac{1}{E - E_R + i\Gamma_R/2} H_{DP}|\psi_0^+\rangle, \tag{2.4}$$

The first term is called direct term and the second semi-direct one. The excitation of giant dipole state from the elastic channel is governed by the operator H_{DP}.

The form factor for inelastic transition of nucleon to a bound state is defined as:

$$\langle \psi_{n,l,j}(r_0)\{\langle 0_t|(H_\gamma H_{DP}|0_t\rangle\}\psi_0^+(r_0)\rangle = \langle \psi_{n,l,j}(r_0)\{H'(r_0)\}|\psi_0^+(r_0)\rangle. \tag{2.5}$$

The form factor was derived [2, 8] from the isospin dependent component of the short range two-body force which is responsible for excitation of giant multipole state in the target nucleus. The Hamiltonian H_{DP} is therefore supposed to be:

$$V' = \sum_i V_\tau \delta(\mathbf{r_i} - \mathbf{r})\tau \cdot \tau_\mathbf{i}. \tag{2.6}$$

The multipole expansion of τ_3 term of V' is:

$$V' = V_\tau \sum_i \tau_{03}\tau_{i3} \frac{\delta(r_i - r_0)}{r_0^2} \sum_{l\mu} Y_{l\mu}(\hat{\mathbf{r}}_i) Y^*_{l\mu}(\hat{\mathbf{r}}_0). \tag{2.7}$$

The form factor H' could be calculated if we evaluate the matrix element:

$$\langle\phi_D|V'|0_t\rangle = -2V_\tau\tau_{03}Y^*_{l\mu}(\hat{\mathrm{r}}_0)h'(r_0)\langle\phi_D|H_\gamma|0_t\rangle. \tag{2.8}$$

The multipole expansion of V' together with the equation 2.8 gives the normalization condition [8] [2] for h':

$$\int r^3h'dr = 1. \tag{2.9}$$

The same normalization should be applied if $h'(r_0)$ is complex. Imaginary component may be in principle present even in free form factor, related to isospin dependent part of imaginary optical potential. For known radial dependence of h' the free form factor follows using this condition and the dipole sum rule for the square of the matrix element $\langle\phi_D|H_\gamma|0_t\rangle$. In [8] two radial dependences of $h_r(r_0)$ are reported and since then widely used in nucleon capture calculations. Older is surface shaped [1]

$$H' = -\tau_{03}\frac{2NZ}{A^2}\frac{\hbar^2}{2mE_R}\frac{V_1}{4}(-\frac{df(r_0)}{dr_0})Y^*_{1\mu}(\hat{\mathrm{r}}_0) \tag{2.10}$$

and volume shaped one, more frequently used [2]:

$$H' = -\tau_{03}\frac{2NZ}{A^2}\frac{\hbar^2}{2mE_R}\frac{V_1}{4}(\frac{5}{R^2}r_0f(r_0))Y^*_{1\mu}(\hat{\mathrm{r}}_0) \tag{2.11}$$

In our calculations we have used the volume shaped form factor with parameter $V_1 = 135MeV$.

The form factor for heavy nuclei has large imaginary component, which is surface peaked and of the order of the real one [4]. The parameter W_1 in the complex form factor, parametrized as $\propto V_1r_0f(r_0) - iW_1r_0df(r_0)/dr_0$ is for heavy nuclei of the order of 100 MeV. Possible source of the imaginary part of the form factor is discussed in [5]

3 Nuclear Dicke state

The giant dipole state play the role of a doorway state, which is strongly coupled to the continuum channel and at the same time not strongly coupled to the complicated states. The giant dipole state is supposed to exhaust the whole dipole sum rule and at the same time the only state the nucleon can excite in early stage of the scattering process. Sokolov and Zelevinsky pointed out that the state which is strongly coupled to the nucleon channel may be different from the state which collects all dipole strength. There are generally two types of collectivity. Internal collectivity forms the giant dipole

resonance absorbing the total dipole strength but is stationary, without any coupling to the continuum. This coupling is introduced by introducing a decay width to the state. Open channels, however, force another collectivization of the nuclear intrinsic excitations (1p-1h excitations to be specific). The so called nuclear Dicke state collects the decay widths from intrinsic excitations leaving them almost stationary. The Dicke state itself decays rapidly to an open channel and is therefore the only state which is coupled to the continuum. The giant dipole resonance and specific Dicke state may not be the same states. In an extreme case the giant dipole state may be totally de-coupled from the continuum. The more realistic possibility where giant dipole state is partially de-coupled from the continuum will be studied in the following.

Following [6] we consider N intrinsic 1p-1h states with the same energy ϵ and decay widths w due to access to decay channels. Let us for a moment have only one nuclear decay channel, that of the incoming nucleon. If the decay channel is closed, the residual interaction governing the system is in the simples case taken to be factorizable, [9]:

$$H_{mn} = \epsilon\delta_{mn} + \lambda d_m d_n. \tag{3.12}$$

The moments d_m are matrix elements $d_m = \langle m|d|0\rangle$. It is well known that Hamiltonian 3.12 leads to the so called intrinsic collectivization: one state is shifted to higher energies with all the dipole strengths, other states are not shifted and with no dipole strength. In presence of open decay channel, the Hamiltonian 3.12 should be changed to an effective one. We still work in the system of N intrinsic states without explicit channel variables. The effective Hamiltonian accounts for finite decay amplitudes $\mathbf{A}_n$ of intrinsic states:

$$H_{eff} = H_{mn} - \frac{i}{2}A_m A_n. \tag{3.13}$$

For the system which is invariant to time-reversal, the amplitudes d_m and A_m could be chosen as real numbers. Here separability is not a suitable approximation but necessity, following from unitary condition of the S matrix:

$$S(E) = 1 - i\sum_{mn} A_m^* \mathcal{G}_{mn}(E) A_n. \tag{3.14}$$

The effective propagator $\mathcal{G}(E)$ is given by:

$$\mathcal{G}(E) = \frac{1}{E - \mathcal{H}}. \tag{3.15}$$

The separable imaginary part of the effective Hamiltonian then forces collectivization of widths, where one state collects all the decay widths of the intrinsic states therefore de-coupling them from the decay channel. The state only coupled to the decay channel in

called nuclear Dicke state. Generally for each decay channel there exists specific nuclear Dicke state.

In nucleon capture process let us assume only two open channels, gamma and nucleon. The effective Hamiltonian for this case is:

$$H_{eff} = H_{mn} - \frac{i}{2}(A^p_m A^p_n + A^\gamma_m A^\gamma_n). \tag{3.16}$$

The decay amplitudes for γ channel are denoted with A^γ_m and for nucleon channel by A^p_m. The amplitudes to the γ channel are proportional to the dipole matrix elements:

$$A^\gamma_m = \sqrt{\alpha} d_m.$$

The shift of the giant dipole state from the unperturbed energy ϵ is in this notation:

$$E_R = \epsilon + \lambda \mathbf{d}^2 \tag{3.17}$$

where $\mathbf{d}^2$ stands for the sum $\sum_n d_n^2$ so the vector $\mathbf{d}$ is defined as:

$$\mathbf{d} = \{d_n\}.$$

The total width w acquired by the Dicke state is:

$$w = \mathbf{A}^2 \tag{3.18}$$

where we introduced another vector $\mathbf{A}$ similarly as $\mathbf{d}$:

$$\mathbf{A} = \{A_n\}.$$

The transition matrix T^{ba} for reaction $b \to a$ could be calculated most directly from $\hat{K}$ matrix $\hat{K} = \mathbf{A}^+ \mathbf{G}(\mathcal{E})\mathbf{A}$ using:

$$T^{ba} = \frac{\hat{K}}{1 + \frac{i}{2}\hat{K}} \tag{3.19}$$

The propagator $G(\mathcal{E})$ for closed system is used in definitions above:

$$G(\mathcal{E}) = \frac{1}{\mathcal{E} - H}.$$

Explicit calculation of transition matrix is straightforward but somewhat lengthy. The result for (n, γ) reaction depends on angle ϑ between the vectors $\mathbf{A}$ and $\mathbf{d}$:

$$T^{n\gamma} = \frac{\sqrt{\alpha \mathbf{d}^2 w}\cos\vartheta}{E - E_R - \frac{\alpha \mathbf{d}^2 w \sin^2\vartheta}{2(E-\epsilon)} + \frac{i}{2}[w + 2\alpha\mathbf{d}^2 - \frac{\lambda \mathbf{d}^2 w \sin^2\vartheta}{(E-\epsilon)}]}. \tag{3.20}$$

In parallel case $\vartheta = 0$ we get familiar expression for semi-direct part of the reaction. The total width of the doorway state is sum of particle width w and γ width $\alpha \mathbf{d}^2$. The decay width $\Gamma^{\downarrow}$ to more complicated states of the nucleus is in this simple model neglected. The coupling to the nucleon channel is in the DSD model given by the matrix element $\langle \phi_D | H_{DP} | \psi_0^+ \rangle$ and in 3.20 with $\sqrt{w}$. The coupling to the photon channel is in the DSD model obtained from $\langle 0 | H_\gamma | \phi_D \rangle$ and in 3.20 from $\sqrt{\alpha \mathbf{d}^2}$. The increasing angle ϑ therefore decrease the strength of the form factor and in this way de-couples the giant resonance from the continuum.

When vectors $\mathbf{d}$ and $\mathbf{A}$ are not parallel the resonance energy is slightly shifted to higher energies. The shift could be neglected if we are few MeV from unperturbed energy ϵ. The width of the resonance is diminished and is slightly energy dependent being smaller below the resonance energy E_R.

4 Discussion

The different free form factors proposed in 2.10,2.11 are not equally successful in reproducing the experimental data. There is general opinion that surface peaked form factor 2.10 does not properly account for actual process of excitation of giant dipole state. Close look at the derivation of both free form factors suggests another interpretation. The derivations are equivalent, the difference arises only in different forms of operator a^+ for creation of giant dipole state from the ground state. In one case the form of a^+ is proportional to $rY_{1\mu}(\hat{r})$ and in other $\epsilon \nabla$. For excitation of linear harmonic oscillator in the ground state both operators lead to the same state, the first excited state. The same state is reached with creation operator $a^+ \propto (x - x_0 d/dx)$. This suggests alternative form factor as a combination of volume and surface ones and indeed such form factor was suggested in [3] The difference in results may also be probably due to improper optical model used to generate the initial wave functions since the effect of D component of the initial wave function should be excluded from the optical model potential. Such an elimination is not done in the DSD model calculations.

In the calculation of cross sections with nuclear Dicke state one should include the $\Gamma^{\downarrow}$ component of resonance decay width. We supposed in the calculation that entire width is $\Gamma^{\uparrow}$ component and therefore neglect the coupling of the resonance with more complicated states (Q) of the nucleus. Some estimates suggest that as much as 70% of the resonance decay width is $\Gamma^{\downarrow}$ component. If such estimates are correct, the effect of nuclear Dicke state is overestimated in our calculation. It is clear that angles ϑ close to $\pi/2$ are excluded by experimental (n,γ) data compared with our calculations. The effect of nuclear Dicke state may be, however, important at energies $E \approx \epsilon$, at the lower energy tail of the

resonance. The effect of this changes for neutron capture in ^{208}Pb is shown on Figs.1 and 2. We see that moderate angle $\vartheta \approx 30°$ improves the fit to the data.

5 Conclusion

The collectivization of widths of the intrinsic states cause the width of the giant resonance state in the energy denominator may also be energy dependent being narrower at lower energies. Analysis of the cross section for capture to the single particle states in ^{208}Pb show, however, that the angle ϑ may not be too far from 0° even if the decay width $\Gamma^{\downarrow}$ is neglected.

References

[1] C. F. Clement, A. M. Lane, and J. A. Rook, Nucl. Phys. **66**, 273, 293 (1965)

[2] G. Longo, S. Saporetti, Phys. Let. **42B**, 17 (1972); Nucl. Phys. **A199**, 530 (1972)

[3] J. Zimanyi, I. Halpern, V. A. Madsen, Phys. Lett. **33B**, 205 (1970)

[4] M. Potokar, Phys. Lett. **46B**, 346 (1973)

[5] A. Likar, contribution to the NEANSC Meeting on Measurement, Calculation and Evaluation of Photon production Data, Bologna, 9.-11. nov. 1994

[6] V. V. Sokolov and V. G. Zelevinsky, Fizika **22**, 303 (1990)

[7] H. Feshbach, Theoretical Nuclear Physics, Nuclear Reactions, J. Wiley, 1992

[8] C. F. Clement, S. M. Perez, Nucl. Phys. **A165**, 569 (1971)

[9] G. E. Brown and M. Bolsterli, Phys. Rev. Lett. **3**, 472 (1959)

[10] I. Bergqvist, D. M. Drake and D. K. McDaniels, Nucl. Phys. **A198** 641 (1972)

[11] L. Rosen, J. G. Beery, A. M. Goldhaber, E. M. Auerbach, Ann. of Phys. **34**, 96 (1965).

Figure captions

Fig.1 The effect of angle $\vartheta = 30°$ on neutron capture cross section (dotted line) to the single particle state $2g_{9/2}$. The solid line denotes DSD calculation with $\vartheta = 0°$. The decay width $\Gamma^{\downarrow}$ to complicated states is neglected in the calculation. Optical potential from [11] was used, the experimental points are from [10].

Fig.2 The same as on Fig.1 but for capture to the $1i_{11/2}$ state.

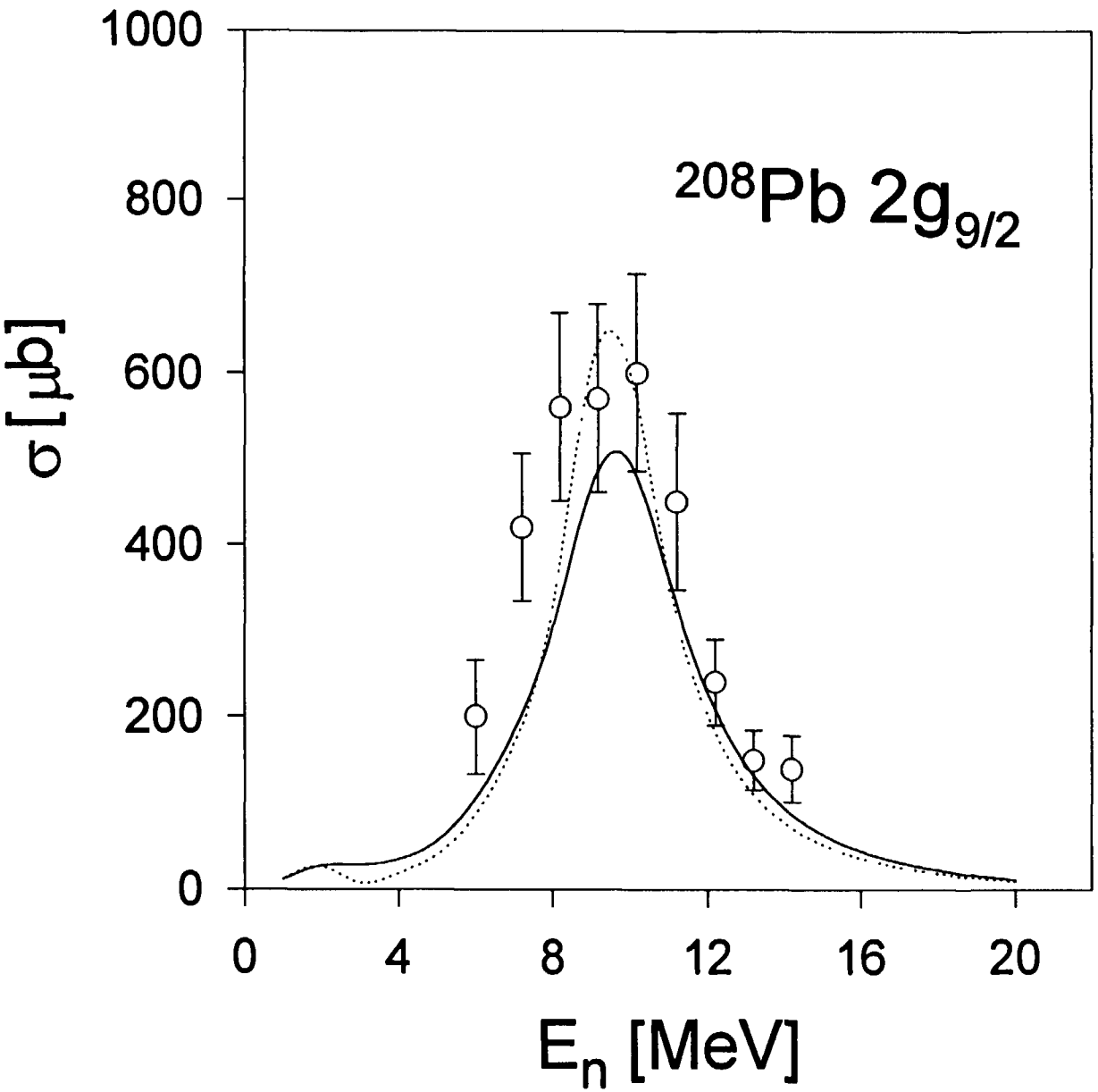
1000
800
600
400
200
0
σ [μb]
^{208}Pb 2g$_{9/2}$
0
4
8
12
16
20
E$_n$ [MeV]

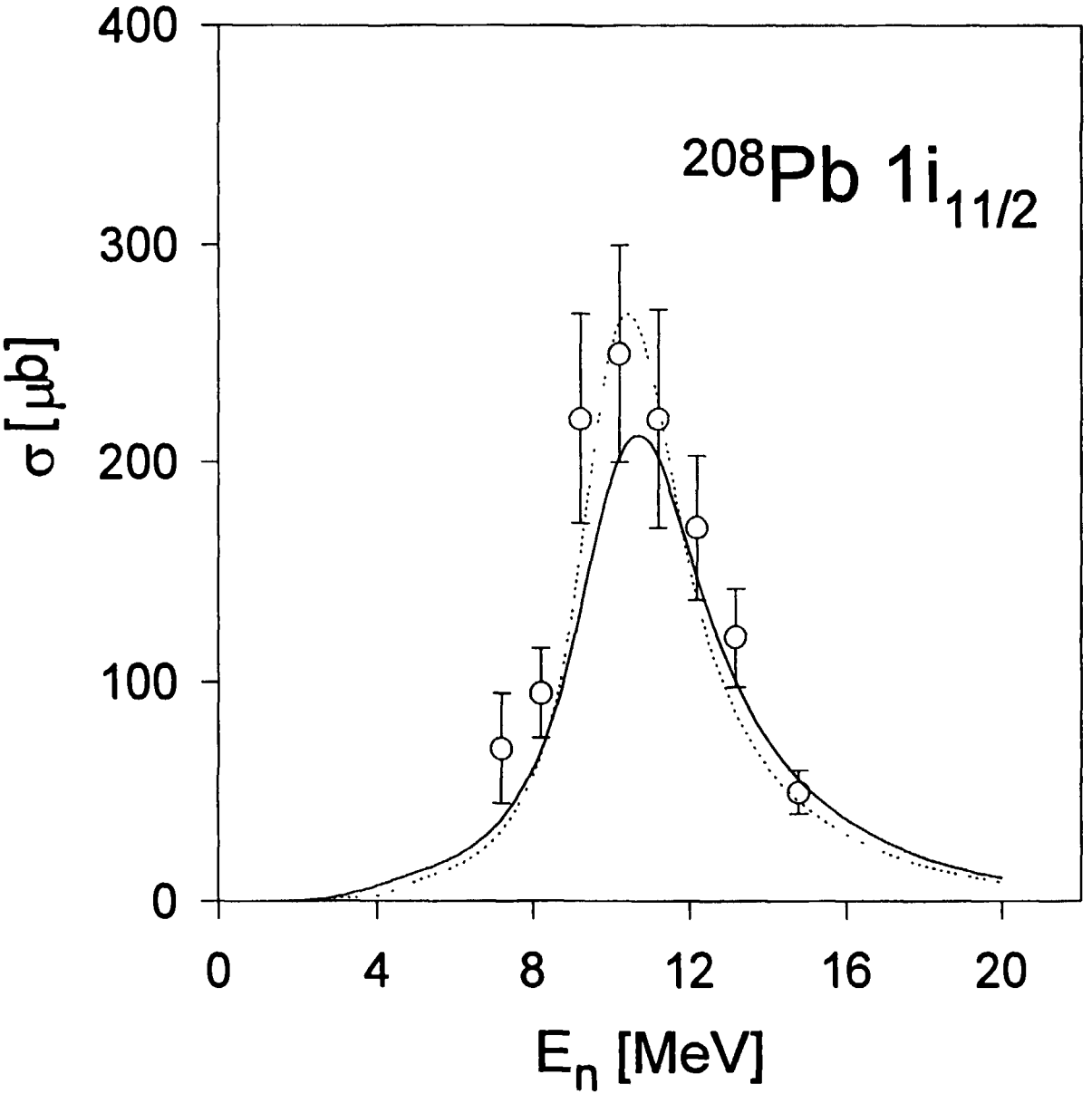
400
300
200
100
0
σ [μb]
^{208}Pb 1i$_{11/2}$
0
4
8
12
16
20
E_n [MeV]

THE EFFECT OF COLLECTIVE EXCITATIONS ON THE FORMATION OF PREEQUILIBRIUM GAMMA RAY SPECTRA FOR THE RADIATIVE NEUTRON CAPTURE REACTION

A.I. DITYUK, Yu.N. SHUBIN, G.Ya. TERTYCHNY
Institute of Physics and Power Engineering
Obninsk, 249020, Russia

ABSTRACT

The high-energy gamma ray emission from fast neutron capture on 208-Pb has been analysed in the frame of direct-semidirect (D-SD) mechanism using the realistic parameters for Giant Dipole Resonance, collective form factors and effective isovector interaction. It is shown that collective D-SD process based on particle-vibrational nature of entrance channel plays significant role in primary gamma ray emission, but this mechanism enables to explain not more than one half of observed cross section. This result corrects the early D-SD calculations of Longo and Saporetti which assumed the predominance of this process in high-energy gamma emission. On the other hand our results differ essentially from recent calculations of Herman et al., which manifest the negligible role of SD process as compared with MSC one. The main reason of these differences is that in latter calculations entrance neutron channel was considered as a noncollective one.

1. Introduction

Cross section for production of high energy gamma rays resulting from fast neutron capture is small as compared with total cross section for (n,γ) reaction but it is of great importance for many applications. During last decade multistep compound reaction theories[1-2] were used to develop various quantum mechanical models for description of high energy gamma ray production[3-6]. However the results obtained in the frame of new models do not give better description of cross sections and spectra in comparison with more phenomenological exciton model[7]. Moreover the results differ in conclusions relatively the role of various mechanisms in preequilibrium gamma spectrum formation. In paper[3] the conclusion has been made that multistep direct process contribution to 14 MeV neutron capture is 50-80%. On the other hand the calculations performed for the same nuclei in paper[5] lead to opposite results: the contribution of this mechanism is small, not more than 10%. The results of these papers contradict both each other and many calculations on the base of direct-semidirect mechanism which describe total cross sections, excitation functions and gamma spectra with the accuracy ≈90% for some light, medium weight and heavy nuclei[10-13].We consider it important to have conclusion about real contribution of direct-semidirect mechanism to (n,γ) reaction cross section. The aim of the present work is to estimate absolute contribution of combined direct (D) and collective SD processes to the observed gamma spectra. In our calculations for Pb we used the realistic parameters for GDR, effective nucleon-nucleon interaction and radial form factors that are consistent with experiment and recent nuclear structure calculations

In our opinion this is the first necessary step to develop the combined SD-MSC model that would be free of arbitrary choice of the main input parameters.

2. Collective semidirect mechanism of radiative neutron capture

Soon after the appearance of the fast nucleon capture experiments it became apparent that statistical evaporation and direct single-particle models fail to reproduce the observed cross sections and specific form of high-energy tail of γ ray emission spectra For the first time in Brown's paper [8] it has been noticed that because of γ ray energies in this case cover the energy location of GDR observed in photonuclear reactions then the two- step collective process of excitation and deexcitation of GDR in target nucleus must dominate in primary γ rays production. The simple evaluation for (p,γ) reaction on Pb and Ge confirmed the validity of this hypothesis. This paper followed by papers of Clement, Lane, and Rook [9] for the long time became the keystone for the following experimental and theoretical studies of fast neutron radiative capture [10-13].

Let us to dwell on the main points of this model. Due to well-known dominance of electric dipole mode in full operator of electromagnetic transitions the matrix element determining the combine D-SD radiative capture can be represented as follows

$$M_{i\Rightarrow f} = \langle \Psi_f | H_\gamma | \Psi_i \rangle + \frac{\langle \Psi_f | H_\gamma | \Psi_d \rangle \cdot \langle \Psi_d | F | \Psi_i \rangle}{E_\gamma - E_1 + \frac{i}{2}\Gamma_1} \qquad (1)$$

where Ψ_i, Ψ_f are the wave functions (w.f.) corresponding to initial (continuum) and final (bound) states of captured neutron. $\Psi_d = \Psi_f * \Psi_1$ is the w.f. of quasibound doorway state built as direct product of final neutron state and GDR which has the mean energy E_1 and total width Γ_1 , $E_\gamma = E_i - E_f$ is the energy of emitted γ rays. The operator of E1 transition has usual form

$$H_\gamma = \frac{e}{2}\sum_{\mu i}(1-\tau_{3i})r_i Y_{1\mu}(\Omega_i)$$
$$\tau_{3n} = 1, \quad \tau_{3p} = -1 \qquad (2)$$

If the matrix element (1) is known then radiative capture cross section is determined as follows

$$\sigma_{i\Rightarrow f}(E_i, E_\gamma) = \frac{\pi}{k_i^2}\sum_{(i)}\left|M_{(i)\Rightarrow f}\right|^2 \qquad (3)$$

where summation is performed over all partial continuum waves permitted by parity and momentum conservation $\pi_i = \pi_f (-1)^l$, $|j_f - 1| \le j_i \le j_f + 1$. The main contribution to cross section arises from SD-part which can be represented in compact Breit-Wigner form

$$\sigma^{SD}_{i\Rightarrow f}(E_i, E_\gamma) = \frac{\pi}{k_i^2}\sum_{(i)}\frac{\Gamma_{in}\Gamma_\gamma}{(E_\gamma - E_1)^2 + \frac{1}{4}\Gamma_1^2}, \qquad (4)$$

In the frame of collective SD model the integral characteristics of GDR are used, therefore it is convenient to use collective E1 coordinate $\alpha_{1\mu}$ to generate the GDR w.f.

$$\alpha_{1\mu} = \sum_k \tau_{3k} r_i Y_{1\mu}(\Omega_k), \ |\Psi_{1\mu}\rangle = \frac{\alpha_{1\mu}|0\rangle}{\langle 0|\alpha^+\alpha|0\rangle^{1/2}} \tag{5}$$

and to normalise it on bremsstrahlung sum rule [14]:

$$\sigma_{-1} = \int (\sigma_{\gamma,tot} / E)dE = \frac{16\pi^3 e^2 NZ}{3\hbar c A^2}\langle 0|\alpha^+\alpha|0\rangle \cong \beta A^{4/3}(mb),$$
$$\beta=(0.145 \div 0.200) \tag{6}$$

Since GDR is isovector excitation mode the effective interaction between captured neutron and doorway state is isovector operator. In r-local approximation it is determined[10-13] as follows

$$F_{ik} = \frac{V_1}{4\rho_0}\tau_{3i}\tau_{3k}\delta(r_i - r_k) \tag{7}$$

where $\rho(r)$ is the ground state density of nucleus, $\rho_0 = \rho(r=0)$. Simple calculations using (5), (7) and expansion of δ-function in spherical harmonics result in following representation for particle-vibrational matrix element that determines partial width Γ_m.

$$\langle \Psi_d|F|\Psi_i\rangle = \int d^3 r_i \Psi_f^*(r_i)H(r_i)\Psi_i(r_i)$$
$$H(r_i) = \sum_\mu \frac{V_1}{4\rho_0}\langle 0|\alpha^+\alpha|0\rangle^{1/2}\tau_{3i}Y_{1\mu}^*(\Omega_i)h(r_i) \tag{8}$$

In practice either surface or volume radial form factors are used [10-13]

$$h_s(r) = -\frac{4\pi}{3A}\frac{d\rho(r)}{dr}$$
$$h_v(r) = \frac{4\pi}{A\langle r^2\rangle}r\rho(r), \ \int r^3 h_{s(v)}(r)dr = 1 \tag{9}$$

These form factors correspond to GDR transition densities from the earliest hydrodynamic description of GDR given by Goldhaber and Teller (ρ^{GT}, h_s) and Jensen and Steinwedel (ρ^{JS}, h_v). The following investigations of Myers and Swiatecky [15] within the refined hydrodinamic model showed an appreciable mixing of both dipole modes For light nuclei GT mode dominates, whereas for heavy ones they are comparable. This conclusion agrees results obtained in the frame of self-consistent theory of finite Fermi systems [16] and can be a base for more realistic parameterization of collective form factors.

The strength V_1 (7) is the next important parameter determining the width Γ_m. It is worthy to identify F_{ik} (7) with isovector effective interaction that is used in microscopic calculations of GDR and other isovector multipole giant resonances in nuclei [17]. This

Landau-Migdal interaction is r-local also but in addition it is density-dependent to account for the finite size of nuclei:

$$F_{ik}^{LM} = C_0 f'(\rho(r))\tau_{3i}\tau_{3k}\delta(r_i - r_k)$$

$$f'(\rho(r) = f'_{ex} + (f'_{in} - f'_{ex})\rho(r) / \rho_0$$

$$\rho(r) = \sum_i^A \frac{2j_i + 1}{4\pi}\left(\Psi_i(r)\right)^2,$$

$$f'_{ex} = 2.300, \quad f'_{in} = 0.76, \quad C_0 = 300\text{MeV Fm}^3 \qquad (10)$$

It is this interaction we used in our numerical calculations for ^{208}Pb but in order to compare obtained results with ones of Longo, and Saporetti [12,13] one have to average F_{ik}^{LM}. There is some ambiguity of this procedure because of the final results are dependent on shape of form factor (9) used in calculations of Γ_m. If form factor $h_v(r)$ is used then it is more appropriate to use the following average procedure

$$\langle f'(\rho(r)) = \frac{4\pi}{A}\int \rho(r) f'(\rho(r)) r^2 dr \qquad (11)$$

Using the realistic parameters for Saxon-Woods potential [17] and formulas (7,10,11) the following evaluation can be obtained:

$$\rho_0 \cong 0.167\text{Fm}^{-3}, \quad \langle f'(\rho(r))\rangle \cong 1.35, \quad V_1 \cong 270\text{MeV} \qquad (12)$$

All main details of calculations has been discussed, so we summarise the final expressions for the widths:

$$\Gamma_{in} = \frac{1}{8\pi}\left(\frac{V_1}{\rho_0}\right)^2 \frac{Mk_1}{\hbar^2}\langle\alpha^+\alpha\rangle\left|\int r^2 dr \Psi_f^*(r) h(r) \Psi_i(r)\right|^2 *$$

$$S_f(2j_f + 1)(2j_i + 1)\langle j_f \frac{1}{2} j_i - \frac{1}{2}|10\rangle^2,$$

$$\Gamma_\gamma = \frac{4\pi}{9} e^2 \left(\frac{E_\gamma}{\hbar c}\right)^3 \langle\alpha^+\alpha\rangle \qquad (13)$$

where S_f is the spectroscopic factor for the final state [12]. In numerical calculations we take into account direct capture and D-SD interference in total cross section also. It is worthy to note, while the contribution of D-capture rather small, $\sigma^D \approx 0.01\sigma^{tot}$, it is important to take into account D-SD interference because of $\sigma^{D\text{-}SD} \approx 0\ 1\ \sigma^{tot}$.

3. Analysis of the ^{208}Pb(n,γ) reaction

We have chosen the nucleus Pb because there are most complete experimental information on the total (n,γ) reaction cross section energy dependence, excitation functions for residual levels of ^{209}Pb and γ-ray spectra [13]. Besides that this reaction has been investigated in detail in the frame of D-SD approach in papers [12,13], and the results obtained are the subject for our analysis. As in papers [12,13] single particle neutron levels

are defined from Schroedinger equation solution using Saxon-Woods potential. The parameters for Saxon-Woods potential were obtained so as to describe binding energies for these levels that are known from the experimental data. The geometrical parameters were taken the same. Optical model parameters were used from Becchetti-Greenlis systematics. It should be noted that the choice of other parameters can result in (10-20) % changes for the cross sections. In our calculations more realistic spectroscopic factors S_f for the "single particle" neutron states in ^{209}Pb were used as compared with [12,13]. They were taken from experiment [18] This resulted in reduction of the total cross section by ≈ 10%.

In comparison with the papers [12,13] we used also more realistic values for the energy of E1-resonance, E_1 = 13.43MeV, and for its width, Γ_1 = 4.07MeV [14], instead of 13.0MeV and 3.5MeV, correspondingly [12,13]. Because of strong dependence of cross sections on these parameters (see formula (4)) the cross sections calculated are 1.4 times less on condition that other parameters are the same. The results depend strongly also on the normalisation of collective dipole operator to inverse sum rule σ_{-1} (see relation (6)). This value enters into the definition of Γ_{in} and Γ_γ, and, consequently, the cross section appears to be quadratic function of this parameter. We used in our calculations the experimental value σ_{-1} = 229 mb [14]. This value 1.26 times less than σ_{-1} used in [12,13] so the cross section is 1.6 times less! On the other hand the strength parameter used in our calculations, V_1 = 270MeV instead of 184MeV [13] results in cross section increase to 2.2 times, because of quadratic dependence of cross section on V_1 value (see (12)). However, joint action of these three factors gives close results for these two calculations, the difference being only 20 % in the region of neutron energies E > 10MeV. The difference of cross sections at lower energies is connected with the fact that in addition to "main" E1-resonance we included into calculations resonance with energy E = 11MeV and width Γ = 1.5MeV that takes 10 % of sum rule. This resonance is observed well in photoabsorption cross section and is interpreted in the frame of microscopic theory [17] as an intermediate structure connected with collective one-phonon state 2^+. In these calculations (curves 2,3 in Fig.1) the volume form factor $h_v(r)$ was used, besides the difference of ours, consistent calculations, from experimental cross sections is approximately 27 %. Using of surface form factor $h_s(r)$ increases these differences up to 65% (curve 1 in Fig.1). Supposing for simplicity that realistic form factor $h(r) = 0.5*(h_v + h_s)$ (see preceding section) we can conclude that D-SD mechanism explains ≈50-60 % of the observed cross section. This conclusion agrees with the results of paper [3] and contradicts [5]. Main reason of these discrepancies consists in different interpretation of SD mechanism in paper [5] in comparison with authors [8,9] in that aspect that in the first paper entrance channel is considered statistically and is characterised by width $\Gamma_{in} \approx 0.1$ KeV while the average value in our calculations is ≈400 KeV (both entrance channel and exit channels are collective!). If we imitate additive contribution of multistep compound process simply by increasing of parameter V_1 up to 300 MeV, the result is obtained that is shown in Fig.1 (curve 4). Following investigations will show in what degree this procedure is justified. Let us note that the results obtained agree rather well with the experimental data. The same is confirmed by results shown in Figs. 2-5, where partial components of cross sections connected with the excitation of discrete levels for ^{209}Pb are shown (excitation functions). Let us note once more the important role of low-lying E1-structure with energy E = 11 MeV. It allows to adjust the calculation and experimental data at the left

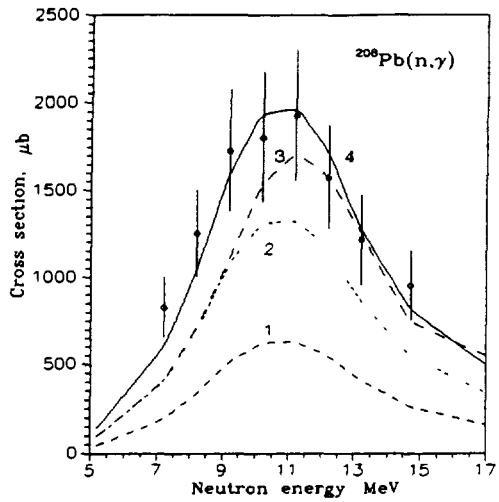

Fig. 1 Total cross section for ^{208}Pb(n,γ) reaction as a function of neutron energy. Curves 1,2 and 4 show the results of this work using various values for interaction amplitude V_1 and form factor h(r) (see text). Curve 3 - results calculated in paper[13]. Experimental data were taken from[13]

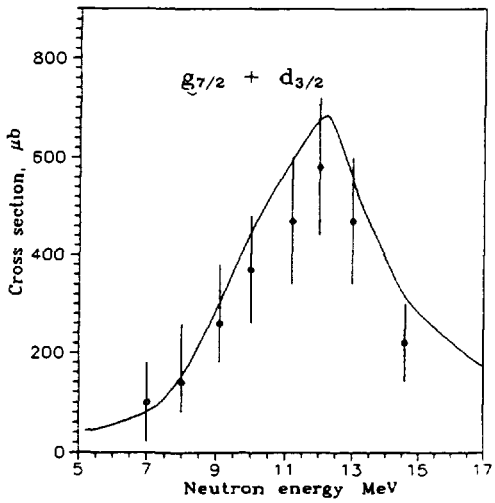

Fig. 3. The same as in Fig. 2 but for excitation $2g_{7/2}$ and $3d_{3/2}$ single particle level. Experimental data were taken from[13].

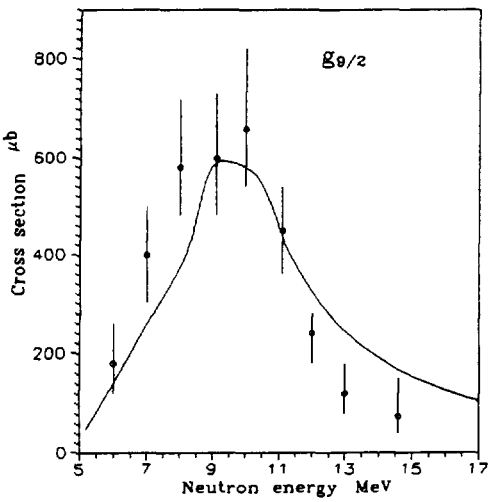

Fig. 2. Calculated partial cross section for ^{208}Pb(n,γ) reaction with excitation of $2g_{9/2}$ single particle level in ^{209}Pb. Experimental data were taken from[13].

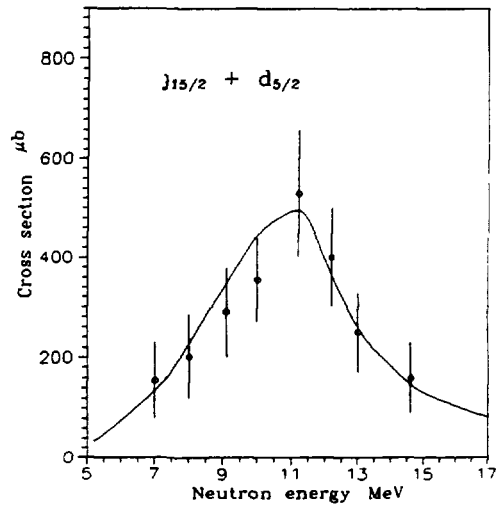

Fig. 4. The same as in Fig. 2 but for excitation $1j_{15/2}$ and $3d_{5/2}$ single particle level. Experimental data were taken from[13]

side of curve (Fig. 1) and to amend the excitation function description for $g_{9/2}$-level (Fig.2). The most convincing evidence of D-SD physical assumptions correctness is the correlation of structures in γ-spectra with the discrete levels position for daughter nucleus ^{209}Pb (see Figs.6-8). As can be seen the theory explains these structures successfully. In some sense they have been predicted because the theory has been developed before such experimental data appeared. Nevertheless we can not speak about absolute agreement between theory and experiment because there is obvious deficiency of calculated cross section near neutron binding energy (see Fig.6-8). Whether this discrepancy is connected with low-energy local E1- structures, tails of quasistationary states or with some features of energy dependence of multistep compound process should be found out in a future.

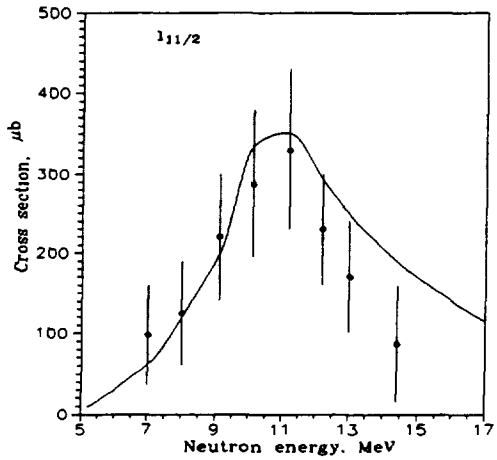

Fig. 5. The same as in Fig. 2 but for excitation $1i_{11/2}$ single particle level.

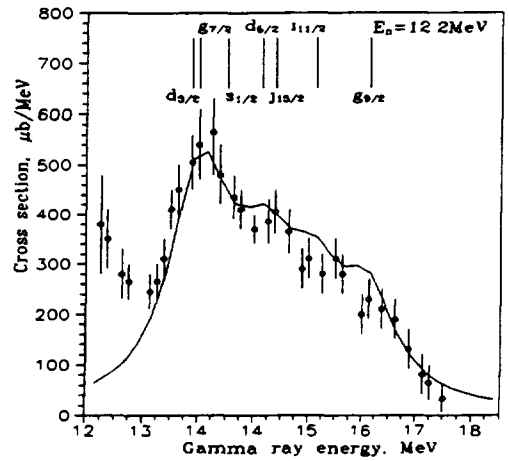

Fig. 7. The same as in Fig. 6 but for neutron energy E_n = 12.2MeV.

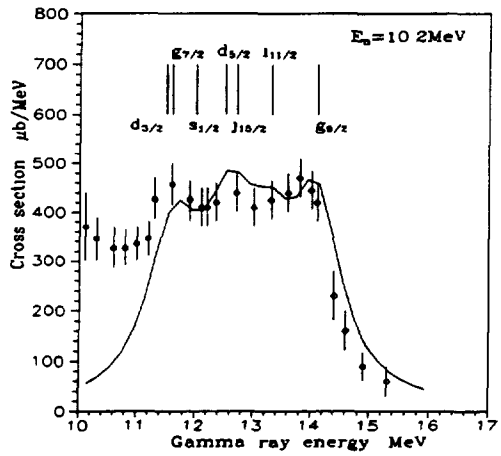

Fig. 6. Calculated spectrum of hard γ-rays from ^{208}Pb(n,γ) reaction for neutron energy E_n = 10.2MeV. At upper part of Figure position of single particle levels in ^{209}Pb is shown.

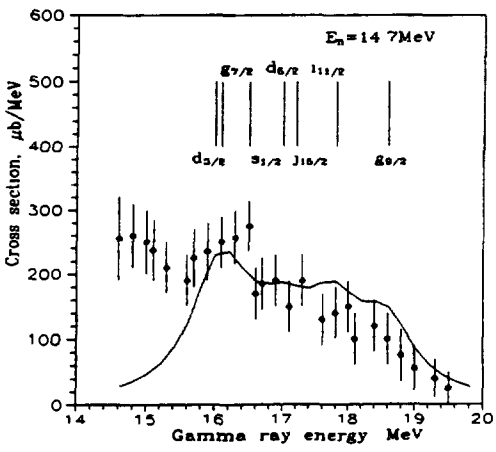

Fig. 8. The same as in Fig. 6 but for neutron energy E_n = 14.7MeV.

4. Conclusions

Considering the results of investigations outlined we can conclude:

It is shown that 50-60 % of total radiative fast neutron capture cross section for ^{208}Pb is explained by D-SD mechanism. The remaining part of cross section can be explained apparently by competing multistep compound reaction. This conclusion is in agreement with the results of paper [3] and contradicts to paper [5] conclusion where D-SD mechanism role is lowered obviously. Main reason of this conclusion consists in underestimation of collective nature of entrance channel connected with particle-vibrational interaction of incident neutron and intermediate E1- resonance.

The results of papers [10-13] based on a priori assumption that D-SD mechanism is dominant for (n,γ) reaction require additional examination. This is connected with some arbitrariness and inconsistency in the parameter choice, that define cross section absolute value, namely isovector interaction amplitude V_1, E1- resonance parameters (E_1, Γ_1, σ_{-1}) and transition potential form factor h(r). Our results show that using consistent parameter choice one can see that absolute cross section values for SD process explain half of observed cross section only.

The importance of taking into account local E1-resonance structures for total cross section calculations, excitation functions and γ-rays spectra. The influence of such structures should be more pronounced for light and medium weight nuclei, where the effects of E1-fragmentation connected with quasiparticle-phonon correlations play a significant role [17].

References

1. H.Feshbach, A.Kerman, and S.Koonin, *Ann. Phys.* **v.125** (1980) 429
2. H.Nishioka, J.J.M.Verbaarschot, and H.A.Weidenmuller, *Ann.Phys.* **v.172** (1986) 67.
3. P.Oblozinsky and M.Chadwick, *Phys.Rev.* **v.C41** (1990) 1652
4. A.Horing and H.Weidenmuller, *Phys.Rev.* **v.C46** (1992) 2476.
5. M.Herman, A.Horing, and G.Reffo, *Phys.Rev.* **v.C46** (1992) 2493
6. M.Herman, G.Reffo, and H.A.Weidemuller, *Nucl.Phys.* **v.A536** (1992) 124
7. J.M.Akkermans and H.Gruppelaar, *Phys.Lett.* **v.157B** (1985) 95.
8. G.E.Brown, *Nucl.Phys.* **v.57** (1964) 339.
9. C.F.Clement A.M.Lane, J.R.Rook, *Nucl.Phys.* **v.66** (1965) 273; **v.66** (1965) 293
10. G.Longo and F.Saporetti, *Nucl.Phys.* **v.A127** (1969) 503.
11. F.Rigaud, J.Roturier et al., *Nucl.Phys.* **v.A154** (1970) 243.
12. G.Longo and F.Saporetti, *Nucl.Phys.* **v.A199** (1973) 530.
13. G.Longo and F.Saporetti, *Nucl.Sci.and Eng.* **v.61** (1976) 40.
14. S.Dietrich, B.Berman, *Atom. Dat. and Nucl. Dat. Tab.* **v.38** (1988) 199.
15. W.D.Myers, W.J.Swiatecky et al., *Phys.Rev.* **v.C15** (1977) 2032..V.Tolokonnikov, S.A.Fayans, *JETP Lett.* **v.5** (1982) 403.
16. S.Kamerdzhiev, G.Tertychny, J.Speth, *Nucl.Phys.* **v.A555** (1982) 90; **v.A569** (1994) 313
17. W A.Lanford et al , *Phys. Rev* **v.C9** (1974) 646

Average Angular Distribution of 14 MeV Neutron capture γ-rays

F. Cvelbar and A.Likar
"J. Stefan" Institute and Faculty of Natural Sciences
and Technology, University of Ljubljana, Slovenia

IAEA First Research Co-ordination Meeting on Measurement, Calculation and Evaluation of Photon production Data
Bologna November 14-17, 1994

Abstract

Angular distribution of 14 MeV neutron radiative capture prompt γ-rays, averaged over the transitions to bound states, is calculated for $^{40}_{20}Ca(n,\gamma)^{41}_{20}Ca$, $^{56}_{26}Fe(n,\gamma)^{57}_{26}Fe$, $^{88}_{38}Sr(n,\gamma)^{89}_{38}Sr$, $^{89}_{39}Y(n,\gamma)^{90}_{39}Y$, $^{140}_{58}Ce(n,\gamma)^{141}_{58}Ce$, and $^{208}_{82}Pb(n,\gamma)^{209}_{82}Pb$ reactions. The direct -semi-direct model extended to cover, besides dipole, also the isovector and isoscalar qaudrupole giant resonance contributions has been applied. Results indicate that calculated angular distribution of 14 MeV neutron capture γ-rays is somewhat anisotropic (a_2 typical value is about -0.3), but practically forward-backward symmetric (a_1 being typically less than + 0.03). In the calculation of energy and angle integrated cross-section multiplying the 90^0 experimental value by 4π, one obtains the result which is 10% to 20% too high.

1 Introduction

Study of the fast neutron radiative capture has been initially aimed to determine the prompt γ-ray spectra and corresponding integrated cross sections (direct transitions to the bound states) and activation cross sections (cascade transitions included). Intensity of prompt γ-ray spectra measured at about 90^0 and multiplied by 4π has been considered as a sort of angle integrated cross section [1]-[3] though e.g. in the case that only the a_2 coefficient of the Legendre polynomial expansion (see the text) is different from zero, the following relation holds:

$$\int \frac{d\sigma}{d\Omega} d\Omega = 4\pi \frac{\sigma_{90}}{1 - a_2/2} \tag{1}$$

For the $sin^2\theta$ and $1 + cos^2\theta$ distribution the coefficient a_2 is -1 and + 0.5 respectively, and therefore the denominator in eq. 1 equals 0.66 and 1.33. At the same time, by the use of the special experimental arrangement [4]-[6] , the 4π (or 2π for heavy nuclei) solid angle integrated prompt γ-ray spectra were measured. Due to a rather poor accuracy it was hopeless to extract from comparison of these measurements and the ones at 90^0 even an indication of e.g. average a_2 value. It could be done only from comparable spectral measurements at different angles. This possibility opened after the development of improved experimental technique. From the first measurements of this kind [7] it was evident that physically clear picture can be obtained only for transitions to the well separated ground states and eventually also to the low excited states. Angular distributions of these transitions were then measured

rather intensively at different bombarding energies [8]-[13]. By the help of the direct-semi-direct (DSD) capture model [14]-[17] these measurements became the source of the additional knowledge about GDR. Even more, from such analyses interesting new phenomena e.g the isovector quadrupole giant resonances (IQGR) were studied [9]-[11].

Here the calculated average angular distribution coefficients of prompt neutron capture γ-rays are presented as a function of the neutron energy for $^{40}_{20}\mathrm{Ca}(n,\gamma)^{41}_{20}\mathrm{Ca}$, $^{56}_{26}\mathrm{Fe}(n,\gamma)^{57}_{26}\mathrm{Fe}$, $^{88}_{38}\mathrm{Sr}(n,\gamma)^{89}_{38}\mathrm{Sr}$, $^{89}_{39}\mathrm{Y}(n,\gamma)^{90}_{39}\mathrm{Y}$, $^{140}_{58}\mathrm{Ce}(n,\gamma)^{141}_{58}\mathrm{Ce}$, and $^{208}_{82}\mathrm{Pb}(n,\gamma)^{209}_{82}\mathrm{Pb}$ reactions using different optical model potentials. From these neutron energy functions the 14 MeV data are extracted and evaluated by the help of some additional calculated and experimental results.

2 Direct-semidirect (DSD) model

In DSD model the transition matrix element T_{if} is the sum of the term describing the direct capture of the bombarding nucleon to the (single particle) final state, accompanied by the emission of γ-photon, and the resonant term, resulting from the two step process in which first the giant resonance mode is excited and, later on, deexcited by the emission of γ-ray:

$$T_{if} \propto \sum_j \langle \psi_f | d_j | \chi^+ \rangle + \frac{\langle \psi_f | D_j | \chi_d \rangle \langle \chi_d | H_{\tau j} | \chi^+ \rangle}{E - E_{Rj} + i\Gamma_j/2} = T_{DIR} + T_{RES} \qquad (2)$$

Here $\langle \psi_f |$ is the wave function of the captured nucleon into the bound state, $|\chi^+\rangle$ is the optical model continuum wave function, d_j and D_j stand for the single particle and collective electromagnetic operator of multipolarity j, respectively. E_{Rj} and Γ_j refer to the position and the width of the (multipole j) giant resonance of the combined target plus nucleon system, respectively. Symbol $H_{\tau j}$ means the coupling interaction of the incident nucleon to the target nucleus vibration. There were proposed several radial forms of this interaction. The complex form [15], in which the real and imaginary strengths V_j and W_j (though in some way connected to the corresponding strengths of the isospin part of the optical model potential) are treated as free parameters, has been in the last decade considered as the most adequate. Parameters V_1 and W_1 are usually extracted a) by fitting the GDR excitation function at $\theta = 90^0$ (e.g. ref. 16) and b), less accurately, from the description of the 14 MeV neutron capture γ - ray spectra [18]. Initially DSD model was formulated to treat only the dipole giant resonance contribution, appearing on the average at the excitation energy $E_{R1} = 77A^{1/3}$ MeV. Later on it has been enlarged to cover also higher multipole giant resonances [19] e.g. isovector giant quadrupole resonance (IVQR) apearing at $E_{VR2} = 130A^{1/3}$ MeV and also the isoscalar giant quadrupole resonance (ISGQR) observed at excitation energy $E_{IR2} = 65A^{2/3}$ In this formulation of the DSD model besides the dipole resonance transition matrix element, also those of quadrupole resonances appear. As we are summing up coherently the contributions of different parity, due to the interference effect, the odd Legendre coefficients become different from zero. If one remains within the original (dipole) version [20] of the DSD model, this is true only for a_2 Legendre coefficient. In this case at 14 MeV neutron energy the angular distribution is of the type of $\sin^2\theta$ + const, or $\cos^2\theta$ + const.

In the complete DSD calculation different multipole transitions, either direct (DIR) or resonant (RES) therefore take place. It is worth of mentioning here, that, due to the low neutron quadrupole effective charge, intensities of the direct neutron quadrupole capture transitions are very small in comparison with that of the direct-dipole , resonance-dipole

or resonance- quadrupole transitions. If we limit ourselves to the dipole and quadrupole processes the DSD neutron radiative capture matrix element is therefore the sum,

$$T_{if} = T_{DIR-DIP} + T_{RES-DIP} + T_{RES-SQGR} + T_{RES-IVQGR} \ .$$

As already mentioned, resulting angular distribution is generally forward - backward asymmetric and the odd Legendre coefficients are different from zero. The most sensitive is the coefficient a_1 . It is in fact the neutron energy dependence of a_1 which offers the possibility to extract the information about QGRs by the study of fast neutron radiative capture. Till now mostly the IVQGR has been considered [9]-[11]. Observable contribution of the ISQGR was possibly found in Ca-41 [9].

3 Experimental techniques

Sample to be measured is put [8]-[13] in the collimated neutron beam and prompt γ-rays are detected by a large (recently up to $25cm^2$ x 25cm) high quality NaJ(Tl) spectrometer, usually embodied by the anticoincidence shield. Pulses belonging to the unproper neutrons, e.g. those hitting the NaI(Tl) crystal directly, are eliminated by the time of flight discrimination technique. For this purpose the neutron source is nanosecondly pulsed. Mentioned before Legendre expansion coefficients a_i, usually extracted from the measured angular distribution, are defined by the equation:

$$\frac{d\sigma}{d\Omega} = A_0(1 + \Sigma a_i P_i(\cos\theta)) \ , \tag{3}$$

so that,

$$\int \frac{d\sigma}{d\Omega} d\Omega = 4\pi A_0 \ . \tag{4}$$

Usually the angular distribution is measured at three angles i.e. $55°, 90°, and\ 125°$. From it two combinations, $A_1 = (I_{55} - I_{125})/(I_{55} + I_{125}) = (0.57a_1 - 0.02a_2 - 0.38a_3)/(1 - 0.39a_4)$ measuring the fore-aft asymmetry, and $A_2 = 2 - 4I_{90}/(I_{55} + I_{125}) = 2 - (2 - a_2 + 0.67a_4)/(1 - 0.39a_4)$, indicating the anisotropy of the distribution are determined. If higher coefficients are small, $A_1 \simeq 0.57a_1$ and $A_2 \simeq a_2$.

4 Results

Angular distribution asymmetry coefficients A_1 and anisotropy coefficients A_2 as a function of neutron energy and averaged over all bound state transitions for $^{40}_{20}Ca(n,\gamma)^{41}_{20}Ca$, $^{56}_{26}Fe$-$(n,\gamma)^{57}_{26}Fe$, $^{88}_{38}Sr(n,\gamma)^{89}_{38}Sr$, $^{89}_{39}Y(n,\gamma)^{90}_{39}Y$, $^{140}_{58}Ce(n,\gamma)^{141}_{58}Ce$, $^{208}_{82}Pb(n,\gamma)^{209}_{82}Pb$ reactions are shown, respectively, in Fig.1. and in Fig.4. for different optical potentials. One observes that below neutron energy of about 15MeV the A_1 value is practically zero, independently on optical model used in the calculation. In this energy region the angular distribution is therefore symmetric with respect to 90^0.

There are no corresponding average experimental data to be compared with the present results. Experimental and DSD study of the capture transitions to the individual levels, might indirectly help us in this respect. From Fig.2. and Fig.3. one observes that also in these cases the measured and DSD calculated A_1 coefficients are not much different from zero. As it follows from Fig.3, this result does not dependent on such details of the calculation as

it is its width (Γ) b) or the integral (EWSR) of the IVQGR c). These findings are easily explained by the fact that in the neutron energy region below about 15 Mev the tail of the IVQGR is so low that its effect is not observed even in the interference process.

Behaviour of the average anizotropy coefficient A_2 is much more dynamic. Even though, from our results (Fig.4) one is allowed to conclude that in the neutron energy region below about 15MeV the DSD A_2 values practically do not depend on the optical model used in the computation. It is interesting that in all cases presented in Fig.4 the average A_2 coefficients are negative, meaning that the γ - ray angular distribution of the spectral integral is of the shape of $\sin^2\theta$. Our DSD model values of A_2 calculated for individual states of $^{95}_{141}$Nb, on the other hand, are of both signs (Fig.5.) The same result follows from the experimental data for transitions to the individual bound states. (Fig.6.)

Table 1: Interval of the average asymmetry coefficient values A_2 for 14 MeV neutron radiative capture (averaged over all prompt bound state transitions) calculated within DSD model using different optical model parametrization.

Target	$A_{2averageDSD}$
$^{40}_{20}$Ca	$-(.5-.6)$
$^{56}_{26}$Fe	$-(.32-.36)$
$^{88}_{38}$Sr	$-(.38-.41)$
$^{89}_{39}$Y	$-(.2-.27)$
$^{140}_{58}$Ce	$-(.33-.36)$
$^{208}_{82}$Pb	$-(.48-.49)$

Table 2: Comparison of experimental and DSD model A_1 and A_2 coefficients for the capture transitions to the individual (single particle levels). Symbols h,d,g, mean the $1h_{11/2}$, $2d_{3/2}$ and $1g_{7/2}$ levels, respectively.

Target	E_n MeV	Level	A_1	A_2
^{40}Ca	14	$f_{7/2}$	$+(.00\pm.05)$	$-(.15\pm.08)$
DSD			$-(.02-.06)$	$-(.2-.3)$
^{88}Sr	11	$d_{5/2}$	$+(.17\pm.02)$	$-(.6\pm.08)$
DSD				$-.7$
^{88}Sr	11	$s_{1/2}$	$-(.25\pm.10)$	$-(.7\pm.4)$
DSD			$+.07$	-1.0
^{89}Y	14	$d_{5/2}$	$+(.05\pm.01)$	$-(.75\pm.1)$
DSD			$+.05$	$-.7$
^{89}Y	14	h, d, g	$+.02$	$-(.08\pm.02)$
DSD			$+.03$	$-.03$
^{208}Pb	13	$g_{9/2}$	$+(.10\pm.05)$	$-(.9\pm.3)$
DSD			$+.04$	$-.25$
^{208}Pb	13	$i_{11/2}$	$-(.05\pm.10)$	$-(.16\pm.2)$
DSD			$+.01$	$+(.25$ - $.40)$

Values of the angular distribution anizotropy coefficients A_2 at about 14 MeV neutron energy, extracted from Fig.4. are shown in Table I. (A_1 values are typically less than 0.03). Their reliability these values can be estimated from the analysis of the reported

experimental data for the transitions to the individual excited states (Table II.). In these cases the agreement between the measured and DSD model calculated data is quite good. Strong disagreement is found only for the population of the $g_{9/2}$ level in ^{209}Pb. In Table II. there are not included rather inacurate experimental data [7] for the population of the $g_{9/2}$ ground state in ^{208}Pb, being $A_1 = +(.06 \pm .08)$ and $A_2 = +(.03 \pm .20)$ [7].

5 Conclusion

Using the Direct - Semi - Direct capture model, enlarged to include also the qudrupole giant resonances, the angular distribution asimmetry coefficients A_1 and anizotropy coefficients A_2 were calculated. From their dependence on the neutron energy the 14 MeV data ($A_1 \simeq 0$ and $A_2 \simeq -0.3$) were extracted. Results practically do not depend on the optical model used in the computation.

Acknowledgement
Technical assistance of A. Perdan is highly acknowledged.

References

[1] F.Rigaud, J.Roturier, J.L.Irigaray, G.Y.Petit, G.Longo, and F.Saporetti, *Nucl. Phys.* **A154** (1970), 243,

[2] F.Rigaud, J.Roturier, G.Y.Petit, G.Longo, and F.Saporetti, *Nucl. Phys.* **A173** (1971), 551 and **A176** (1971) 545,

[3] I.Bergqvist, D.M.Drake, and D.K. McDaniels *Nucl. Phys.* **A191** (1972), 641,

[4] F.Cvelbar, A.Hudoklin, M.V.Mihailović, M.Najžer, and V.Ramšak *Nucl. Phys.* **A130** (1969), 401,

[5] F.Cvelbar, A.Hudoklin, and M.Najžer, *Nucl. Phys.* **A158** (1970), 251,

[6] M.Budnar et al. Prompt γ -ray Spectra and Integrated Cross Sections for Radiative Capture of 14MeV Neutrons in 28 Natural Targets in the mass region from 12 to 28, IAEA, INDC(YUG) 6/L, 1979, for some evaluations see F.Cvelbar and A.Betak *Z.Phys.* **A332** (1989), 163

[7] E.D. Arthur, D.M.Drake, and I. Halpern, *Phys.Rev.Lett.* **35** (1975) 914,

[8] A.Likar, A.Lindholm, L.Nilsson, I.Bergqvist and B.Pålson, Nucl. *Nucl. Phys.* **A298** (1978), 217,

[9] I.Bergqvist, R.Zorro, A.Hakanson, A.Lindholm, L.Nilsson, N.Olsson and A.Likar, *Nucl. Phys.* **A419** (1984), 509,

[10] R.Zorro, I.Bergqvist, S.Crona, A.Håkansson, A.Likar, A.Lindholm, L.Nilsson and N.Olsson, *Nucl. Phys.* **A472** (1987), 125,

[11] A.Håkansson, J.Blomgren, A.Likar, A.Lindholm, L.Nilsson, N.Olsson and R.Zorro, *Nucl. Phys.* **A512** (1990), 399,

[12] S.E.King, M.Potokar, N.R.Robertson, H.R.Weller, D.R.Tilley *Nucl. Phys.* **A384** (1982), 129,

[13] C.M.Laymon, R.O.Nelson, S.A.Wender, and L.R.Nilsson *Phys.Rev.* **C46** (1992) 1880,

[14] C.F. Clement, A.M, Lane, and J.R. Rook, sl Nucl.Phys. bf 66 (1965), 273; *ibid.*, 293,

[15] M.Potokar, *Phys.Let.* **B46** (1973), 346,

[16] F.S. Dietrich and A.K. Kerman, *Phys.Rev.Lett.* **43** (1979),114,

[17] M.Potokar, *Phys.Let.* **B92** (1980), 1,

[18] F. Cvelbar, R. Martinčič and A. Likar, *Atomkernenergie - Kerntechnik* **45** (1984), 179,

[19] G.Longo, F. Saporetti and R.Guidotti, *Nuovo Cim.* **46A** (1978), 509,

[20] A.Likar, *Fizika* **10** (1978) 187,

[21] J.Speth and A. Van der Woude, *Rep. Prog. Phys.* **44** (1981) 719.

6 Figure captions

Fig. 1 (a-f). DSD model fore-aft asymmetry coefficient A_1 for radiative neutron capture in ^{40}Ca, ^{56}Fe, ^{88}Sr, ^{89}Y, ^{140}Ce and ^{208}Pb, averaged over all bound state transitions, as a function of neutron energy, for different optical models.

Fig. 2 (a-c). Examples of the agreement between the experimental and DSD model values of the A_1 coefficient for the capture transitions to the selected individual states (ground states): $f_{7/2}$ in ^{41}Ca a) [9], [13] and $d_{5/2}$ in ^{90}Y b). One observes also insensitivity of the results on the width Γ b) and on the strength (EWSR) c) of the IVQGR connsidered in $^{89}_{39}\mathrm{Y}(n,\gamma)^{90}_{39}\mathrm{Y}$ reaction [10].

Fig. 3. Neutron energy dependence of the DSD model fore-aft asymmetry coefficients A_1 a) and of the anisotropy coefficients A_2 b) for the neutron capture to the individual states in the $^{95}_{141}$Nb.

Fig. 4. (a-f). DSD model anisotropy coefficient A_2 for radiative neutron capture in ^{40}Ca, ^{56}Fe, ^{88}Sr, ^{89}Y, ^{140}Ce and ^{208}Pb, averaged over all bound state radiative transitions, as a function of neutron energy for different optical models.

Fig. 5. An example of the unability of the DSD model to reproduce the experimental neutron energy dependence of the Legendre coefficient values a_2 for the neutron capture into the ground state $g_{9/2}$ a) and first excited state $i_{11/2}$ b) of ^{209}Pb. Disagreement is typical for the neutron radiative capture in heavy nuclei [12].

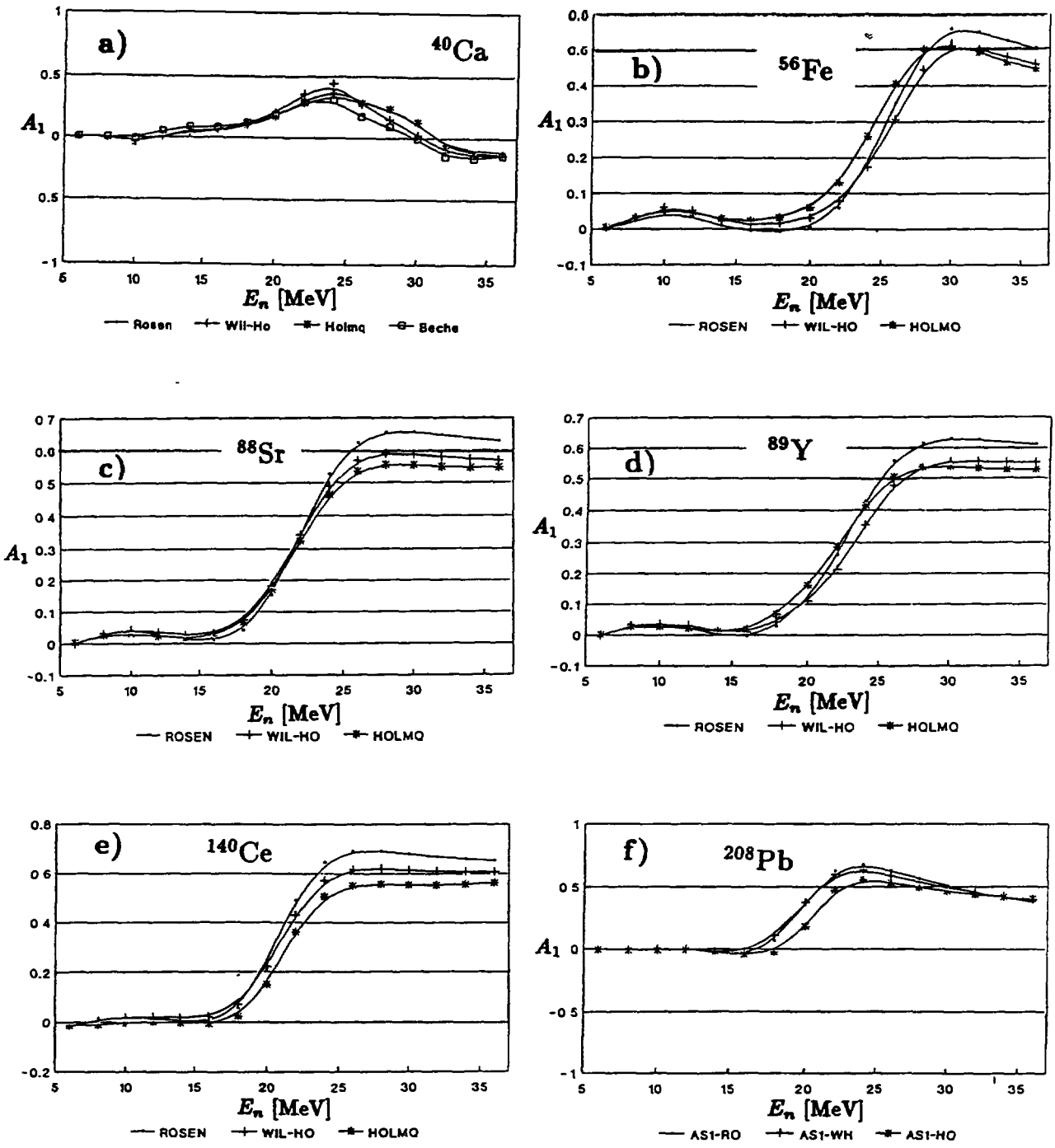
a)
40Ca
A1
En [MeV]
Rosen
Wil-Ho
Holmq
Beche
b)
56Fe
ROSEN
WIL-HO
HOLMQ
c)
88Sr
d)
89Y
e)
140Ce
f)
208Pb
AS1-RO
AS1-WH
AS1-HO

Fig.1.

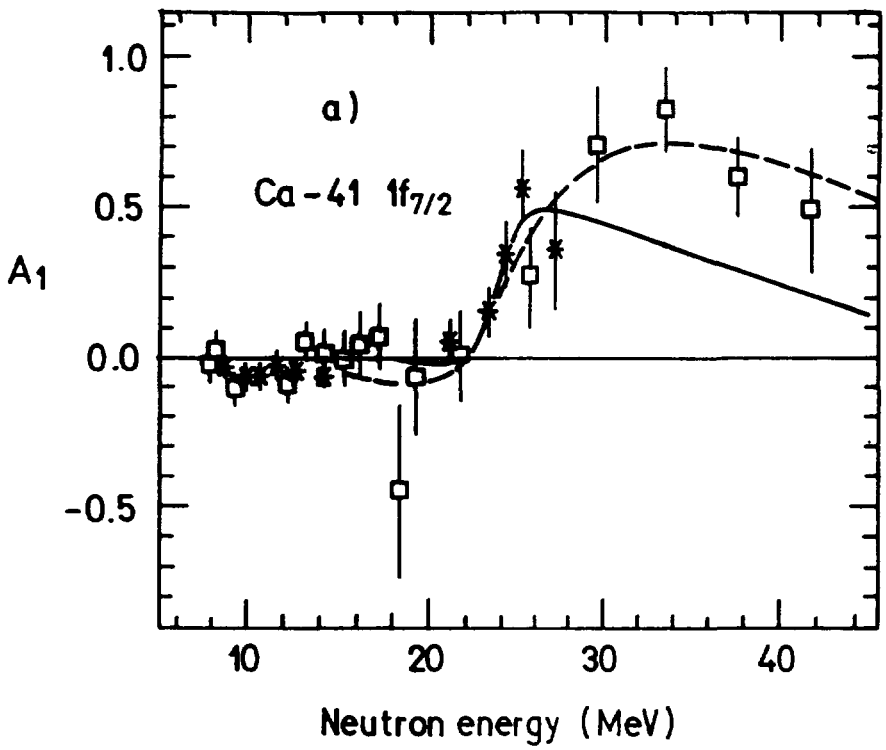
a)
Ca-41 1f7/2
A1
1.0
0.5
0.0
-0.5
10
20
30
40
Neutron energy (MeV)

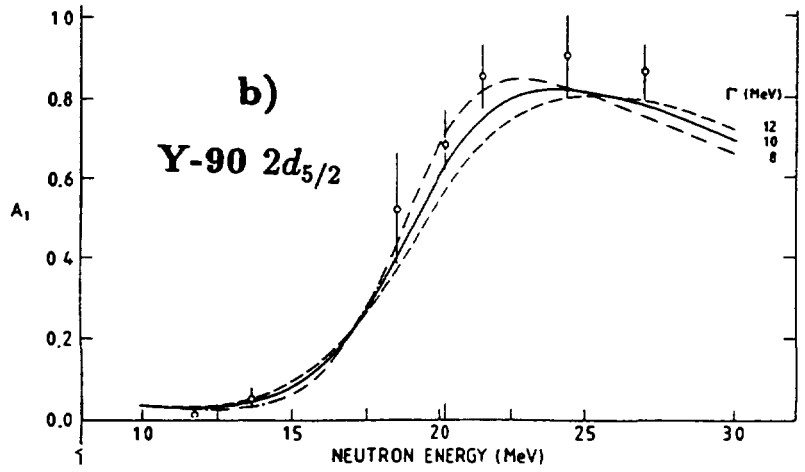
b)
Y-90 2d5/2
A1
Γ (MeV)
12
10
8
NEUTRON ENERGY (MeV)

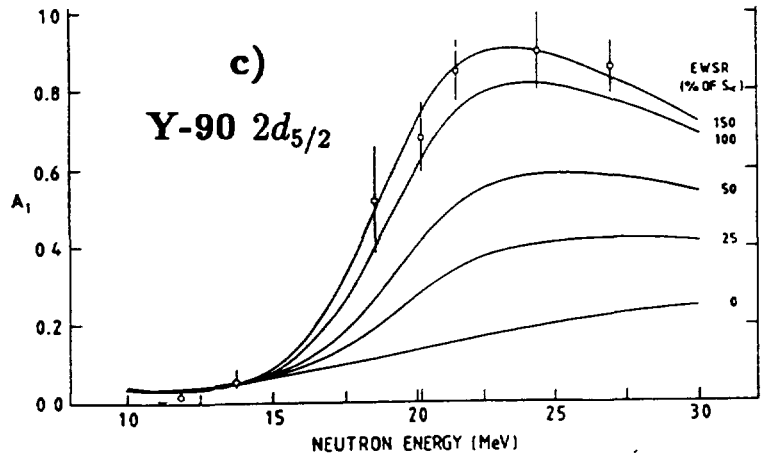
c)
Y-90 2d5/2
A1
EWSR
150
100
50
25
0
NEUTRON ENERGY (MeV)

Fig.2.

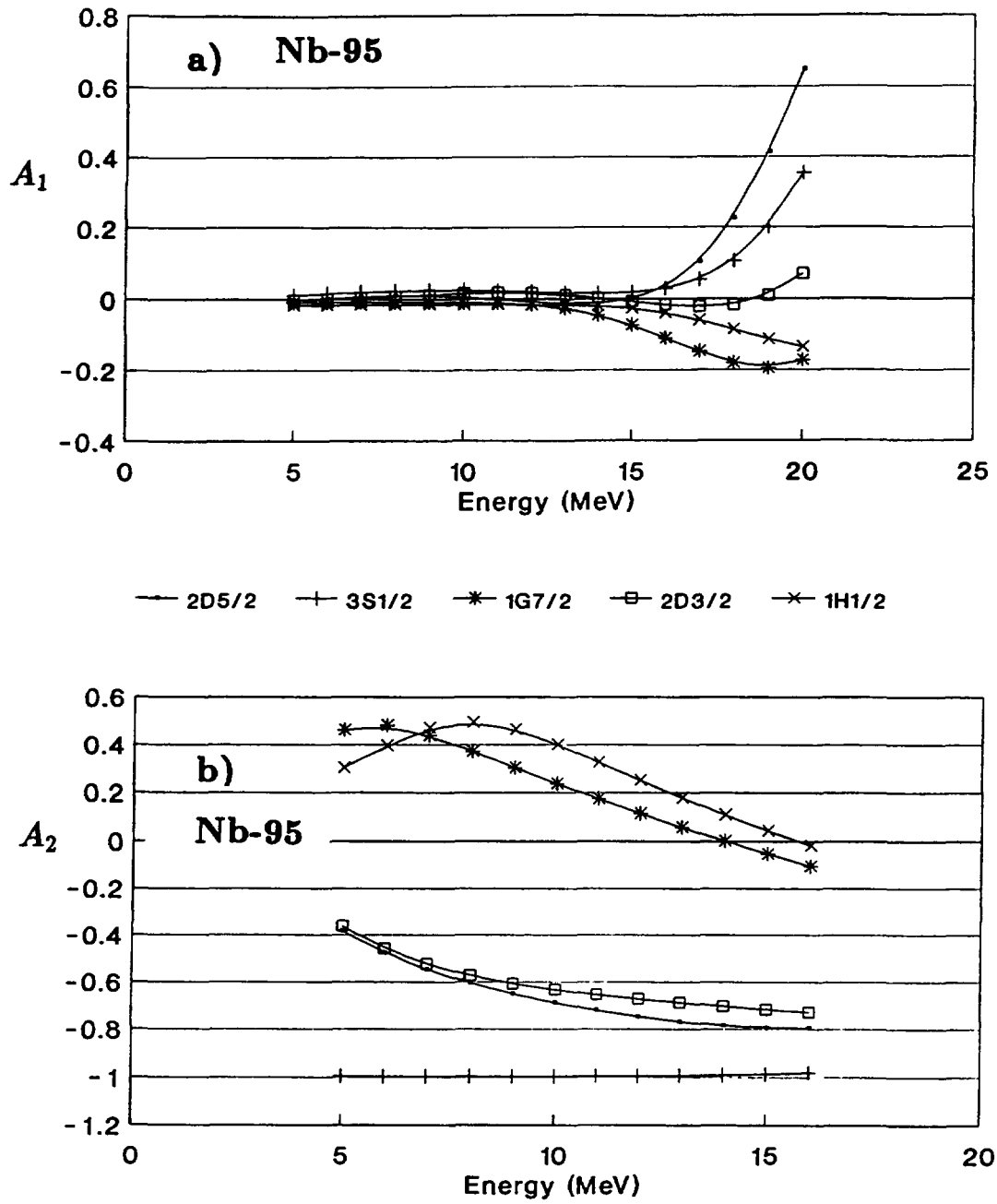
a) Nb-95
A_1
0.8
0.6
0.4
0.2
0
-0.2
-0.4
0
5
10
15
20
25
Energy (MeV)
2D5/2
3S1/2
1G7/2
2D3/2
1H1/2
b)
Nb-95
A_2
0.6
0.4
0.2
0
-0.2
-0.4
-0.6
-0.8
-1
-1.2
0
5
10
15
20
Energy (MeV)

Fig.3.

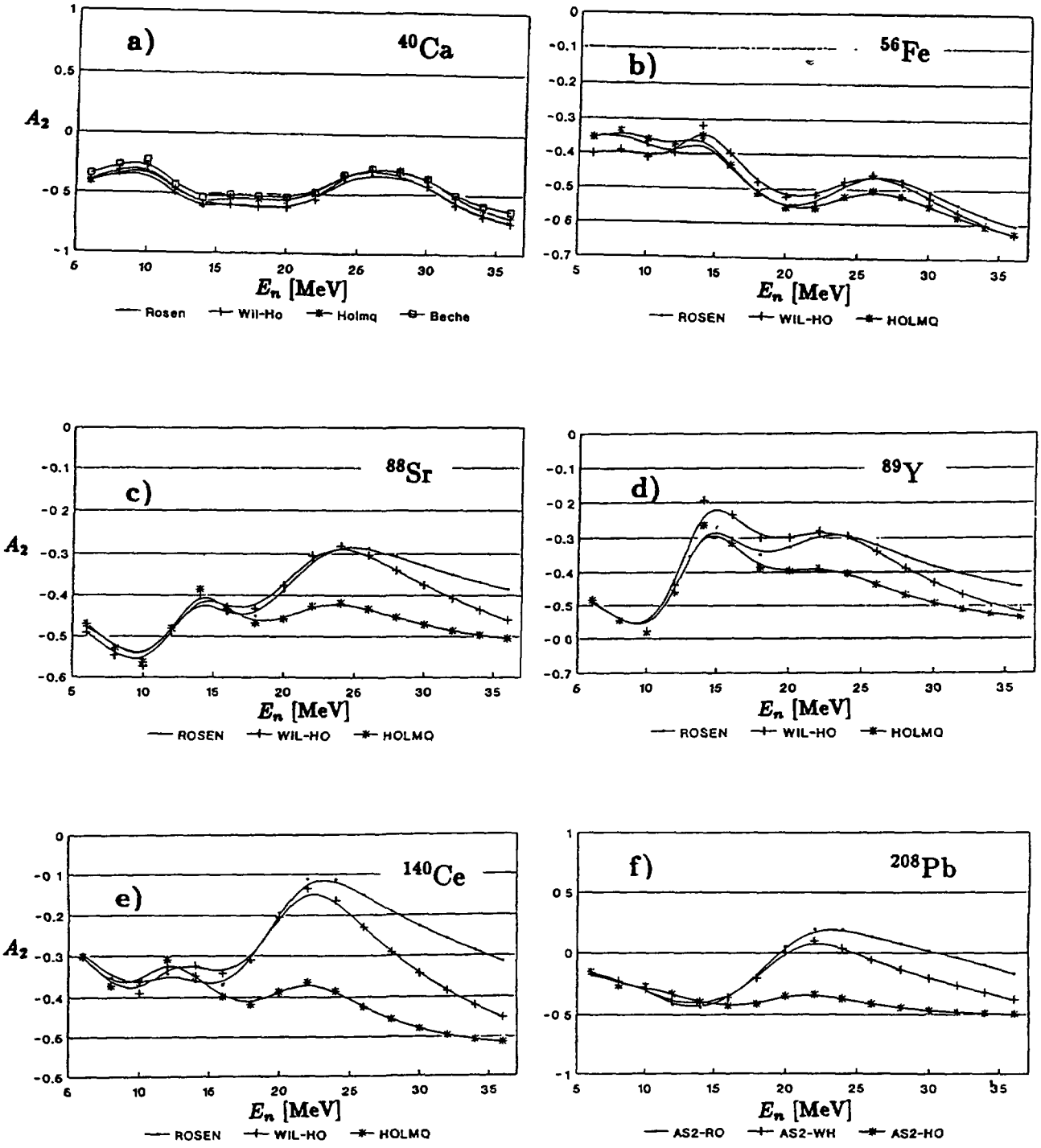
a)
^{40}Ca
A_2
E_n [MeV]
Rosen
Wil-Ho
Holmq
Beche
b)
^{56}Fe
E_n [MeV]
ROSEN
WIL-HO
HOLMQ
c)
^{88}Sr
A_2
E_n [MeV]
ROSEN
WIL-HO
HOLMQ
d)
^{89}Y
E_n [MeV]
ROSEN
WIL-HO
HOLMQ
e)
^{140}Ce
A_2
E_n [MeV]
ROSEN
WIL-HO
HOLMQ
f)
^{208}Pb
E_n [MeV]
AS2-RO
AS2-WH
AS2-HO

Fig.4.

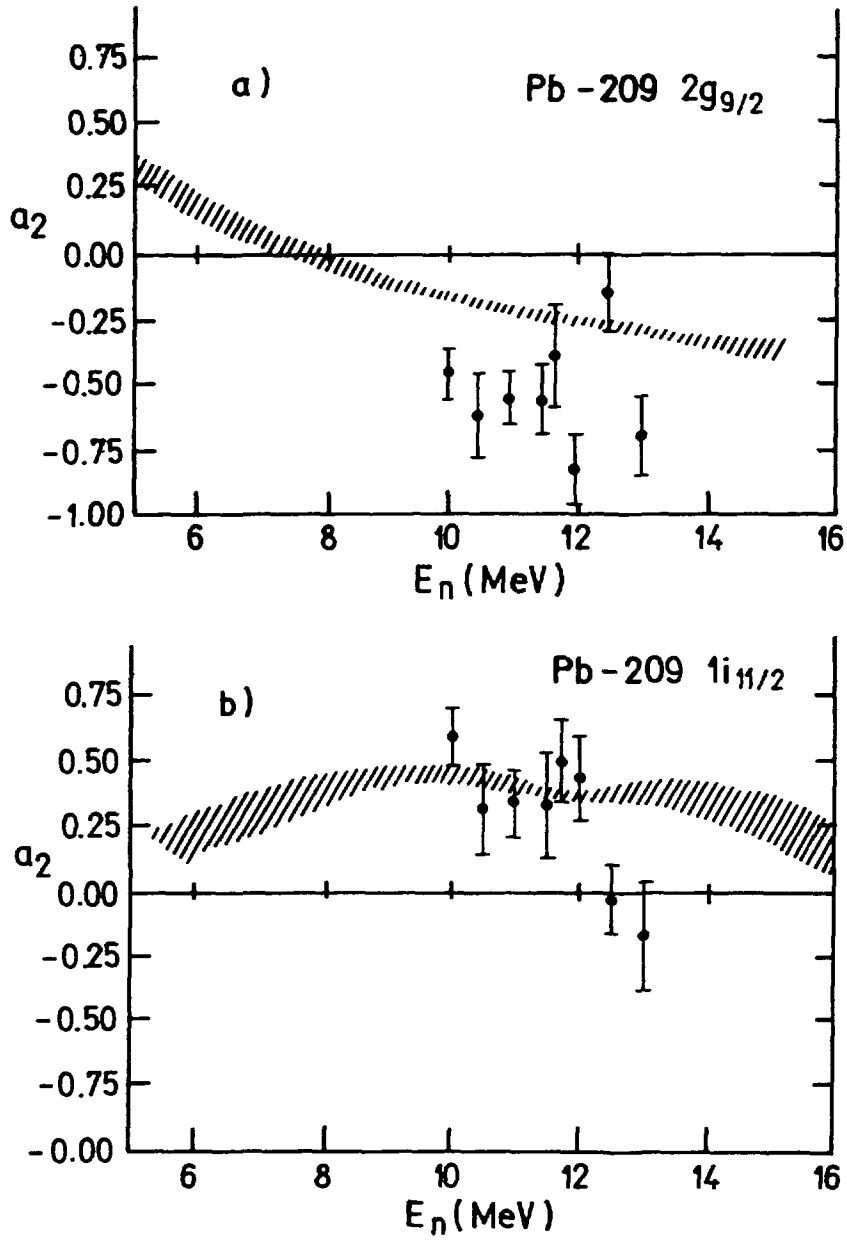
a)
Pb - 209 $2g_{9/2}$
0.75
0.50
0.25
a_2
0.00
-0.25
-0.50
-0.75
-1.00
6
8
10
12
14
16
E_n (MeV)
b)
Pb - 209 $1i_{11/2}$
0.75
0.50
0.25
a_2
0.00
-0.25
-0.50
-0.75
-0.00
6
8
10
12
14
16
E_n (MeV)

Fig.5.

PRE-EQUILIBRIUM GAMMA EMISSION: SPIN-DEPENDENT CALCULATIONS

E. Běták

Institute of Physics, Slovak Academy of Sciences,
*84228 Bratislava, Slovakia**

IAEA Research Co-ordination Meeting of the Agency's CRP on Measurement, Calculation and Evaluation of Photon Production Data, Bologna, November 1994

Abstract

We calculated γ energy spectra within the pre-equilibrium (exciton) model of nuclear reactions with full account for both the spin couplings as well as for couplings of different nuclei and cascades of γ's. This has been done using the computer code PEGAS.

The calculations presented are those for two 14 MeV neutron-induced reactions, namely ^{56}Fe+n and ^{93}Nb+n, which differ significantly in the target spin. We have found a difference with respect to the spin-independent version of the pre-equilibrium code; this difference depends on the choice of projectile-target combination (and their spins), the incident energy, as well as on the channel studied. In both cases, it does not influence the γ spectra drastically.

The study of spin effects in the presence of discrete levels is of special interest and the code PEGAS is being modified as to enable such a possibility.

1 Introduction

We studied the spin effects on the observable quantities in nuclear reactions. We benefited from the code PEGAS [1], which enables to take consistently into account both particle and γ pre-equilibrium emission (including cascades) and the spin-coupling effects. This is probably the first and till now the only one fully pre-equilibrium master equations code with a rigorous treatment of spin coupling effects, where the pre-equilibrium description is consistently used at all stages of the reaction. The code PEGAS is in its strucure and in the input data very similar to its spin-independent predecessor, code PEQAG [13]. This closeness enabled us to study spin effects in detail, especially the influence of the inclusion of spin coupling formalism on the calculated γ (and particle as well) spectra.

The pre-equilibrium model combines in a natural way the pre-equilibrium nuclear reaction concept with the equilibrium statistical decay. This is enabled via the master equations approach, that allows one to follow the time evolution of the reaction system up to its

*E-mail: betak@savba.sk

complete decay. The master equations description of a nuclear reaction is used for all stages of a nuclear reaction. Specifically, all subsequent emissions, including the equilibrium (= the compound nucleus) one, are treated within the pre-equilibrium formalism, where the compound nucleus is just its equilibrium limit. In order to handle properly the cascades of γ rays, the ususal set of master equations (tens of equations) has been enlarged to couple also different excitation energies as well as various nuclei. The great advantage of such a model is a consistent calculation of multiple particle emission as well as multiple γ emission. The model has been quite recently extended to account for angular momenta [2], opening thus a possibility to calculate also discrete γ ray production. It is important that the nucleon as well as the γ emission rates of the pre-equilibrium decay automatically take over their correct equilibrium (Hauser-Feshbach) form in the angular-momentum version of the model.

2 Master equations with spin coupling

The set of master equations used with explicite treatment of spin variables and all possible couplings and cascades is (see e.g. [1])

$$\begin{aligned}\frac{\mathrm{d}P(\imath,E,J,n,t)}{\mathrm{d}t} &= P(\imath,E,J,n-2,t)\,\lambda^{+}(i,E,J,n-2)\\ &+ P(i,E,J,n+2,t)\,\lambda^{-}(i,E,J,n+2)\\ &- P(\imath,E,J,n,t)\,\left[\lambda^{+}(\imath,E,J,n)+\lambda^{-}(i,E,J,n)+L(i,E,J,n)\right]\\ &+ \sum_{\imath',J',n',x}\int P(\imath',E',J',n',t)\;\lambda_x([\imath',E',J',n']\xrightarrow{\epsilon}[\imath,E,J,n])\mathrm{d}\epsilon\;, \qquad (1)\end{aligned}$$

where $P(\imath,E,J,n,t)$ is the occupation probability of a nucleus $\imath$ at the excitation energy E, spin J and the exciton number n, λ^{+} and λ^{-} are the transitional rates to neighbouring states, and L is the total integrated emission rate of particles (protons π and neutrons ν) and γ rays.

The nucleon emission rate per energy and time unit is in its usual shape

$$\lambda_{\pi,\nu}([E,J,n]\xrightarrow{\epsilon}[U,S,n-1]) = \frac{1}{h}\frac{\omega(n-1,U,S)}{\omega(n,E,J)}\mathcal{R}_{\pi,\nu}(n)\sum_{\jmath=|S-1/2|}^{S+1/2}\sum_{\imath=|J-\jmath|}^{J-\jmath}T_{\imath}(\epsilon)\;, \qquad (2)$$

where $\omega(n,E,J)$ is the particle-hole state density defined below, T_l's are the transmission coefficients of the emitted nucleon and $\mathcal{R}_x(n)$ is the charge factor for a given type of a nucleon [3]. At any stage of the reaction $\mathcal{R}_\nu(n)+\mathcal{R}_\pi(n)=1$; the initial values as well as those at equilibrium depend on the type of reaction and neutron-proton composition of the system.

The particle-hole state density $\omega_n(E,J)$ is

$$\omega(n,E,J) = \frac{g(gE-A_{ph})^n}{p!h!(n-1)!}R_n(J)\;, \qquad (3)$$

where g is the single-particle level density, the exciton number n is divided into particles p and holes h, $n=p+h$, A_{ph} is the correction term due to the Pauli principle, and the spin part is

$$R_n(J) = \frac{2J+1}{2\sqrt{2\pi}{\sigma_n}^3}\exp\left(-\frac{(J+1/2)^2}{2{\sigma_n}^2}\right), \qquad (4)$$

where σ_n is the spin cut-off parameter.

The transition rate from an n-exciton state to a more complicated one, $n \rightarrow (n+2)$, is taken factorized

$$\lambda^+(E,J,n) = \frac{2\pi}{\hbar}|M|^2 Y_n{}^{\downarrow} X_{nJ}{}^{\downarrow} \ . \tag{5}$$

In eq. (5), $|M|^2$ is the energy part of the average squared transition matrix element of the residual interaction, $Y_n^{\downarrow}$ is the energy part of the accessible final states, and $X_{nJ}^{\downarrow}$ represents the angular momentum part of the squared transition matrix element together with the angular momentum part of the accessible final states. The energy part $Y_n^{\downarrow}$ is just that of the spin-independent case (see e.g. [4]), and the spin part $X_{nJ}{}^{\downarrow}$ is given as [2]

$$X_{nJ}{}^{\downarrow} = \frac{1}{R_n(J)} \sum_{j_4 Q} R_1(Q)\tilde{F}(Q)R_{n-1}(j_4)\Delta(Q j_4 J) \ , \tag{6}$$

where $\Delta(Q j_4 J)$ is 1 for $|Q - j_4| \leq J \leq Q + j_4$ and 0 otherwise, and

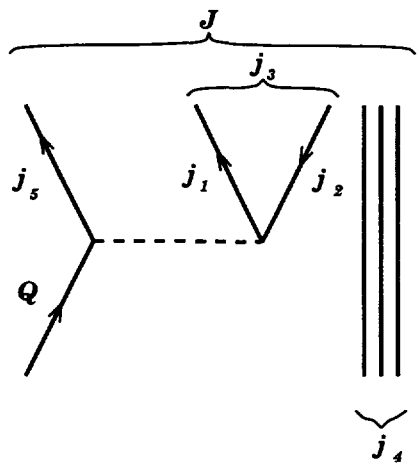

Figure 1: Diagram of the $X_{nJ}^{\downarrow}$ function for the intranuclear transitions.

$$\tilde{F}(Q) = \sum_{j_3 j_5}(2j_5+1)R_1(j_5)(2j_3+1)F(j_3)\begin{pmatrix} j_5 & j_3 & Q \\ \frac{1}{2} & 0 & -\frac{1}{2} \end{pmatrix}^2 , \tag{7}$$

and the angular momentum density of pair states is

$$F(j_3) = \sum_{j_1 j_2}(2j_1+1)R_1(j_1)(2j_2+1)R_1(j_2)\begin{pmatrix} j_1 & j_2 & j_3 \\ \frac{1}{2} & -\frac{1}{2} & 0 \end{pmatrix}^2 . \tag{8}$$

In eqs. (6) to (8), the notation of spins is explained in Fig. 1.

3 Gamma emission

The γ emission mechanism encoded into the PEGAS code is based on the $E1$ single-particle γ radiative transition, Brink-Axel hypothesis, and it uses the giant dipole resonance γ-ray strength function [5, 6]. The γ emission is associated with the change of the energy of

a single nucleon (which eventually may fill in the corresponding hole, decreasing thus the exciton number by -2). With full angular momentum couplings, the γ emission rate λ_γ from an n-exciton state is [2]

$$\lambda_\gamma([E,J,n] \stackrel{\epsilon_\gamma}{\rightarrow} [U,S,m]) = \frac{\epsilon_\gamma^2 \sigma_{GDR}(\epsilon_\gamma)}{3\pi^2\hbar^3c^2} \frac{b_{mS}^{nJ}\,\omega(m,E-\epsilon_\gamma,S)}{\omega(n,E,J)} \ , \tag{9}$$

where $U = E - \epsilon_\gamma$ and the branching ratios are

$$b_{mS}^{nJ} = \frac{y_m^n x_{mS}^{nJ}}{y_m^m x_{mS}^{mJ} + y_m^{m+2} x_{mS}^{m+2J}} \ . \tag{10}$$

In eq. (9), $\sigma_{GDR}(\epsilon_\gamma)$ is the photo-absorption cross section. Within the equidistant-spacing scheme, the energy terms y's are

$$y_n^n = gn \ , \qquad\qquad y_n^{n+2} = g^2\epsilon_\gamma \ , \tag{11}$$

and the corresponding spin coupling terms

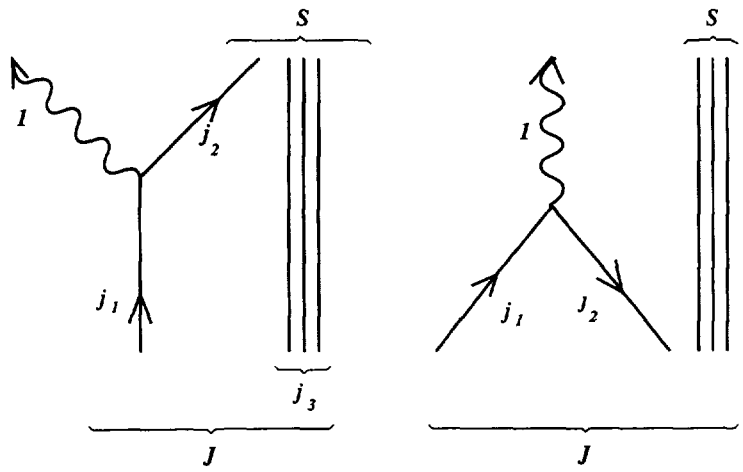

Figure 2: Diagram of x_{nS}^{nJ} (left) and x_{nS}^{n+2J} (right) functions for the γ emission.

$$x_{nS}^{nJ} = \frac{3(2J+1)}{R_n(S)} \sum_{j_1 j_2 j_3} (2j_1+1)R_1(j_1)(2j_2+1)R_1(j_2)R_{n-1}(j_3) \times \begin{pmatrix} j_2 & 1 & j_1 \\ \frac{1}{2} & 0 & -\frac{1}{2} \end{pmatrix}^2 \begin{Bmatrix} j_2 & j_3 & S \\ J & 1 & j_1 \end{Bmatrix}^2 \ , \tag{12}$$

$$x_{nS}^{n+2J} = \frac{2J+1}{2S+1} \sum_{j_1 j_2} (2j_1+1)R_1(j_1)(2j_2+1)R_1(j_2) \begin{pmatrix} j_2 & j_1 & 1 \\ \frac{1}{2} & -\frac{1}{2} & 0 \end{pmatrix}^2 \Delta(S1J) \ . \tag{13}$$

The notation of spins involved is depicted in Fig. 2.

By solving the set of master equations, we get the time integrals of the occupation probabilities,

$$\tau(i,E,J,n) = \int_0^\infty P(i,E,J,n,t)\mathrm{d}t \ , \tag{14}$$

which are essential in calculations of spectra, cross sections, and other interesting quantities. Thus, the angle-integrated energy spectrum of γ's or particles emitted from the originally created composite system ($i = 0$) at its initial excitation energy E_c is

$$\left(\frac{\mathrm{d}\sigma_x}{\mathrm{d}\epsilon_x}\right)_0 = \sum_{J_c,n} \sigma(E_c,J_c)\tau(0,E_c,J_c,n)\lambda_x([0,E_c,J_c,n] \xrightarrow{\epsilon_x} [\text{anything}]) \ . \tag{15}$$

Here, $\sigma(E_c,J_c)$ is the cross section of a creation of the composite system. The full γ and/or particle production spectrum is obtained by the summation over all nuclei within the reaction chain and an integral over all possible excitation energies E,

$$\frac{\mathrm{d}\sigma_x}{\mathrm{d}\epsilon_x} = \sum\!\!\!\!\!\!\int_{E,J,J_c,n,i} \sigma(i,E_c,J_c,E,J)\tau(i,E,J,n)\lambda_x([i,E,J,n] \xrightarrow{\epsilon_x} [\text{anything}]) \ . \tag{16}$$

Here, $\sigma(i,E_c,J_c,E,J)$ represents the population cross section of a nucleus with the excitation energy E and spin J, when the original composite system was created with the cross section $\sigma(E_c,J_c)$. The population cross section incorporates the preceding history of the system by cascade deexcitation and particle emissions before the present emission.

One should emphasize that our approach differs significantly from the standard one. Commonly, only the particle emission is (or could be) considered to proceed at the pre-equilibrium stage of the reaction (even that applies often to the first emitted particle only), and the weaker (and therefore also slower) γ emission is considered to occur already from an equilibrated compound nucleus. The only exception from this simple rule is the calculation of the hard γ emission in reactions without (or prior to) the particle emission, like (n,γ) and/or (p,γ) ones. In this paper, however, all the emission, both that of particles and of γ's, is considered consistently within the pre-equilibrium formalism. Our approach obviously incorporates the equilibrium (compound nucleus) emission as its natural limit, and — in practice — a significant portion of the emission occurs at or very close to the equilibrium stage.

All what has been said above is fully valid for both continuum and discrete γ emission. There is no artificial difference between the two, both are described in the same way. The continuum states are spreaded over all allowed exciton states and distributed over spins; the discrete states often prefer a specific information in all variables (one usually specifies the spin and eventually also the corresponding exciton (quasiparticle) number in addition to the energy of a given state).

4 Parameters

The initial configuration to be used for the calculations is generally accepted to be $n_0 = A_{proj}$. This means $n_0 = 1$ for nucleon-induced reactions (on an even-even target). Thus, both the direct and semi-direct terms of the nucleon capture are effectively described within the pre-equilibrium statistical formalism. We pay for this consistency of description by some loss of

detailed information, which could be employed in more refined microscopic models (as e.g. the DSD model is), but not so easily in a phenomenological model.

The second quantity to be fixed is the intensity of intranuclear transition rates (eq. (5)). To do that we have used the average squared matrix element of the residual interaction $|M_{nonspin}|^2$ of spin-independent calculations according to the parametrization of Kalbach [7], where it depends on the per exciton excitation energy, $e = E/n$. The value of $K' = 100$ MeV^3 has been found to yield reasonable results [8]. The squared matrix element $|M|^2$ for the spin version of the model is established from the condition [2]

$$|M|^2 < X_{nJ}{}^{\downarrow} >= |M_{nonspin}|^2 \ , \tag{17}$$

where the averaging is performed over J This procedure ensures consistency of nucleon emission spectra obtained in both the spin and the nonspin versions of calculations. The condition (17) is evaluated at $n = 3$, the most dominant exciton state for the nucleon emission in nucleon-induced reactions. We adopt the same approach of fixing the value of the matrix element for other reactions as well.

In our calculation, a simple equidistant-spacing scheme of states has been used with $g = A/13$; the pairing corrections have not been considered here. The spin cut-off parameter has been taken in the form of Herman and Reffo [9]

$$\sigma_n{}^2 = (0.24 + 0.0038E)nA^{2/3}. \tag{18}$$

The particle trasmission coefficients were approximated by the use of formulae by Murthy et al. [10]. Similarly, the γ photoabsorption cross section is used in the Lorentzian form

$$\sigma_{GDR}(\epsilon_\gamma) = 53.2\text{mb}\ \frac{NZ}{A}\frac{\Gamma^2}{(\epsilon_\gamma{}^2 - E_{GDR}{}^2)^2 + \epsilon_\gamma{}^2\Gamma^2} \ , \tag{19}$$

with peak energy [11]

$$E_{GDR} = 29\sqrt{(1 + 2/A^{1/3})/A^{1/3}} \tag{20}$$

and width $\Gamma = 5$ MeV.

As the aim of our present study was to demonstrate the influence of the proper spin description on the calculated quantities, we did not adjust the parameters as to be able to follow the data more closely, but we simply preferred their global (*a priori*) values.

5 Results and discussion

The first comparison of spin-dependent and spin-independent formulation has been presented in [2]. It was based only on the primary γ contribution to the γ emission from the original composite system of ^{56}Fe+n, mainly that from the lowest exciton state. The conclusion therein (and till now the only pre-equilibrium one) reported only negligible differences between the two calculations for the case studied. Today, spin effects in the pre-equilibrium decay are one of topical items (see e.g. the recent paper by Chadwick et al. [12]).

Here, we have considered three reactions with projectiles at energies close to 14 MeV, namely those induced by 14 MeV neutrons on ^{56}Fe and ^{93}Nb and by 17 MeV ^{3}He on ^{93}Nb, to perform a comparison of spin-dependent and spin-independent versions of the pre-equilibrium exciton model. The first two reactions differ mainly by their target spin, which

(obviously) influences directly the spin distribution of the composite system. The target spins are 0^+ for ^{56}Fe, and $(9/2)^+$ for ^{93}Nb. The third reaction is not shown in detail herew. It differs from the two preceding by additional amount of angular momentum introduced by impacting ^{3}He, as well as by higher excitation energy (due to different binding of the projectile). The comparison of spin distributions in the initially created composite system is given in Fig. 3.

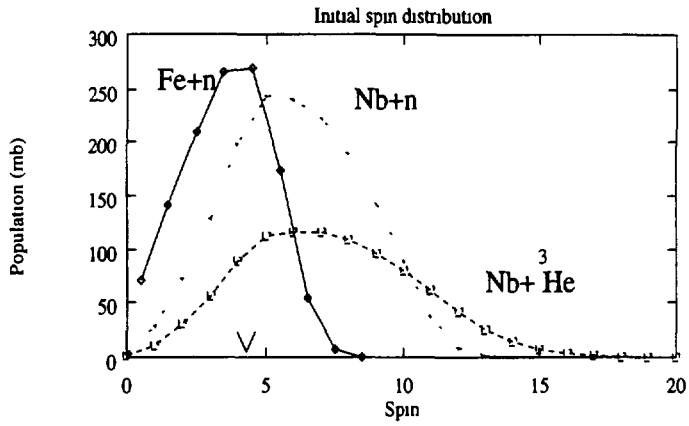

Figure 3: Initial spin distributions in three investigated reactions. The arrow denotes the Nb-target spin.

The inverse cross sections for both neutrons and protons were those obtained from a formula of Murthy et al. [10]. For a reference spin-independent calculation, we have used the PEQAG code [13], with properly adjusted input parameters, so that both the codes (PEGAS and PEQAG) should yield results very close one to the other. The only difference included is just the presence of spin coupling.

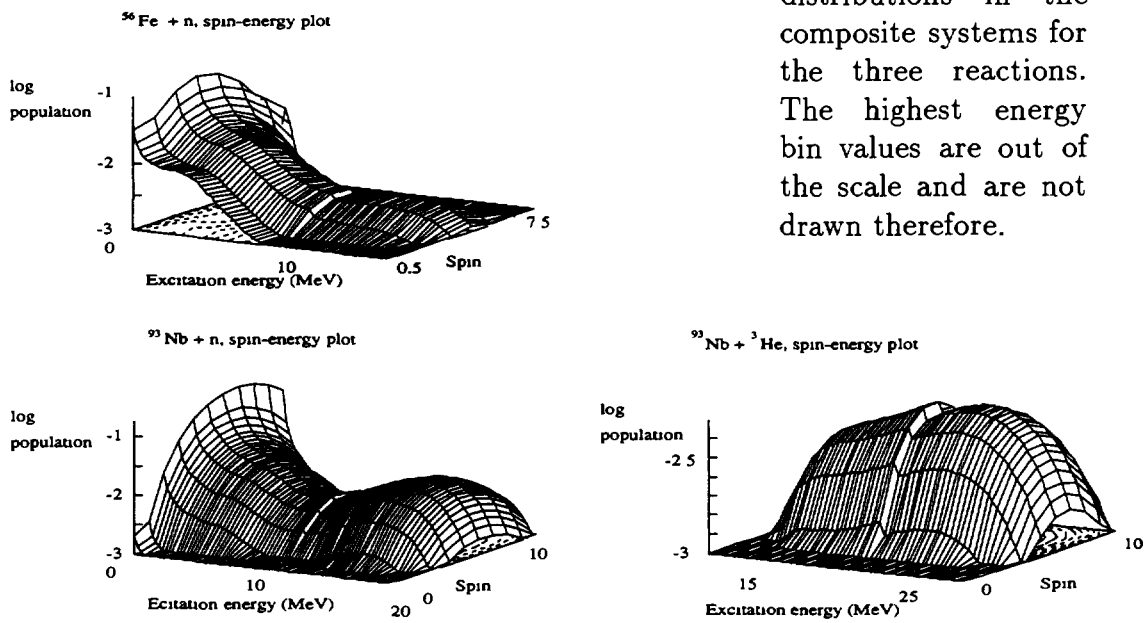

Figure 4: Spin-energy distributions in the composite systems for the three reactions. The highest energy bin values are out of the scale and are not drawn therefore.

Fig. 4 depicts spin-energy distributions as obtained within the equilibration process in a composite system prior to particle emission. The original excitation energy spin distribution (identical to that in Fig. 3) is not drawn, because it is several orders of magnitude higher than all the rest of the distibution. We see significant differences among all three participating systems, fully in accord with their specification.

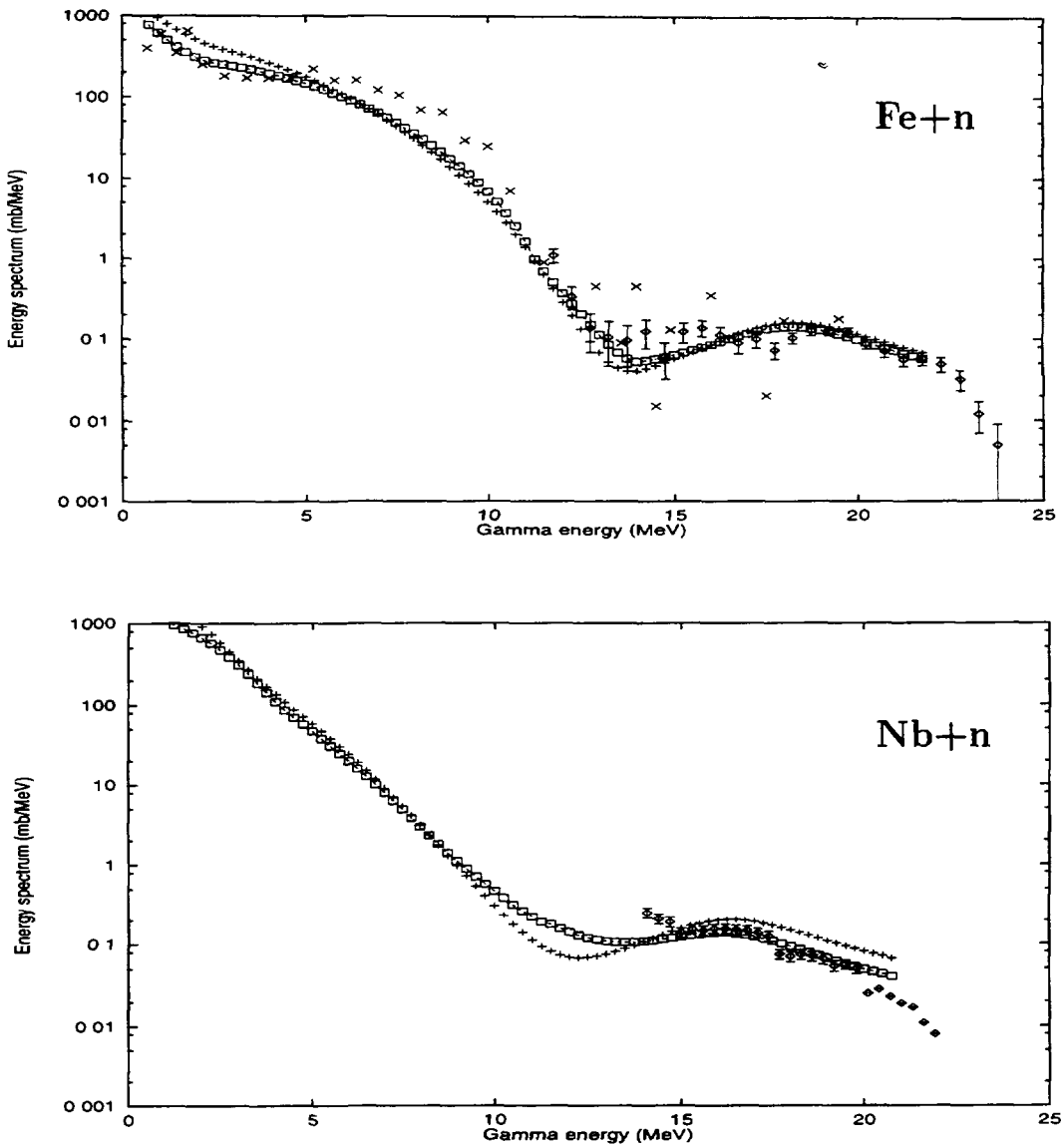

Figure 5: Gamma spectra from ^{56}Fe+n (upper part) and ^{93}Nb+n (lower part) at 14 MeV. The experimental data are drawn as isolated diamonds with errorbars (Fe+n: Ref. [14]; Nb+n: Ref. [15]) or $\times$'s (Fe+n, Ref. [16]). The spin-dependent calculations are drawn by squares; the spin-independent ones by +'s.

Figs. 5 brings the resulting γ energy spectra from two reactions, namely ^{56}Fe+n and ^{93}Nb+n at 14 MeV. They are a kind of *a priori* calculations, as there has been no free parameters: the matrix element and the initial exciton number were fixed from analyses of the nucleon emission (see the preceding chapter), and the γ calculation itself has been performed with the same values.

The influence of the spin coupling is negligible in ^{56}Fe+n (this confirm the earlier finding of Obložinský [2]), and more seen — though not yet a dramatic one — in the other reaction. The particle spectra (especially the proton ones), which are not a subject of this study, are however influenced more significantly (see [17]).

6 Conclusions

We have studied influence of the spin effects on the particle and γ spectra in three selected reactions at excitation energies of several tens of MeV. Whereas the presence of spin couplings yields no significant effect on the neutron (and γ) spectra at the reactions induced by neutrons at zero-spin target, departures from this condition give rise to significant effects, especially in the case of proton emission, where the effect can reach more than a factor of three in some cases.

Therefore, the further use of spin-independent calculations is a kind of oversimplification which may lead to improper results and it should be taken with extreme caution only.

The other areas of pre-equilibrium decay where a proper treatment of the angular momentum couplings are expected to be important, are the discrete γ transitions and consequently isomeric cross sections. Within other approaches, they have been studied in Ref. [12]; and the are one of our nearest aims within the pre-equilibrium exciton model with full account of the spin couplings.

Acknowledgements
The work has been supported in part by International Atomic Energy Agency contract No. 7811/RB. The author is indebted to P. Obložinský for valuable discussions.

References

[1] E. Běták and P. Obložinský, *Code PEGAS*, Report INDC(SLK)-001 (IAEA Vienna 1993).

[2] P. Obložinský, Phys. Rev. **C35** (1987), 407.

[3] C.K. Cline, Nucl. Phys. **A193** (1973), 417.

[4] E. Běták, Comp. Phys. Comm. **9** (1975), 92.

[5] E. Běták and J. Dobeš, Phys. Lett. **84B** (1979), 368.

[6] J.M. Akkermans and H. Gruppelaar, Phys. Lett. **157B** (1985), 95.

[7] C. Kalbach, Z. Phys. **A287** (1978), 319.

[8] F. Cvelbar and E. Běták, Z. Phys. **A332** (1989), 163;
F. Cvelbar, E. Běták and J. Merhar, J. Phys. **G17** (1991), 113.

[9] M. Herman and G. Reffo, *in* Nuclear Level Densities Bologna 1989 (World Scientific, Singapore 1992), p. 103.

[10] K.H.N. Murthy, S.K. Gupta and A. Chatterjee, Z. Phys. **A305** (1982), 73; E **A307** (1982), 374.

[11] S.A. Fayans, lecture (1982).

[12] M.B. Chadwick et al., Phys. Rev. **C49** (1994), R2885.

[13] E. Běták, *Code PEQAG*, Report INDC(CSR)-016/LJ (IAEA Vienna 1989).

[14] M. Budnar et al., Report No. INDC(YUG)-6/L (IAEA Vienna 1979).

[15] F. Rigaud et al., Nucl. Phys. **A173** (1971), 551.

[16] S. Hlaváč and P. Obložinský, Report No. INDC(CSR)-5/GI (IAEA Vienna 1983).

[17] E. Běták and P. Obložinský, *in* Proc. 7th International Conference on Nuclear Reaction Mechanisms, Varenna 1994 (Ed. E. Gadioli). Univ. Milano, 1994, p. 186.

PRESENT STATUS OF EXPERIMENTAL GAMMA-RAY STRENGTH FUNCTIONS

J. KOPECKY

Netherlands Energy Research Institute ECN, P.O. Box 1,
1755 ZG Petten, The Netherlands

M. Uhl

Institut für Radiumforschung und Kernphysik,
Universität Wien, A-1090 Wien, Boltzmanngasse 3, Austria

ABSTRACT

Earlier compilations of photon-strength functions, based on experimental data from resonance- or thermal-neutron capture and photonuclear reactions, have been reviewed and updated with recent data. The assigned f_{E1} and f_{M1} uncertainties are discussed, especially those due to uncertainties of relevant quantity such as the s-wave spacing D_0 and in the absolute calibration of the radiative capture width Γ_γ. Possible corrections due to strong non-statistical contributions are discussed. Derived systematics of f_{E1} and f_{M1} values as a function of atomic mass A are reviewed in view of their use in statistical-model calculations.

1. Introduction

The compound nucleus mechanism is dominant for the neutron capture process up to several MeV incident neutron energy. Therefore the statistical model is generally used to describe and calculate the (n,γ) cross sections and spectra for these energies. An exception to this can occur in thermal and resonance regions (thus at low neutron energies) in mass regions, where non-statistical processes (potential and valence capture) may become important.

The γ-ray transmission coefficient T_{XL}, usually used in the model calculations, is related to the γ-ray strength function f_{XL} as

$$T_{XL}\ (E_\gamma) = 2\pi\ E_\gamma^{2L+1}\ f_{XL}(E_\gamma), \qquad (1)$$

where E_γ is the γ-ray energy and L indicates the multipolarity of the radiation. Therefore both theoretical and experimental knowledge of γ-ray strength functions is a very important ingrediant for description and calculation of photon-production data in all reaction channels, not only for the (n,γ) reaction. The impact of different theoretical formulations of E1, M1 and E2 gamma-ray strength functions on the statistical model calculations have been recently studied in several publications[1-7].

In this study we concentrate on experimental γ-ray strength functions, collected over a period of about 40 years and based on measurements of partial radiative widths $\Gamma_{\gamma i}$. Such data originate from three different experiments. Most of the data are derived from **discrete resonance-capture** experiments using the method of slow neutron time-of-flight spectrometry. In some cases, the **thermal neutron-capture data** can be used, however, with some restrictions. The last source of data is set of the **photonuclear data**. Common in the analysis of all these experiments is a need to average over Porter-Thomas fluctuations, which govern the distribution of partial radiative widths.

The first compilation of McCullagh et al.[8] included about 50 nuclides with absolute partial widths originating from (n_{res},γ) and (γ,n) reactions, selected from data published before 1980 and averaged over the observed resonances. These data were analysed in the frame of model dependent (single-particle model and Brink-Axel approximation) strength functions for E1 and M1 radiation. The mean energy for this data set was about 7 MeV. From fits to these data Kopecky[9] derived global formulae for the additional dependence of f_{E1} and f_{M1} on the mass A compared to the above models. We prefer the model independent definition of strength functions for dipole radiation, written as

$$f_L(E_{\gamma i}) = \langle \Gamma_{\gamma i}/E^3_{\gamma i} \rangle \times 1/D_0 . \qquad (2)$$

A first update of this data set was made by Kopecky and Uhl[10] in 1990. In their study a few new data have been added and the general reliability of the data was addressed. It has been noticed that for a meaningful application of the experimental $f_L(E_{\gamma i})$ values in the statistical-model calculations it is necessary to check (and correct) the data for the presence of a non-statistical component in the total or partial radiative widths. Such corrections have not been applied yet and the use of data, if a non-statistical mechanism is strongly present in the resonance region, may lead to a significant overestimation of normalization in the calculation. The aim of this paper is to develop the γ-ray strength function systematics, based on the recently updated

set of experimental data. A further objective of this work is to address the accuracy and reliability of f_{XL} data in general in view of all possible sources of uncertainties.

2. Update, accuracy and revision of selected data

2.1 Data additions

The original set of data[8] has been extended with data published between 1981 and 1994 with, however, no claim on completeness. The recent extension includes resolved-resonance measurements[16-22], thermal-capture measurements[23-25] and photonuclear data[26-28].

Two comments should be made concerning the interpretation of **thermal capture** data in terms of strength functions. Firstly, Bollinger[29] has demonstrated that the distribution of γ-ray intensities following the thermal capture follows only approximately the Porter-Thomas distribution, and in cases that both spin components contribute in thermal region, the distribution should be intermediate between χ^2 distributions with one and two degrees of freedom. Secondly, the conversion of thermal γ-ray intensities into partial radiative widths is based on the average value of the total radiative width, as derived from all measured resonances. This quantity, especially if resonances in a wide energy region are considered, may not be a good representation of the radiave width for the thermal region. Three of such measurements have been included in our data set; we have selected only those where the authors derived the $f_{E1,M1}$ values by themselves[23-25]. However, it should be mentioned that a huge wealth of thermal capture data is available and it would certainly be worthwhile to consider making effort to convert well selected data into the γ-ray strength functions.

The final data sets of f_{E1} and f_{M1} values are listed in Table 1. In the original data[8], only a small number of minor corrections have been carried out, most of the data have been adopted without changes. Values for two different resonance spins, treated separately in Ref.[8], have been combined. Given errors include statistical, normalization (assumed 20%) and Porter-Thomas uncertainties. Data posterior to Ref.[8] have been adopted without changes and their origin is quoted in first column of Table 1 by their reference. Further, the number of resonances and γ-rays used in evaluation of $f_{E1,M1}$ values is quoted, just to indicate the quality of averaging.

Another assessment concerned the mean energy E_γ at which $f_{E1,M1}$ values have been derived. Following Eq. (1) only the partial E^3_γ reduction factor has been applied and no additional energy dependence was assumed. This is reasonably true if the

energy region is narrow and the additional energy dependence which comes from the E1(M1) giant-resonance model is negligible. The quoted $f_{E1,M1}$ value is then the mean value over all partial $f_{E1,M1}(E_{\gamma i})$ entries considered, assumed to correspond approximately to the mean value $\langle E_\gamma \rangle$. This energy is quoted in Table 1 between columns 1 and 2. An inspection of these values shows, that the majority of data do not significantly deviate from earlier quoted $\langle E_\gamma \rangle \simeq 6 - 7$ MeV. A fraction of the $f_{E1,M1}$ scatter may, however, stem from internal differences in distributions of partial data within the $\langle E_\gamma \rangle$ range. The only data outside 6 - 7 MeV to be considered are the actinide data with $\langle E_\gamma \rangle \simeq 4.2$ MeV. The energy correction due to additional energy dependence (e.g. assumed E^2_γ for E1 radiation) increases f_{E1} values by factor of 2.5. The global trend of $f_{E1,M1}$ data is, however, not significantly influenced due to a relatively small number of such data points, as was shown in Ref. [9].

2.2 Additional uncertainties in f_{E1} and f_{M1} values

In order to get a feeling for additional uncertainties, two of their main sources are discussed now in detail.

Firstly we review uncertainties in $f_{E1,M1}$ coming from the **s-wave resonance spacing D_0**. This quantity may severely influence the "experimental" $f_L(E_\gamma)$ values. Recent evaluations of D_0 values at ENEA Bologna, Obninsk and CNDS published in Refs.[11-13], compared to the original BNL evaluation[14] showed in several cases significant disagreements, despite the fact that a similar methodology (corrections for missed or wrongly assigned resonances), was applied. All D_0 evaluations[11-14] are quoted in columns 2 and 3 of Table 1 together with the value used in the original $f_{E1,M1}$ analysis. It turned out that in some cases an incorrect D_0 value was applied in the derivation of $f_{E1,M1}$ values and a correction is proposed here. A general word of caution, however, has to be given here. As an example of such significant differences the ^{93}Nb(n,γ) reaction can be mentioned. While values of D_0 = 37.8 eV, 44 eV and 45 eV have been deduced in Refs.[8,14,11], respectively, the evaluations[12,13] resulted in 90 eV and 105 eV. Additionally Vertes and Grigoriew[31] quoted the value of 67 eV. Thus the data differ by more than a factor of two.

The $f_{E1,M1}$ data may therefore be categorized into two groups, those with no significant differences among the derived D_0 values and consenquently with a small uncertainty due to resonance spacing and those where significant disagreement among D_0 values occurs. For the last group the additional uncertainty has to be considered and those data are labeled with "D_0" warning in Table 1 or a correction is proposed.

Special attention hasto be paid also to the **absolute calibration** of the radiative width and its accuracy. Several approaches have been applied in the experiments considered, such as **internal normalization** to a strong secondary transition in the spectrum studied or to well known values of the radiative width for individual resonances. As an **external normalization**, either measurements relative to the Au standard (4.9 eV resonance) have been used or measurements relative to well established thermal capture standards, such as e.g. Cl. Recently, Becvar et al.[15] developed a method of calibration relative to the 477 keV γ-line from the $^{10}B(n,\alpha)$ reaction by a simultaneous time-of-flight measurement of the target material with a thin layer of boron. Close inspection of available data, however, raised a suspicion that in many cases the accuracy associated with the normalization procedure is underestimated, with possible consequences for the derived $f_{E1,M1}$ values.

As an example the $^{150}Sm(n,\gamma)$ reaction can be mentioned. The γ-ray intensities, based on the experiment carried out at the BNL fast chopper, were calibrated by two different methods. In the original study[30] the absolute normalization against a secondary transition in the $^{150}Sm(n,\gamma)$ spectrum resulted in a value of $f_{E1} = 4.46(110)\ 10^{-8}\ MeV^{-3}$, while later a new calibration[20] against the boron 477 keV line, gave a value of $f_{E1} = 7.83(157)\ 10^{-8}\ MeV^{-3}$. Their difference lies outside the quoted errors. However, it has to be remembered that it is very difficult to judge the quality of internal calibration without reviewing the original experimental data and the corresponding calibration runs in detail. It seems that an error factor of f=1.5 is a reasonable estimate of the additional global calibration uncertainty.

2.3 Comments on non-statistical capture mechanism

Another inspection was considered for nuclides which can be influenced by a strong **E1 non-statistical component** present in the resonance region. This effect may explain some of the experimental f_{E1} values which significantly exceed values based on pure statistical contributions. Further it is of relevance how large their influence is on the global systematics of f_{E1} as a function of mass. In some data the size of the valence contribution has been discussed and estimated alrea- dy authors as referenced. Here we can list the following reactions: $^{91}Zr(\gamma,n)$, $^{92}Mo(n,\gamma)$, $^{101}Ru(n,\gamma)$, $^{198}Hg(n,\gamma)$ and $^{207}Pb(\gamma,n)$. For the mass region of the 3s-wave giant resonance, $40<A<60$, an estimate of approximately 50% valence contribution to the total radiative width can be quoted. This seems to be a reasonable guess based e.g. on calculations of Allen and Musgrove[32] and comparisons between Γ_γ(s-waves) and Γ_γ(p-waves) values in the above mass region, where the latter is assumed to have a pure statistical nature.

Similar enhancements of E1 radiation may be expected in the 3p-(4s-) giant resonance regions (90<A<110 and 140<A<200).

For nuclides, with very limited number ($\leq$3) of primary transitions (e.g. ground-state transitions), the value of the derived strength function may not be reliable and not representative for the statistical capture, even if a relatively sufficient number of resonances was used for averaging. These transitions may still carry the simple (single-particle) structure through several resonances.

For M1 radiation the situation is more complicated. There is no general theoretical explanation of the non-statistical mechanism, despite the fact that these effects have been experimentally observed (see e.g.[33,34]).

3. Discussion of data

3.1 E1 radiation

All surveyed data with their original values, denoted according to their experimental origin, are displayed in Fig.1 together with a least-squares fit of a power dependence on mass number A (solid curve). Data follow reasonably well the expected smooth global trend with two exceptions, where some deviations above the general scatter of data may be considered. These large deviations belong to data in mass regions with A<40 and 170<A<210. There is no difference detected in data trend among the three experimental methods applied. For indication how the extension and revisions of tha data set have influnced the general trend in f_{E1} data, the fitted curve from 1981[9] is plotted in Fig.1 for a comparison.

Reasons for a large scatter of the low-mass data (A<40) can be surely attributed to an insufficient averaging together with pronounced single-particle character of many transitions. However, it seems that their mean value reasonably represents the general trend, as expected from the other data. The situation in the mass region with 170<A<210 is more complex. Several strongly enhanced data points can be explained by the presence of a non-statistical mechanism, in particular those around the double-closed shell region. However, this enhancement is not a general feature of all data, some values seem to follow the general trend, as determined by data from the mass region with 100<A<170. It is noticed, that the general data scatter around the trend curve in Fig.1 can be characterised by a uncertainty factor of **k**=2, which leaves about 10% of data points outside the uncertainty band (see Fig. 1).

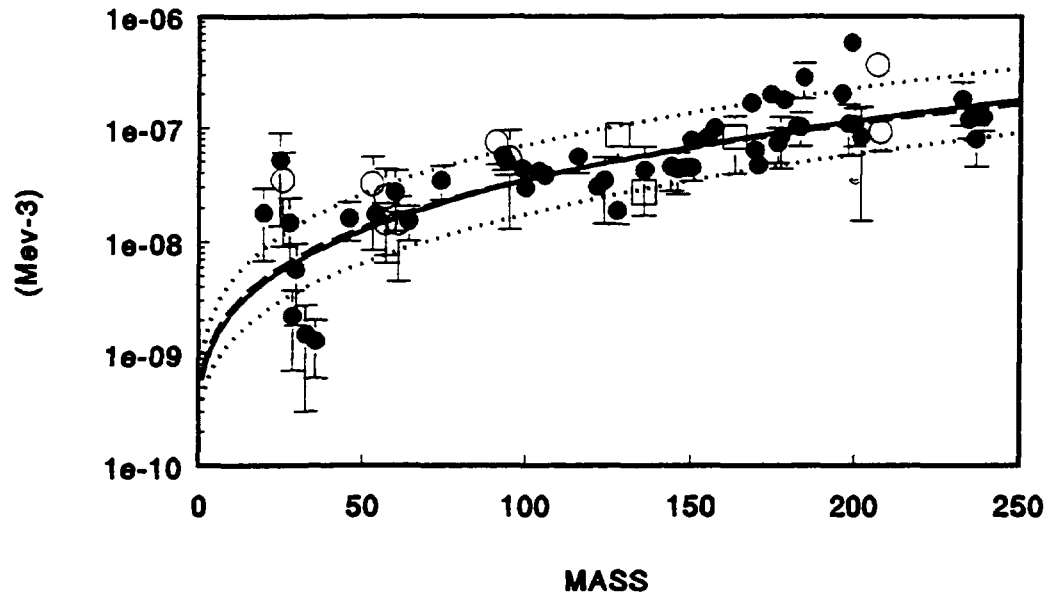

Fig. 1 Plot of f_{E1} values [full circles (n_{res},γ), open circles (γ,n) and squares (n_{th},γ)] against the mass number. The full curve represent a LSQ fit to recent data, the fit from 1981[9] is denoted by the dashed curve. Dotted curves display an uncertainty band with **k**=2 (see Eq. (4)).

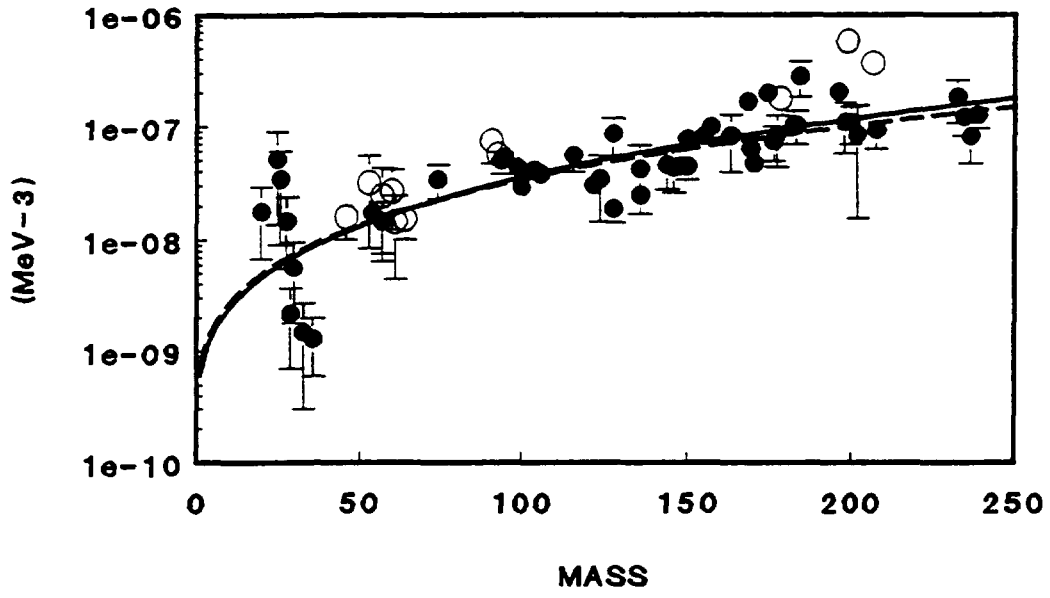

Fig. 2 The same as Fig.1, the open circles denote entries with nonstatistical contributions. The dotted curve results from a LSQ fit to only statistical data (full cirles), while the full curve stems from Fig. 1.

This data scatter probably masks the expected enhancement of f_{E1} values in other mass regions (see Sect. 2.3). This is demonstrated in Fig.2, where data with well established non-statistical contributions have a tendency to lay in the upper half of the data band. It turns out, however, that these non-statistical data influence very little the overall trend and fit to the f_{E1} values. This can be seen in Fig.2, where the fit to data without those labeled as "nonstat" is drawn and differs negligibly from the fit to all data.

A substantial fraction of this scatter can be certainly attributed to uncertainties (see Section 2.2) and to an insufficient averaging of Porter-Thomas fluctuations. All facts discussed above suggest that extensions and changes in basic data including recent revisions (D_0 revi- sions, see comments in Table 1) have a very small influence on global behaviour of f_{E1} values and their fit.

3.2 M1 radiation

For M1 radiation, the situation is more complicated for several reasons. The systematic behaviour of the M1 strength function (see Fig.3) shows a similar mass dependence as E1 radiation. These data, however, are scarce and statistically less accurate, often based on inadequate averaging. The uncertainty representing data scatter, determined in a similar way as for E1 radiation with about 10% data points outside, amounts to a factor of three (see Fig.3). The curve fitted to data available in 1981 (Ref.[9]) differs very little from the present fit.

There is no well established general theoretical expression for f_{M1}. The frequently used single-particle estimate is at variance with a finite energy-weighted sum rule and is also ruled out by the observed mass dependence. The recently proposed giant resonance model[35], based on the Brink hypothesis and the spin-flip M1 resonance, lacks a global description of the sum rule. The data display also some effects, which may be attributed to a non-statistical origin. Some of the enhanced data seem to cluster in a gross structure but a clear identification is difficult. However, their influence on the general trend is marginal, as can be seen in Fig. 4. Only in two original references the nonstatistical origin of data was identified.

4. Recommended systematics

It was shown that there has been no significant influnce on the global trend of the fitted strength functions as a function of mass by updating the basis data set since 1981. It was shown further that this global trend is also not in-

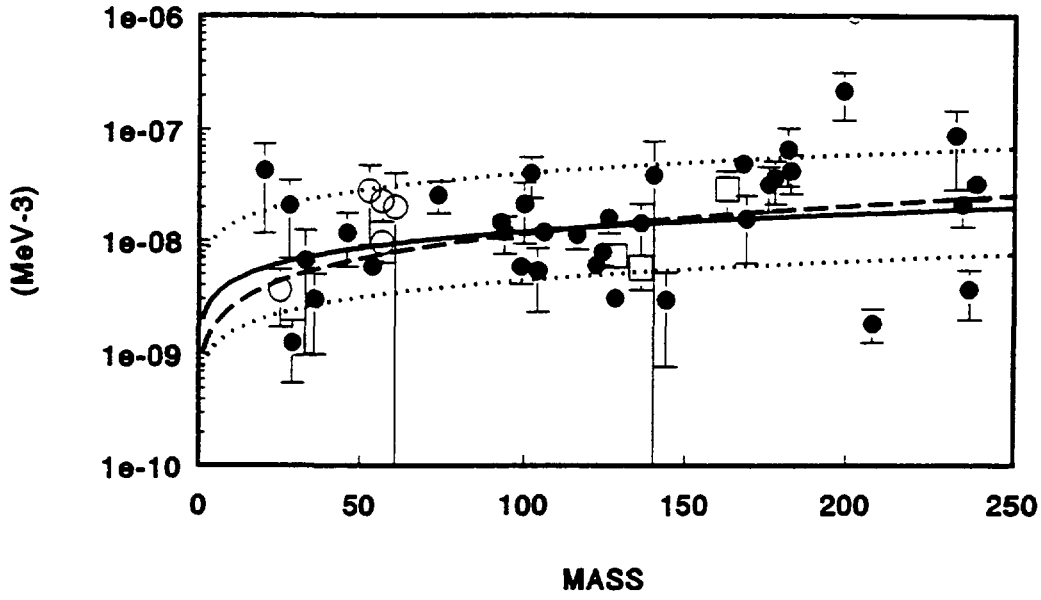

Fig. 3 Plot of f_{M1} values, the uncertainty band has a value of k=3 (used symbols are the same as in Fig.1).

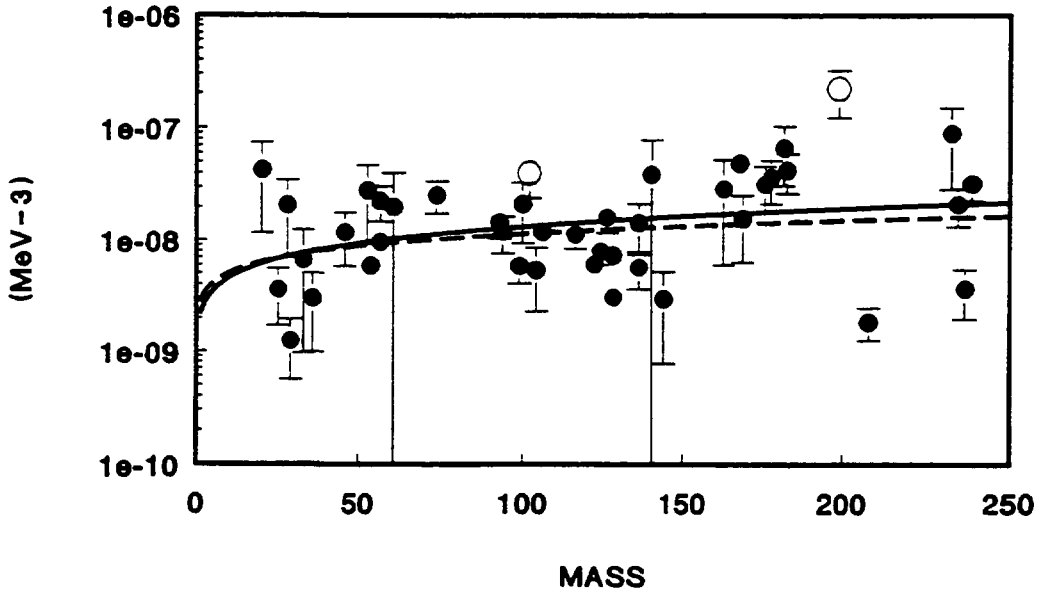

Fig. 4 Non-statistical f_{M1} data, used symbols as in Fig. 2

fluenced by data enhanced by non-statistical effects. The general reason for this is that the associated individual errors, dominated by Porter-Thomas uncertainties, are sometimes comparable to these effects and that the number of non-statistical entries is relatively small. Therefore we have decided to apply only corrections to the those D_0 values in the original entries, which were obviously wrong. These changes are documented in Table 1. The least-square fit to these data resulted in a recommended **experimental (trend) systematics**, which reads as

$$f_{E1}\ (exp) = 9.23\times10^{-11}\ A^{1.34\pm0.14}\ ,$$
$$f_{M1}\ (exp) = 1.58\times10^{-9}\ \ A^{0\ 47\pm0\ 21}\ . \qquad (3)$$

These expressions are recommended for estimates of $f_{E1,M1}$ values in calculation normalizations if the neutron binding energy is not too much different from a value of 6 to 7 MeV. The associated uncertainty factor **k**, defined as

$$f_{E1,M1}/k < f_{E1,M1} < kf_{E1,M1}, \qquad (4)$$

has been proposed in Sect. 3.1 and 3.2 and amounts to **k** = 2(3) for E1(M1) radiation, respectively. These, to some extent arbitrarily chosen uncertainty factors, agree reasonably with asociated errors of the **A** power as derived from the least-squaresd fit, resulting in **k** values 2.1 and 2.9.

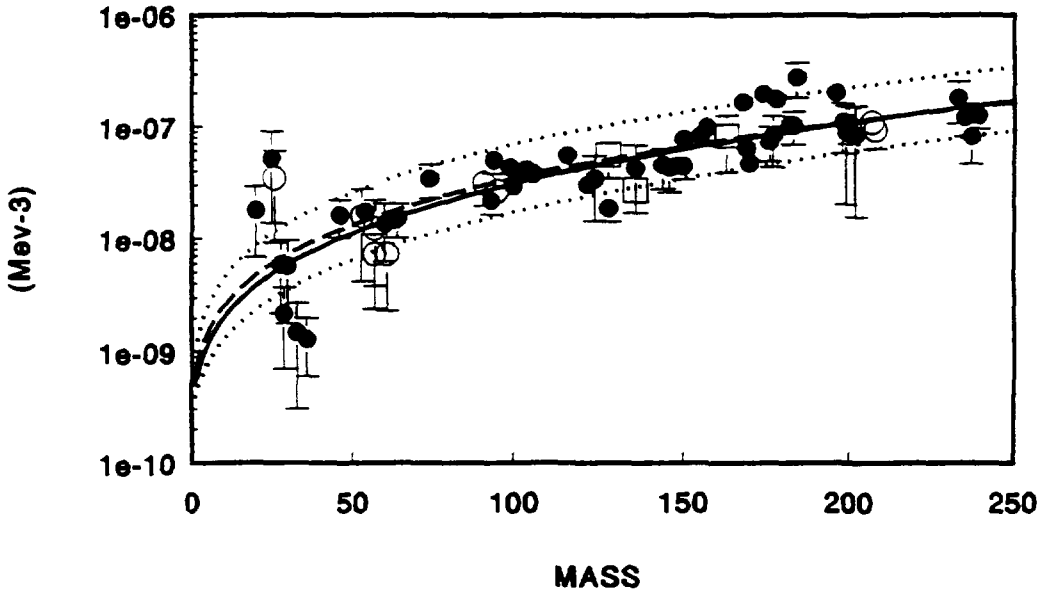

Fig. 5 The f_{E1} data corrected for non-statistical contributions (see Table 1). Fit to these data is denoted by the dashed curve, the other symbols as in Fig. 1.

In the second phase we made an attempt, only for f_{E1}, to produce a set of data representing pure E1 statistical components. Applied corrections for non-statistical contributions have in many cases a rather subjective character, based on an educated guess and should not be taken as a proper quantitative treatment. This exercise resulted in more smoothed data but with a little influence on the global trend. The corrected data are again documented in Table 1 and displayed in Fig.5.

5. Comparison with model predictions

The standard method to relate the surveyed data to model predictions is to display the C/E values from the model considered for comparison. We have chosen, as in all earlier studies, the standard Lorentzian, with an energy independent width, as explored in the Brink hypothesis[36]. Applied parameters of the E1 giant resonance were taken from Dietrich and Berman[37] or, if not available, deduced from the neighbouring isotopes.

There has been longstanding evidence that this formulation overestimates the large body of experimental data both from discrete-resonance and averaged-resonance capture experiments (e.g.[35,38]) and also other pertinent quantities such as $\langle\Gamma_\gamma\rangle$, σ_γ and $d\sigma_\gamma/dE$ (see e.g. refs.[1-7]). If, from obvious reasons, the data below A = 40 and around A $\simeq$ 50 are neglected (nonstatistical region), this overestimation is also confirmed for f_{E1} values as demonstrated in Fig. 6. Additionally, the C/E values have a similar behaviour[1-7] as found for the radiative width $\langle\Gamma_\gamma\rangle$, the σ_γ cross section and the γ-ray spectra $d\sigma_\gamma/dE$, namely, a clear overestimation for mass regions $90<A<150$ and above A = 190, and a reasonable agreement with the standard Lorentzian prediction for the deformed rare-earth region with $150<A<180$.

It has been shown[1-7] that this overestimation is removed by adopting a generalized Lorentzian with an energy dependent width. However, a problem, as mentioned above, remained in the mass region above A = 150, where the modified Lorentzian underestimated the experimental data and in fact the standard Lorentzian gave a reasonable agreement. This was a surprising result especially because it abruptly disappeared at A=180. In order to maintain the global applicability of the physically-sound generalized Lorentzian formulation, Uhl and Kopecky[4-7] introduced an empirical enhancement factor k_0. The size of the enhancement has been determined by a simultaneous adjustment of a large number of calculated $\langle\Gamma_\gamma\rangle$, σ_γ and $d\sigma_\gamma/dE$ in the mass region $90 < A < 210$ against the experimenetal data. This adjustment resulted in a **purely empirical** expression as a function of mass (see Refs.[7,39] for details)

$$k_0(A) = 1.0 \quad \text{for } A \leq 148, \qquad (5)$$
$$= 1.0 + 0.09(A-148)^2\exp[-0.18(A-148)] \quad \text{for } A \geq 148.$$

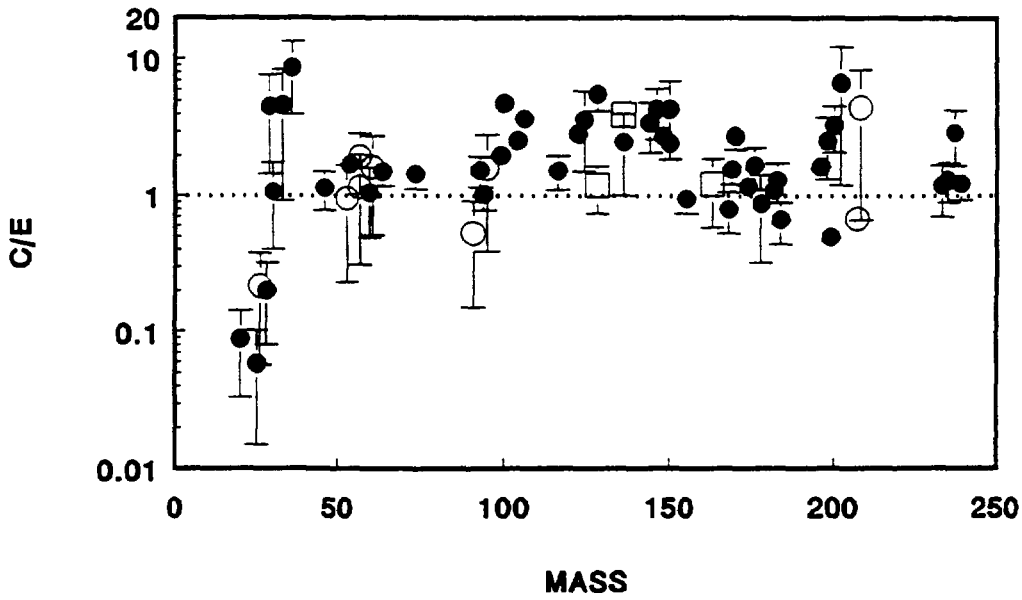

Fig. 6 Ratio of calculated (standard Lorentzian) and experimental f_{E1} values plotted against the mass number.

This enhancement (about factor 2 to 3) remained hidden within the scatter of the present experimental strength function data. However, it seems that it is possible to detect it and explain it globally from the distribution of the total radiative widths. The updated data base of $\langle\Gamma_\gamma\rangle$ (s-wave) values is displayed in Fig. 7 as a function of neutron number. Inspection of these data, plotted with a smooth trend curve, shows three distinct regions of enhanced $\langle\Gamma_\gamma\rangle$ values, which correspond to well established non-statistical regions. Two of them are the well known double magic number regions with A=50-60 and A=200-210, corresponding to the 3s- and 4s-giant resonances in the s-wave neutron strength functions. The less distinct enhancement lies just above A=150 and is again associated with the non-statistical capture in the lower part of the double-humped 4s-giant resonance.

For a graphical comparison with our previous results on these enhancement[7,38], we have plotted the experimental $\langle\Gamma_\gamma\rangle$ values in the discussed mass region together with the calculated enhanced values of $\langle\Gamma_\gamma\rangle$. This calculation was based on application the enhancement factor, as derived in Eq.(5), on

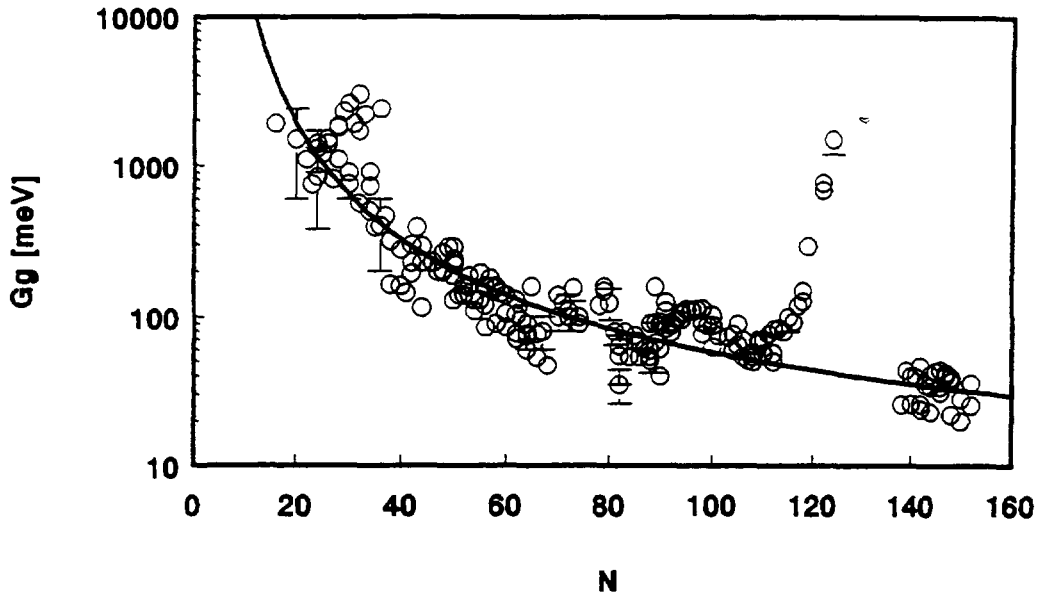

Fig. 7 The average measured s-wave neutron radiative widths plotted against the neutron number. The solid curve is an eyeguide to the trend systematics.

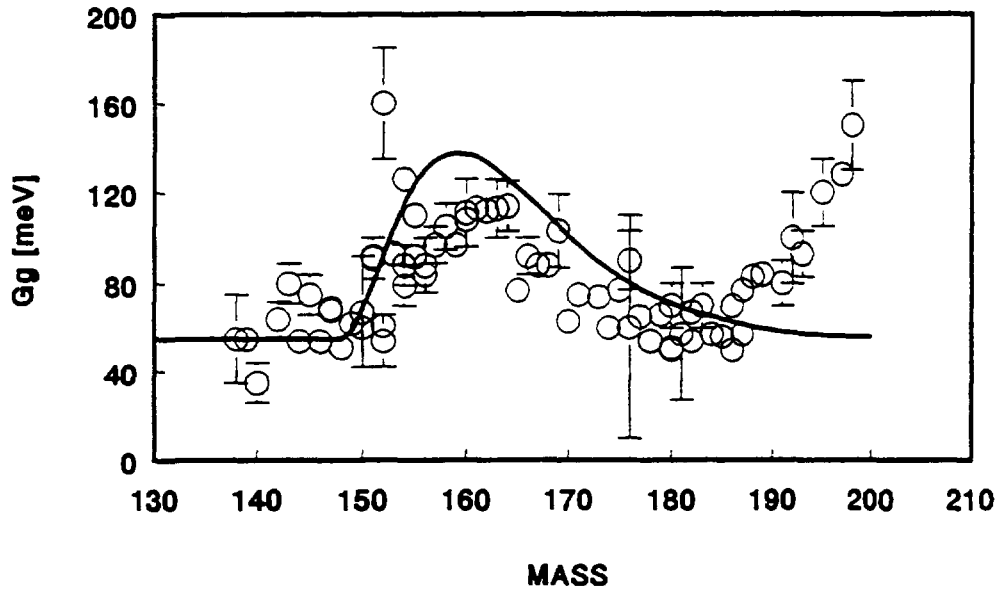

Fig. 8 The f_{E1} enhancement factor (from Ref.[7,39]) plotted together with $\langle\Gamma_\gamma\rangle$ values from Fig. 7 around the rare-earth mass region.

the mean value of $\langle\Gamma_\gamma\rangle$ = 60 meV for nuclides with A $\leq$ 148. The results displayed in Fig. 8 show a very nice agreement and support the explanation of this effect by a global enhancement of the total radiative width in the reaction mechanism.

6. Conclusions

1. The original experimental data set for E1 and M1 gamma-ray strength functions[8] has been reviewed, and extended by recent data. The resulting f_{E1} and f_{M1} values show a smooth increasing dependence on mass A, different to that expected from the single-particle model. Together with an additional energy dependence above the E^3 phase-shift factor (as detected in many averaged-resonance capture experiments), it may be concluded that the use of single-particle model should be disregarded for both E1 and M1 radiation.

2. The data fluctuations around the fitted systematics are dominated by a combined effect of experimental uncertainties (including the averaging properties) and uncertainties in D_0 values, their possible corrections are discussed and in several cases applied. The size of these fluctuations complicates the interpretation of individual data in terms of statistical and non-statistical components, however, a global trend of these effects is detected.

3. The resulting set of f_{E1} values generaly underestimates the predictions by the standard Lorentzian, as expected from previous studies. This behaviour forms a global argument for the use of the generalised Lorentzian with the energy-dependent width. The enhancements of E1 radiation above this model in mass regions 50<A<60 and 150<A<170, which influnces all quantities such as f_{E1}, $\langle\Gamma_\gamma\rangle$, σ_γ and $d\sigma_\gamma/dEm$ may be attributed to global non-statistical effects. However, it is not exluded that some of the $\langle\Gamma_\gamma\rangle$ enhancements are due to experimental effects.

4. For practical applications in statistical model calculations, the experimental ratio of $\langle\Gamma_\gamma\rangle/D_0$ is probably the best normalization check. The derived systematics of f_{E1} and f_{M1}, if necessary combined with the trend in E1/M1 ratios, can be used as a reasonable approximation of the strength functions in model calculations, if experimental values are not available.

7. References

1. J. Kopecky and M. Uhl, *Phys. Rev.* **C41** (1990) 1941.
2. M. Uhl and J. Kopecky, *Proc. IAEA Specialists' Meeting on the Measurement, calculation and Evaluation of Photon Production Cross Sections*, February 5-5, 1990, Smolenice (CSFR), INDC(NDS)-238 (1990) p. 113.
3. J. Kopecky and M. Uhl, *Proc. 7th Int. Symposium on Capture Gamma-Ray Spectroscopy and Related Topics*, Asilomar 1990, (AIP New York 1991) AIP Conf.Proc. No. 238, p.607.
4. M. Uhl and J. Kopecky, *Proc. Int. Conf. Nuclear Data for Science and Technology*, Jülich 1991, (Springer Verlag, Berlin/Heidelberg, 1992), p. 977.
5. J. Kopecky and M. Uhl, *Proc. Int. Symposium on Nuclear Data Evaluation Methodology*, Brookhaven 1992, (World Scientific, Singapore, 1993), p.381.
6. J. Kopecky, M. Uhl and R.E. Chrien, *Phys. Rev.* **C47** (1993) 312.
7. M. Uhl and J. Kopecky, *Proc. Int. Conf. Nuclear Data for Science and Technology*, Gatlinburg 1994, to be published.
8. C.M. McCullagh, M. Stelts and R.E. Chrien, *Phys. Rev.* **C23** (1981) 1394.
9. J. Kopecky, *Neutron-Capture Gamma Ray Spectroscopy and Related Topics 1981*, (The Institute of Physics, Bristol and London, 1982), p. 423.
10. J. Kopecky and M. Uhl, *Proc. IAEA Specialists' Meeting on the Measurement, Calculation and Evaluation of Photon Production Cross Sections*, February 5-7, 1990, Smolenice (CSFR), INDC(NDS)-238 (1990) p. 103.
11. Huang Zhongfu, Zhao Zhixiang and Zhou Delin, *Com. of Nuclear Data Progress*, **No 9** (1993) 60.
12. A.V. Ignatyuk et al., INDC(CCP)-320 (1990) 25, and private communication.
13. G. Reffo, ENEA Bologna, private communication.
14. S.F. Mughabghab, M. Divadeenam and N.E. Holden, *Neutron Cross Sections*, (Academic Press, New York, 1981 and 1984), **Volume 1**, Part A and B.
15. F. Becvar et al., *Journal of Nuclear Physics (Russian)*, **44** (1986) 3.
16. O. Shahal, S. Raman, G.G. Slaughter, C. Coceva and M. Stefanon, *Phys. Rev.* **C25** (1982) 1283.
17. S. Kahane, S. Raman, G.G. Slaughter, C. Coceva and M. Stefanon, *Phys. Rev.* **C30** (1984) 807.

18. C. Coceva, M1 transitions from p-wave neutron resonances of ^{53}Cr, *Contr. to the 8th International Symposium on Capture Gamma-ray Spectroscopy and Related Topics*, Fribourg (Switzerland), September 20-24, 1994.
19. C. Coceva, Radiative transitions from neutron capture in ^{53}Cr resonances, to be published in Il Nuovo Cimento A, 1994.
20. F. Becvar et al., *Journal of Nuclear Physics (Russian)*, **46** (1987) 3.
21. F. Becvar, *Capture Gamma Ray Spectroscopy 1987*, (Institute of Physics Conference Series 88, Institute of Physics, Bristol, 1988) p.649 and private communication.
22. F. Becvar et al., *Proc. of the Int. Conference on Neutron Physics*, Kiev (USSR), 2-6 October, 1983, p.8.
23. M.A. Islam, T.J. Kennett and W.V. Prestwich, *Z. Physik*, **A 335** (1990) 173.
24. M.A. Islam, T.J. Kennett and W.V. Prestwich, *Phys. Rev.*, **C42** (1990) 207.
25. H.H. Schmidt et al., *Nucl. Phys.* **A 504** (1989) 1 and F. Becvar, private communication.
26. C. Coceva, Y.K. Ho, M. Magnani, A. Mauri and P. Bartolomei,*Capture Gamma Ray Spectroscopy 1987*, (Institute of Physics Conference Series 88, Institute of Physics, Bristol, 1988) p.676.
27. C. Coceva, Y.K. Ho, M. Magnani, A. Mauri and P. Bartolomei, idem., p.679.
28. C. Coceva, private communication.
29. L.M. Bollinger, *Phys. Rev.* **C3** (1971) 2071.
30. F. Becvar, R.E. Chrien and O.A. Wasson, *Nucl. Phys.* **A236** (1974) 198.
31. P. Vertes and Y.V. Grigoriew, *Proc. Int. Conference on Nuclear Data for Science and Technology*, Mito, Japan, 1988 (Saikon Publ. Co., Tokyo 1988) p. 623.
32. B.J. Allen and A.R. Musgrove, *Adv. Nucl. Phys.*, Vol. **10** (Plenum, New York 1978) p. 129.
33. C.F. Clement, A.M. Lane and J. Kopecky, *Phys. Lett.* **71B** (1977) 10.
34. R.E. Chrien and J. Kopecky, *Phys. Rev. Lett.* **39** (1977) 911.
35. J. Kopecky and R.E. Chrien, *Nucl. Phys.* **A468** (1987) 285.
36. D.M. Brink, Ph.D. Thesis, Oxford University, (1955).
37. S.S. Dietrich and B.L. Berman, *At. Nucl. Data Tables* **38** (1989) 199.
38. S. Raman, *Neutron-Capture Gamma Ray Spectroscopy and Related Topics 1981*, (The Institute of Physics, Bristol and London, 1982), p. 357.
39. M. Uhl and J. Kopecky, Contr. *IAEA RCM Meeting on Deve lopment of Reference Input Parameter Library for Nuclear Model Calculations of Nuclear Data* , Bologna (Cervia), September 19-23, 1994, to be published.

Table 1. Compilation and revisions of experimental values for gamma-ray strength functions f_{E1} and f_{M1} based on s-(p-) wave neutron capture and photonuclear data.

FN [Ref.] Reaction #res/E1/M1 <$E_{\gamma E1}/E_{\gamma M1}$>	D_0 [eV] Applied in [Ref.]	[2] [3] [4] [5]		$f(E1)^{bc}$	$f(M1)^{bc}$
				[10-8 MeV^{-3}]	
	Revision comment		f^a	Revised values	
F -20	33200	-		1.80(112)	4.26(310)
[1]		200000			
(n,γ)		-			
2/5/3 <4.4>		-			
	D_0 uncertainty				
Mg-25		143500			0.36(19)
[9]		220000			
(γ,n)		120000			
14/1 <8.5>		-			
Mg-25	143000	143500		5.17(380)	
[1]		220000			
(n,γ)		120000			
1/4 <6.0>		-			
Mg-26		-		3.46(255)	
[1]		-			
(γ,n)		14000			
6/1 <11.1>		-			
Al-28	19970	-		1.48(92)	2.08(139)
[1]		54000			
(n,γ)		32000			
2/5/2 <6.6/6.9>		64300			
	D_0 = <50000>		0.40	0.59(37)	0.83(66)
Si-29	40000	-		0.22(15)	0.125(70)
[1]		135000			
(n,γ)		-			
2/5/2 <6.0/5.4>		-			
	D_0 uncertainty				
Si-30	100000	-		0.57(39)	
[1]		-			
(n,γ)		-			
1/2 <6.9>		-			
S -33	203000	17000		0.15(12)	0.66(57)
[1]		60000			
(n,γ)		17000			
1/4/3 <7.5>		-			
	D_0 = 17000		11.9	1.79(143)	7.88(681)

Cl-36	24500	21000	0.13(7)	0.30(20)
[1]		18000		
(n,γ)		28000		
1/9/5 <7.2/5.4>		8428		
		D_0 uncertainty		
Sc-46	1300	1300	1.61(59)	1.17(59)
[1]		1280		
(n,γ)		-		
2/13/9 <7.0/7.2>		1450		
Cr-53		42000	3.19(235)	2.80(188)
[1]		40000		
(γ,n)		45000		
21/1/1 <7.9/7.9>		-		
#5(E1)16(M1) Nonst. effects		0.5	1.60(118)	
Cr-54	7100	7100	1.74(20)	0.59(6)
[12]		6330		
(n,γ)		7100		
23/33/31 <6.7/6.7>		6550		
		Nonst. effects/Averaging		
Fe-57		17000	2.46(181)	2.25(78)
[1]		23000		
(γ,n)		25000		
15/1/1 <7.7/7.7>		-		
#8(E1)7(M1) Nonst. effects		0.5	1.23(99)	
Fe-57		17000	1.46(70)	0.96(33)
[10]		23000		
(γ,n)		25000		
32/1/1 <7.8/7.8>		-		
#14(E1)18(M1)Nonst. effects/Averaging				
Co-60	1060	1100	2.70(146)	
[1]		1560		
(n,γ)		1100		
1/8 <7.0>		1340		
		Nonst. effects	0.5	1.35(73)
Ni-61		16000	1.46(101)	2.00(108)
[1]		13900		
(γ,n)		-		
23/1/1 <7.8/7.8>		14935		
#7(E1)16(M1) Nonst. effects		0.5	0.73(50)	
Cu-64	629	320	1.53(52)	
[1]		504		
(n,γ)		1040		
3/9 <7.5>		1452		

Ge-74	76	82		3.44(115)	2.57(82)
[1]		40			
(n,γ)		82			
5/7/7 <7.1/7.9>		165			
Zr-91		6400		7.48(281)	
[1]		7800			
(γ,n)		8600			
32/1 <7.2>		10500			
Nonst. effects			0.42	3.14(118)	
Nb-94	37.8	44		5.04(124)	1.20(44)
[1]		45			
(n,γ)		90			
7/15/16 <6.5/6.5>		105			
D_0 = 67 eV			0.5	2.84(70)	0.68(25)
Mo-93	1000	2100		5.67(147)	1.46(42)
[1]		1630			
(n,γ)		3600			
8/10/9 <6.6/6.2>		3000			
Nonst. effects			0.20	1.13(29)	
D_0 = <2580>					
Mo-95		975		5.38(41)	
[13]		749			
(γ,n)		1150			
NA/1 <7.3>		2265			
Nonst. effects			0.50	2.69(20)	
Mo-99	429	970		4.32(81)	0.59(18)
[1]		703			
(n,γ)		970			
17/7/8 <5.5/5.5>		-			
Ru-100	31.4	25		2.97(41)	2.12(118)
[1]		14.5			
(n,γ)		17.6			
4/5/10 <6.9/7.4>		26			
Ru-102	24.6	16			4.00(160)
[1]		13.4			
(n,γ)		18			
6/5 <7.8>		94			
Enhanced trans.			0.62		2.46(98)
Rh-104	23.2	16		4.13(33)	0.54(31)
[1]		18			
(n,γ)		31			
6/4/2 <6.9/6.9>		-			
Pd-106	11.9	10		3.79(87)	1.19(27)
[1]		10.2			
(n,γ)		10.3			
8/10/12 <7.0/7.9>		13			

In-116	9.5	9.4	5.56(159)	1.13(30)
[1]		11		
(n,γ)		9.4		
31/12/12 <5.9/6.1>		9.3		
Sb-122	13.5	18	3.05(61)	0.61(12)
[1]		14.1		
(n,γ)		18		
12/9/9 <6.1/5.9>		18.5		
Sb-124	20.7	38	3.48(203)	0.79(20)
[1]		26.9		
(n,γ)		38		
4/11/13 <5.6/5.8>		42		
Te-126	38	38		1.60(44)
[1]		37		
(n,γ)		48		
6/10 <7.7>		56.25		
I -128	13.3	9.7	1.88(46)	0.31(5)
[1]		15.7		
(n,γ)		14.5		
8/7/12 <6.5/6.5>		15		
I -128	9.7	9.7	8.64(329)	0.73(13)
[14]		15.7		
(n,γ) thermal		14.5		
0/11/20 <6.5/6.5>		15		
D_0 = <15>		0.65	5.59(213)	0.47(9)
Ba-136	47.6	40	4.23(254)	1.40(70)
[1]		38		
(n,γ)		40		
6/1/4 <6.6/7.9>		-		
Ba-136	40	40	2.7(7)	0.57(21)
[15]		38		
(n,γ) thermal		40		
0/16/16 <6.5>		-		
Nd-144	44.6	45	4.59(181)	0.30(22)
[1]		24		
(n,γ)		36.5		
10/3/1 <6.6/6.3>		40		
Nd-146	18.7	22	4.31(171)	
[1]		17.5		
(n,γ)		17		
10/2 <6.7>		20		
Sm-148	5.7	5.7	4.5(9)	
[16]		5.8		
(n,γ)		4.7		
12/16 <6.6>		6.9		
Sm-150	2.3	2.2	4.46(110)	
[1]		3.1		
(n,γ)		1.9		
3/31 <6.3>		2.45		
Sm-150	2.2	2.2	7.83(157)	
[17]		3.1		
(n,γ)		1.9		
7/13 <6.5>		2.45		

Gd-155	14.5	14.5	8.3(17)	
[18]		16.5		
(n,γ)		14.5		
15/8 <5.9>		-		
Gd-157	37.8	37.8	10.0(18)	
[17]		44.0		
(n,γ)		38.0		
NA/5 <6.0>		-		
Er-168	3.8	4.0	16.7(152)	4.9(5)
[8]		4.5		
(n,γ)		4.6		
45/6/4 <6.4/6.4>		-		
Er-169	94	94	6.39(147)	1.57(95)
[1]		94		
(n,γ)		100		
7/26/9 <4.9/5.2>		-		
Dy-163	55	64	8.3(4.4)	2.9(1.3)
[19]		51		
(n,γ) thermal		64.6		
0/9/7 <5.5/5.3>		82		
Tm-170	7.3	7.3	4.72(101)	
[1]		9		
(n,γ)		7.3		
9/16 <5.9>		16.5		
Lu-176	3.47	3.45	7.41(251)	3.19(139)
[1]		3.2		
(n,γ)		3.6		
11/8/2 <5.8/5.8>		-		
Lu-177	1.7	1.7	8.46(410)	
[17]		1.8		
(n,γ)		1.7		
6/15 <5.9>		2.3		
Yb-174	7.8	7.8	20.0(33)	
[7]		-		
(n,γ)		7.8		
22/5/5 <6.3>		9.5		
Hf-178	2.5	2.4	17.77(335)	3.65(152)
[1]		2.5		
(n,γ)		2.4		
37/18/3 <6.5/6.2>		2.9		
Abs.cal.uncert.		0.5	8.89(168)	
Ta-182	4.5	4.17	10.47(157)	6.64(356)
[1]		3.96		
(n,γ)		4.4		
19/66/1 <5.2/4.3>		4.0		
W -183	66	66	10.25(338)	4.25(183)
[1]		61		
(n,γ)		66		
7/15/5 <5.2/4.7>		66.8		

W -184	12	12	28.14(970)	
[1]		13		
(n,γ)		13		
6/13 <6.3>		24		
	D_0 uncertainty			
Pt-196	16.3	18	20.31(257)	
[1]		16		
(n,γ)		18		
22/9 <7.0>		15.4		
Au-198	16.2	16.5	11.00(530)	
[1]		15.6		
(n,γ)		16.5		
4/5 <6.4>		16.75		
Hg-199	83	105	58.08(445)	22.1(155)
[1]		93		
(n,γ)		105		
2/3/41 <6.5/5.2>		93.65		
	3 enh.trans.	0.15	8.71(67)	
Hg-200	88.1	100	10.91(404)	
[1]		75		
(n,γ)		100		
3/9 <7.2>		88.3		
Hg-202	100.5	98	8.47(693)	
[1]		126		
(n,γ)		-		
3/3 <7.2>		97.8		
Pb-207		35700	36.61(261)	
[1]		15100		
(γ,n)		37100		
11/1 <7.1>		-		
	Nonst. effects	0.3	10.98(78)	
Pb-208		37500	9.37(800)	0.185(60)
[1]		38000		
(γ,n)		36000		
10/1/1 <7.5/7.6>		-		
	#3(E1)#7(M1) Nonst. effects			
Th-233	18.2	16.8	18.30(766)	8.88(602)
[1]		16.5		
(n,γ)		16.8		
5/3/1 <4.2/4.5>		16.55		
U -235	12.3	10.6	12.14(392)	2.11(78)
[1]		11.8		
(n,γ)		10.6		
4/53/19 <3.9/4.4>		12.15		
U -237	15.4	14.7	8.16(352)	0.37(17)
[1]		15.7		
(n,γ)		15		
7/2/3 <4.6/4.8>		16.45		

U- 239	16.4	20.9	12.74(314)	3.22(96)
[1]		21.2		
(n,γ)		21.7		
23/9/5 <4.1/4.2>		22.3		

FN - final nucleus
D_o values are quoted in the order of:
BNL[14], CNDC[11], Obninsk[12] and ENEA Bologna[13]
[a] Correction factor
[b] Given errors are in quadrature added statistical, normalizations (20%) and Porter-Thomas uncertainties.
[c] The origin of data is the reference quoted in the first column.

In the last line of data sections a comment is given on the quality of data treatment in original references (if doubts exist) and the revised value is presented (if strong arguments for revision exist).

EVALUATED GAMMA-RAY PRODUCTION DATA OF JENDL-3.2

K. SHIBATA, S. IGARASI* and T. ASAMI**

Nuclear Data Center
Japan Atomic Energy Research Institute
Tokai-mura, Ibaraki-ken 319-11, Japan

ABSTRACT

The second revision of JENDL-3 contains gamma-ray production data for 66 nuclides. Evaluated quantities are emitted gamma-ray spectra, production cross sections and multiplicities in the incident neutron energy-range from 10^{-5} eV to 20 MeV. Except for light nuclides, statistical-model calculations were mainly used to obtain these quantities. The evaluated data are presented by comparing with measurements and with other evaluated data libraries.

1. Introduction

The third version of Japanese Evaluated Nuclear Data Library (JENDL-3)[1] was released in 1989. It contained neutron-induced reaction data for 171 nuclides among which gamma-ray production data were stored for 59 nuclides. After slight modification and addition of 172 FP nuclides, the first revision of JENDL-3 (referred to as JENDL-3.1) was made available in 1990. The JENDL-3.1 gamma-ray production data have been used for shielding and nuclear heating calculations, and it was found that some improvements should be needed. There were several problems concerning the gamma-ray production data. A big problem was related to energy balance of capture reactions at thermal energy. Most of the gamma-ray production data were evaluated by using statistical-model calculations, and energy balance was automatically preserved in that case. At thermal energy, however, the calculated data were replaced with experimental data for many nuclides, and total energy was not necessarily conserved. Another problem is concerned with discrete gamma-rays from inelastic scattering to low-lying levels of natural elements. According to the policy of the JENDL-3 project, elemental data of structural materials should be prepared for user's convenience as well as isotopic data. To achieve this, the discrete gamma-rays due to each isotope were embedded in continuum spectra which are represented in a finite energy bin. In other words, sharp discrete lines were somewhat smeared with a finite energy interval. This treatment was

---

* Nuclear Energy Data Center
** Data Engineering, Ltd.

however found to be inadequate from the analysis[2] of an integral experiment[3] performed at KfK. The gamma-ray production data in JENDL-3.1 have been thoroughly re-examined, and some problems were resolved. The revised data were included in the second revision of JENDL-3 (JENDL-3.2) which was released in June 1994.

JENDL-3.2 contains gamma-ray production data for 66 nuclides, which are listed in Table 1. This paper describes the evaluation method of the JENDL-3.2 gamma-ray production data and presents several results of cross sections and spectra.

Table 1 Nuclides for which gamma-ray production data are stored in JENDL-3.2

^{1}H	^{3}He	^{6}Li	^{7}Li	^{9}Be	^{10}B	^{11}B	^{12}C	^{14}N	^{15}N	^{16}O
^{19}F	^{23}Na	Mg	^{27}Al	Si	^{28}Si	^{29}Si	^{30}Si	^{31}P	S	K
Ca	^{40}Ca	Ti	^{51}V	Cr	^{55}Mn	Fe	^{54}Fe	^{56}Fe	^{57}Fe	^{58}Fe
^{59}Co	Ni	^{58}Ni	^{60}Ni	Cu	^{63}Cu	^{65}Cu	Zr	^{93}Nb	Mo	Ag
^{107}Ag	^{109}Ag	Cd	Eu	Hf	^{174}Hf	^{176}Hf	^{177}Hf	^{178}Hf	^{179}Hf	^{180}Hf
^{181}Ta	W	Pb	^{204}Pb	^{206}Pb	^{207}Pb	^{208}Pb	^{209}Bi	^{235}U	^{238}U	^{239}Pu

*) The nuclide without a mass number stands for a natural element.

2. Light Nuclides

2.1. Radiative Capture

For very light nuclides up to carbon, neutron capture reactions play a significant role in gamma-ray production, together with inelastic scattering to several discrete levels. In the low energy region, the capture cross section is assumed to have a dependence of $(E_n)^{-1/2}$, where E_n stands for an incident energy. On the other hand, the inverse reaction is used to evaluate the higher energy part of capture cross section if the measurements on (γ,n) reactions are available.

The capture cross sections of ^{3}He are shown in Fig. 1, where the JENDL-3.2 data are compared with those of ENDF/B-VI and with experimental data. In this case, experimental data are available in a wide energy range, and the evaluated data were obtained as follows:

$$\sigma_{n,\gamma}(E_n)=\frac{8.59\times10^{-6}}{\sqrt{E_n}}+6.37\times10^{-8}\sqrt{E_n}e^{-5.11\times10^{-4}\sqrt{E_n}}$$

,where $\sigma_{n,\gamma}$ and E_n are given in units of barn and eV, respectively. In the above equation, the second term indicates p-wave capture. It should be noted that the ENDF/B-VI data assume a straight line in the entire energy region. P-wave capture is also important in the evaluation of capture cross sections of ^{16}O. It is found from Fig. 2 that the recent measurements[4] indicate a dependence of $(E_n)^{1/2}$ above several tens of keV, while the old

data point is placed on the $(E_n)^{-1/2}$ line. In the energy region above 1 MeV, the JENDL-3.2 data were obtained by using the $^{17}O(\gamma,n_0)$ cross sections measured by Johnson et al.[5]

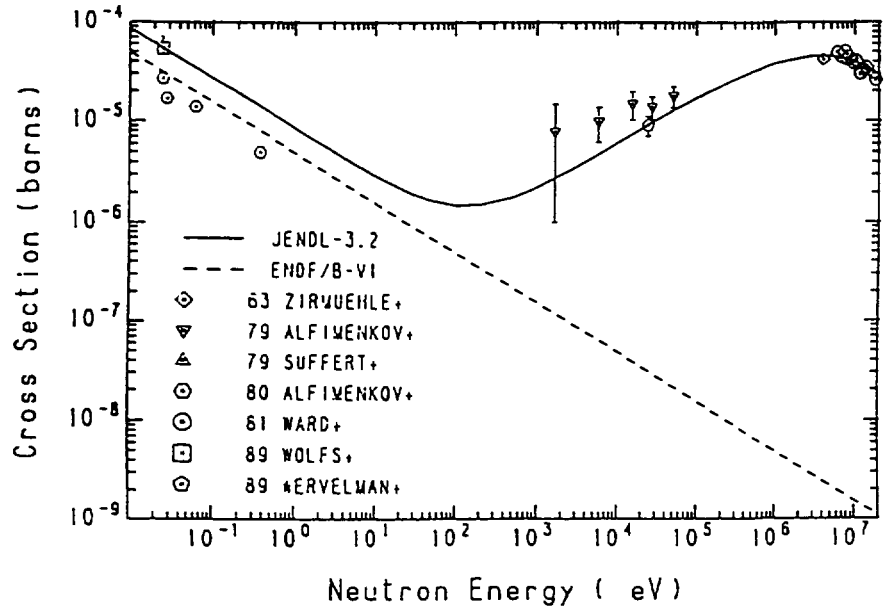

Fig. 1 $^{3}He(n,\gamma)$ reaction cross sections.

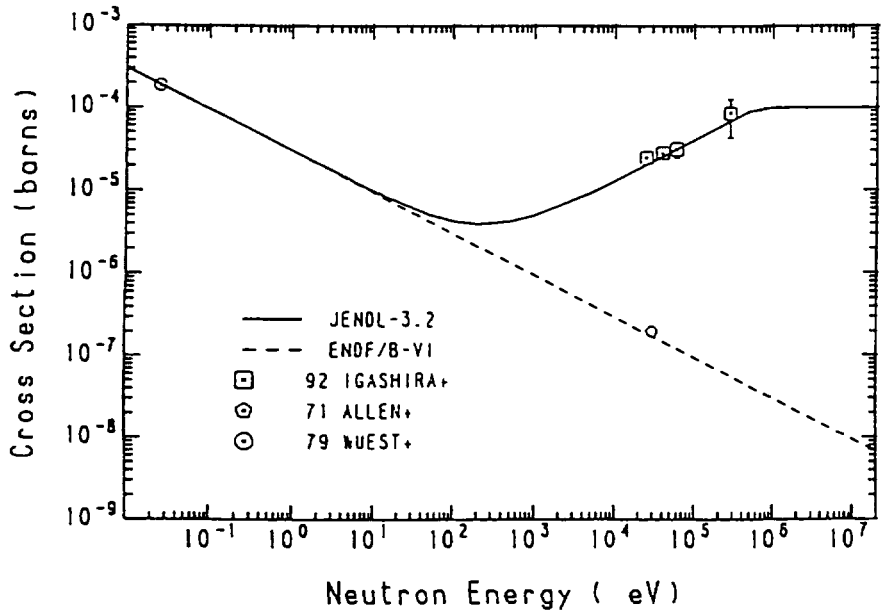

Fig. 2 $^{16}O(n,\gamma)$ reaction cross sections.

2.2. Inelastic Scattering to Discrete Levels

Figures 3 and 4 show (n,n'γ) cross sections of ^{7}Li and ^{12}C, respectively. In either case, there are a lot of experimental data although they are not shown in the figures. As for ^{7}Li only γ-ray measurements are available for this level, while both neutrons and γ-rays can be measured for the 4.439-MeV level of ^{12}C. A small difference between JENDL-3.2 and ENDF/B-VI is seen at the foot of a big resonance around 4 MeV in the case of ^{7}Li. It is found from Fig. 4 that the uncertainty of the evaluated data is relatively large concerning ^{12}C.

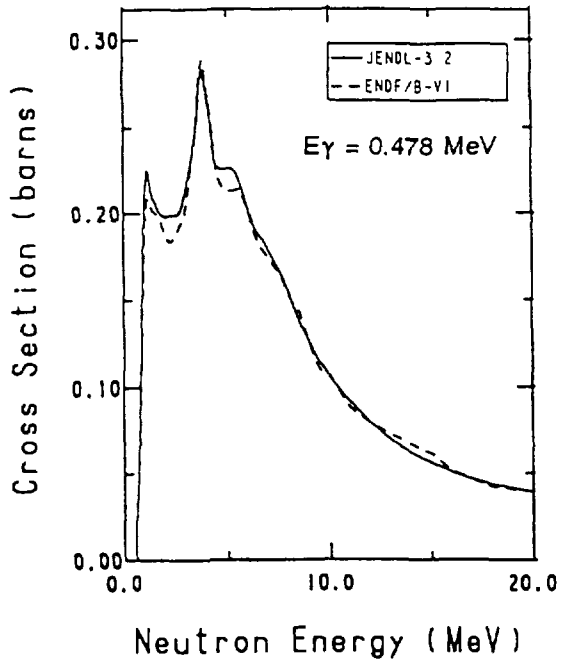

Fig. 3 ^{7}Li(n,n'γ) reaction cross sections.

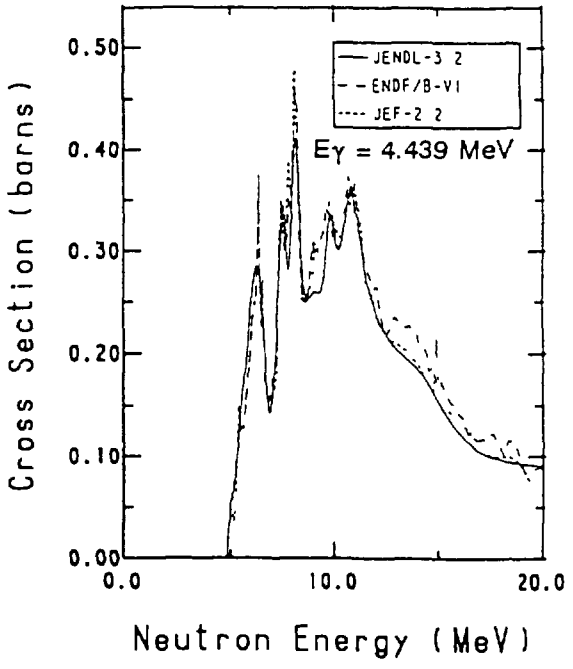

Fig. 4 ^{12}C(n,n'γ) reaction cross sections.

3. Structural-Materials

3.1. Statistical-Model Calculations

The evaluated gamma-ray production data of structural materials were obtained from statistical-model calculations using computer codes CASTHY[6], GNASH[7] and TNG[8]. The composite formula of Gilbert and Cameron[9] was used to represent level density. The profile function of giant dipole resonance is of the Brink-Axel[10] type, i.e., a Lorentzian shape.

In the previous version JENDL-3.1, the calculated thermal spectra were replaced with measured data after a benchmark test[11] had been done, since it was too difficult for the calculations to reproduce the measurements well. As a result of this replacement, total energy was not necessarily conserved at thermal energy. In the present JENDL-3.2, this drawback was removed by taking account of experimentally determined branching

ratios for primary transitions in the calculation of capture gamma-ray spectra. Evaluated thermal spectra from natural nickel are shown in Fig. 5, where the JENDL-3.1 data are based on the experimental data[12] measured at ORNL. It should be noted that the JENDL-3.2 data are almost consistent with those of JENDL-3.1 in this case. On the contrary, the natural zirconium data of JENDL-3.2 differ from those of JENDL-3.1, as seen in Fig. 6.

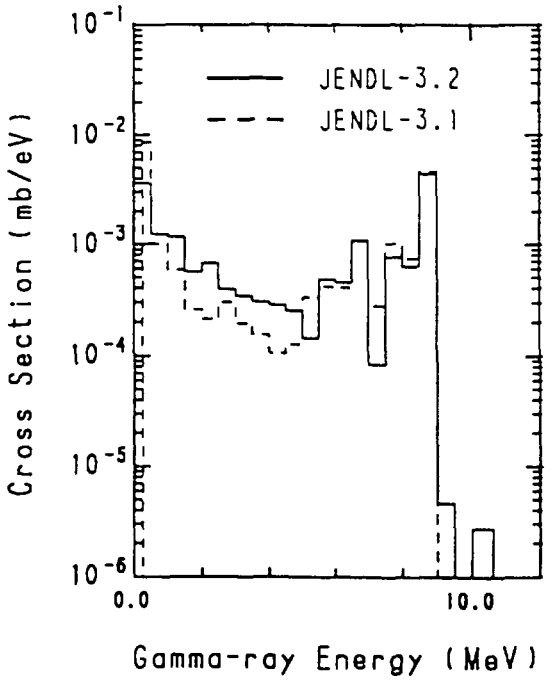

Fig. 5 Capture gamma-ray spectra from natural nickel at thermal energy.

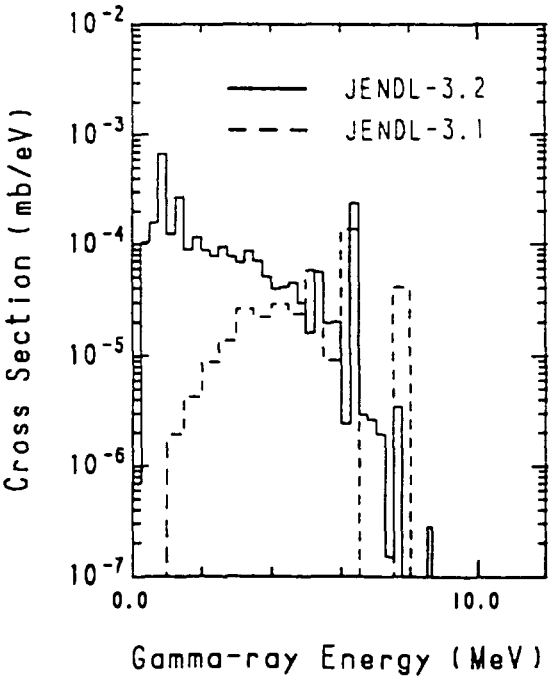

Fig. 6 Capture gamma-ray spectra from natural zirconium at thermal energy.

3.2. Data of Natural Element

According to the policy of the JENDL-3 project, data of natural element should be prepared for users' convenience. In the resonance region, capture reactions contribute to gamma-ray production. Therefore, gamma-ray multiplicities and spectra for a natural element were calculated from each isotope, and were given in MF/MT=12/102 and 15/102 of the ENDF format. Above the resonance region, all the contributions but inelastic scattering were combined into the nonelastic reaction (MT=3). In the JENDL-3.1 evaluation, the contributions from the inelastic scattering to discrete levels were also included in continuum spectra of the nonelastic reaction with a finite (~500 keV) energy bin. This treatment, however, caused a serious problem in the analysis[2] of leakage spectra from iron spheres measured[3] at KfK. The spectrum calculated from JENDL-3.2 reproduces an experimentally observed peak around 850 keV better than that of JENDL-3.1, as seen Fig. 7.

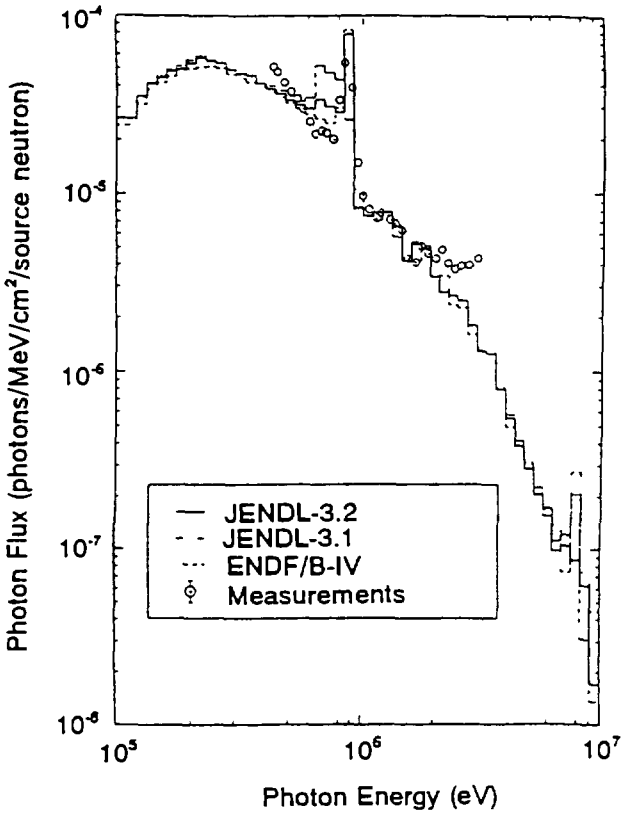

Fig. 7 Leakage spectra from an iron sphere (ref. 2).

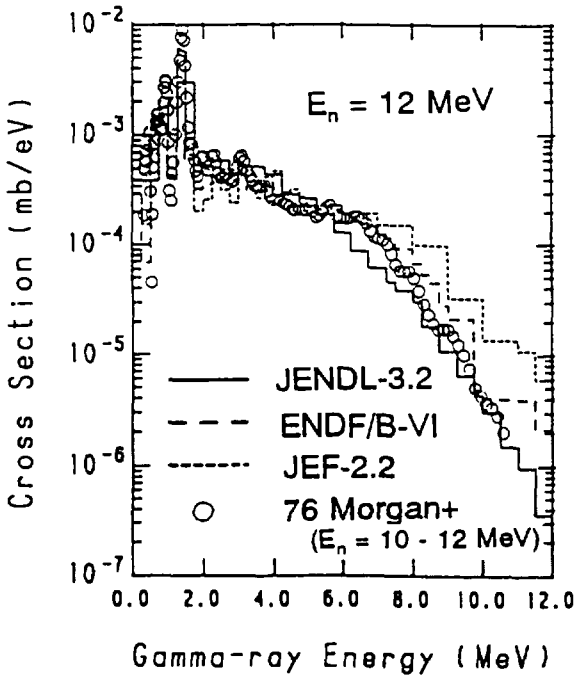

Fig. 8 ^{nat}Cr(n,xγ) spectra at 12 MeV.

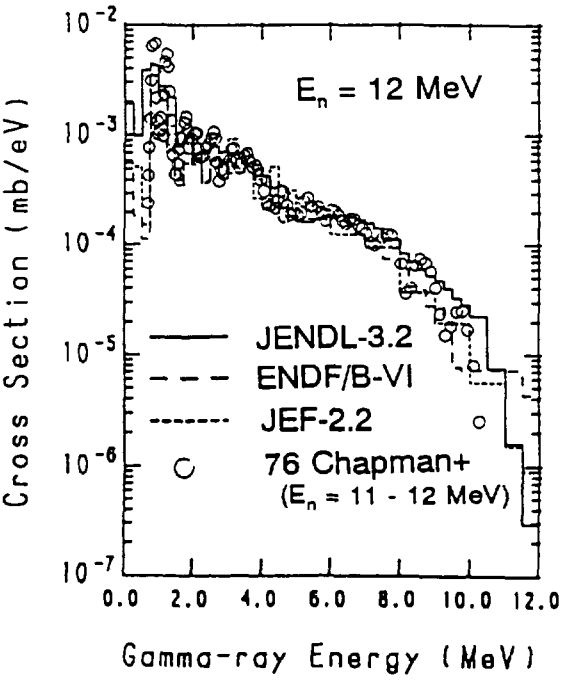

Fig. 9 ^{nat}Fe(n,xγ) spectra at 12 MeV.

3.3. Evaluated Cross Sections and Spectra

Evaluated gamma-ray spectra from natural chromium and iron at 12 MeV are shown in Figs. 8 and 9, together with measurements. In this comparison, the elemental data of ENDF/B-VI and JEF-2.2 were generated from major isotopes, i.e., ^{52}Cr, ^{53}Cr, ^{54}Fe and ^{56}Fe. Total gamma-ray production cross sections are compared with experimental data in Figs. 10 and 11. In these figures, the experimental data were obtained by multiplying the spectral measurements mentioned above by 4π, while the evaluated data were corrected for experimental cut-off energy of gamma-rays. As for chromium, all evaluated data are smaller than the measurements. On the other hand, the iron data of JENDL-3.2 are considerably larger than those of the other two libraries, although the measured data are consistent with JENDL-3.2.

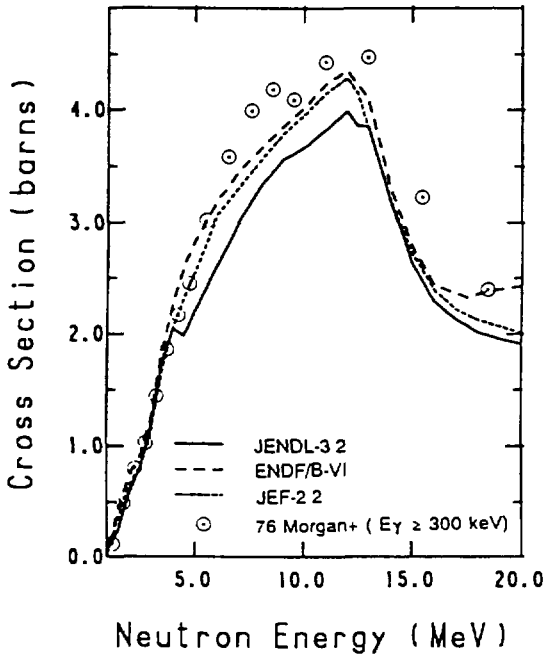

Fig. 10 Total gamma-ray production cross sections of ^{nat}Cr.

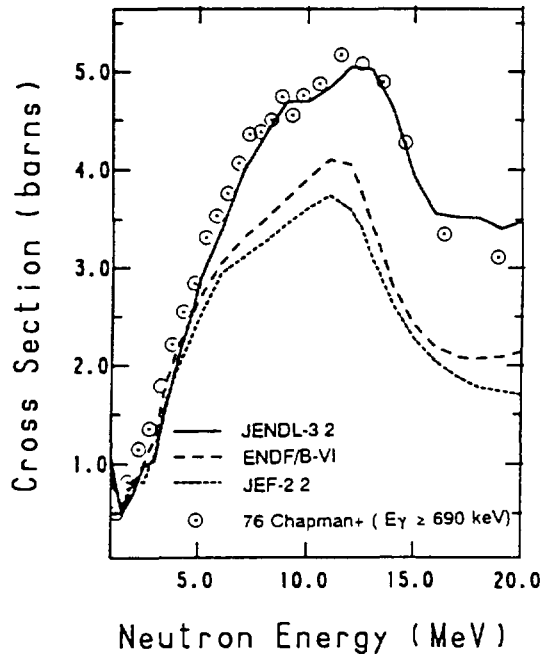

Fig. 11 Total gamma-ray production cross sections of ^{nat}Fe.

4. Actinide Nuclides

4.1. Prompt Gamma-Ray Spectrum from Fission

Verbinski et al.[13] measured prompt gamma-ray spectra from thermal neutron-induced fission of ^{235}U and ^{239}Pu and from spontaneous fission of ^{252}Cf. Their results indicate that the fission gamma-ray spectrum does not depend so much on the fissioning nucleus. The evaluated gamma-ray multiplicities and spectra were obtained from these experimental data. The evaluated data of ^{238}U were deduced from the measurements of ^{235}U. Neglected was the neutron energy dependence of the gamma-ray spectra. According to the Thomas-Grover theory[14], the spectrum will not change much with an

incident neutron energy. In fact, Takahashi[15] calculated the gamma-ray spectra for ^{238}U at several incident energies using the Thomas-Grover theory and found that the energy dependence is quite small.

4.2. Statistical-Model Calculations

Gamma-ray spectra from radiative capture and other nonelastic reactions were calculated by using the GNASH code. The energy dependence of gamma-ray profile function was assumed to be of the Brink-Axel type giant dipole resonance superposed by the so-called pygmy resonance. The parameters of the pygmy resonance were determined so as to reproduce the neutron capture gamma-ray spectrum measured by John and Orphan[16] in the eV region: σ_p = 4.0 mb, E_p = 2.1 MeV and Γ_p = 1.0 MeV.

4.3. Evaluated Cross Sections and Spectra

Total gamma-ray production cross sections are shown in Figs. 12-14, where the evaluated data were corrected for experimental gamma-ray cut-off energy in order to compare with measurements. As for ^{235}U and ^{239}Pu, the JENDL-3.2 data give smaller cross section than those of ENDF/B-VI and the measured data of Drake et al.[17-19] On the other hand, for ^{238}U, the JENDL-3.2 and JEF-2.2 data are larger than those of ENDF/B-VI.

Evaluated gamma-ray spectra are almost consistent with available experimental data, as seen in Fig. 15 for ^{239}Pu.

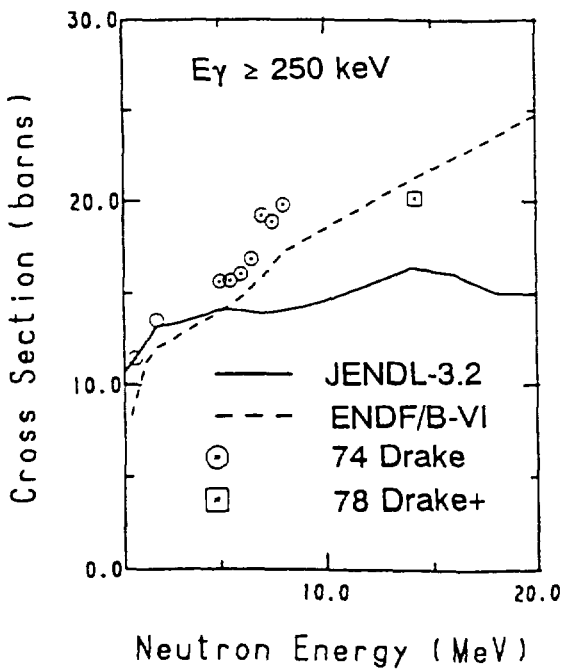

Fig. 12 Total gamma-ray production cross sections of ^{235}U.

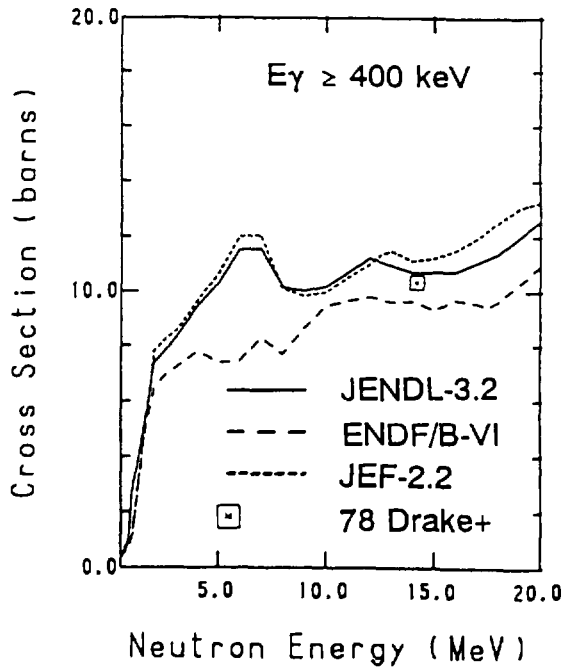

Fig. 13 Total gamma-ray production cross sections of ^{238}U.

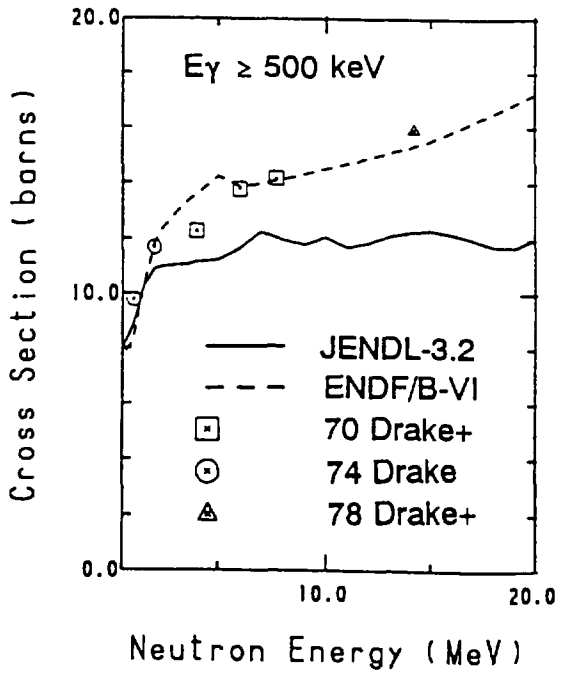

Fig. 14 Total gamma-ray production cross sections of ^{239}Pu.

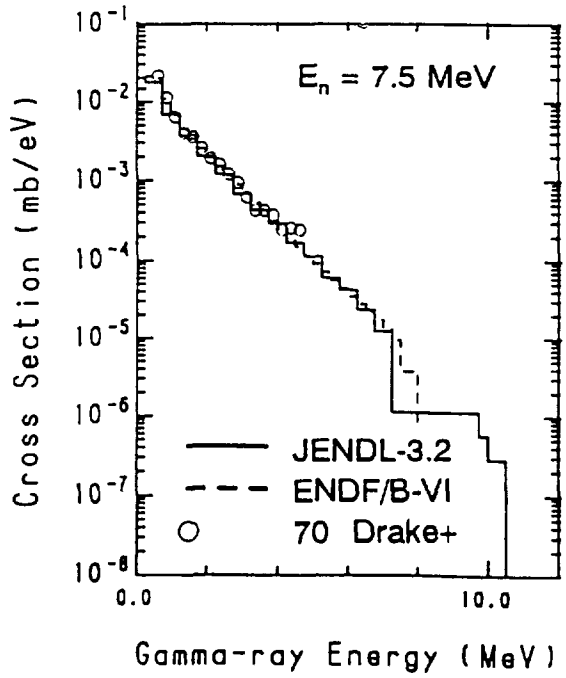

Fig. 15 ^{239}Pu(n,xγ) spectra at 7.5 MeV.

5. Conclusions

The second revision of JENDL-3 contains gamma-ray production data for 66 nuclides. As for light nuclides, p-wave capture plays an important role in gamma-ray production. The statistical model was applied to evaluate medium-heavy and heavy nuclei. Prompt gamma-rays due to fission are important for actinide nuclides. Evaluated gamma-ray spectra were compared with available experimental data. Furthermore, total gamma-ray production cross sections were compared with measurements by taking account of experimental gamma-ray threshold.

Acknowledgements

The authors would like to thank Drs. K. Hida, M. Igashira, H. Kitazawa and M. Mizumoto for their efforts in improving the JENDL-3 gamma-ray production data.

References

1. K. Shibata, T. Nakagawa, T. Asami, T. Fukahori, T. Narita, S. Chiba, M. Mizumoto, A. Hasegawa, Y. Kikuchi, Y. Nakajima and S. Igarasi, *JAERI 1319* (1990).
2. K. Ueki, A. Ohashi and N. Yamano, *JAERI-M 94-019* (1994), p.362.
3. S.H. Jiang and H. Werle, *Nucl. Sci. Eng.* **66** (1978) 354.

4. M. Igashira, H. Kitazawa and K. Takaura, *Nucl. Phys.* **A536** (1992) 285.
5. R.G. Johnson, B.L. Berman, K.G. McNeill and J.G. Woodworth, *Phys. Rev.* **C20** (1979) 27.
6. S. Igarasi and T. Fukahori, *JAERI 1321* (1991).
7. P.G. Young and E.D. Arthur, *LA-6947* (1977).
8. C.Y. Fu, *ORNL/TM-7042* (1980).
9. A. Gilbert and A.G.W. Cameron, *Can. J. Phys.* **43** (1965) 1446.
10. P. Axel, Phys. Rev. **126** (1962) 671.; J.E. Lynn, *The Theory of Neutron Resonance Reactions* (Clarendon, Oxford, 1968).
11. Cai Shao-hui, A. Hasegawa, T. Nakagawa and Y. Kikuchi, *J. Nucl. Sci. Technol.* **27** (1990) 844.
12. R.E. Maerker, *ORNL/TM-5203* (1976).
13. V.V. Verbinski, H. Weber and R.E. Sund, *Phys. Rev.* **C7** (1973) 1173.
14. T.D. Thomas and J.R. Grover, *Phys. Rev.* **159** (1967) 980.
15. H. Takahashi, *Nucl. Sci. Eng.* **51** (1973) 296.
16. J. John and V.J. Orphan, *GA-10196* (1970).
17. D.M. Drake, *Nucl. Sci. Eng.* **55** (1974) 427.
18. D.M. Drake, E.D. Arthur and M.G. Silbert, *Ncul. Sci. Eng.* **65** (1978) 49.
19. D.M. Drake, J.C. Hopkins, C.S. Young and H. Condé, *Nucl. Sci. Eng.* **40** (1970) 294.

An Integral Test of Neutron-Induced Photon Production Data for Iron

H. Freiesleben, K. Seidel and S. Unholzer

Institut für Kern- und Teilchenphysik
Technische Universität Dresden
Mommsenstraße 13, D-01069 Dresden, Germany

Abstract

An iron slab of dimension 1m x 1m x 0.3m is irradiated with 14 MeV neutrons. The neutrons and protons penetrating and leaking the assembly are measured. The spectral photon fluence normalized to one source neutron is compared with Monte Carlo transport calculations (code MCNP) based on data of the European Fusion File EFF-1. Discrepancies are discussed.

Note: Abstract only. Text of the paper has not been received by deadline.

BENCHMARK TEST OF GAMMA-RAY PRODUCTION DATA IN JENDL-3.2 AND FENDL-1

Fujio MAEKAWA and Yukio OYAMA

Department of Reactor Engineering
Japan Atomic Energy Research Institute
Tokai-mura, Naka-gun, Ibaraki-ken 319-11 Japan

ABSTRACT

In regard to verification of secondary gamma-ray data in evaluated nuclear data libraries, there were two useful sets of benchmark experiments conducted at the principal D-T neutron source facilities in Japan; FNS and OKTAVIAN. By analyzing the experimental gamma-ray spectra and heating rates with MCNP-4A, gamma-ray production data in JENDL-3.2 and FENDL/E-1 were tested for fourteen elements of C, F, Al, Si, Ti, Cr, Mn, Fe, Co, Cu, Nb, Mo, W and Pb. Through comparisons between the experiments and the calculations, validity of the secondary gamma-ray data contained in the two nuclear data files was confirmed for most of the nuclei. However discrepancies between them were still observed in some cases, and improvements of the data were recommended for more accurate data libraries.

1. Introduction

Neutron induced secondary gamma-ray data in evaluated nuclear data libraries are highly important from a view point of applications for nuclear heating and shielding designs of fusion devices. There were some previous studies [1-4] so far for verification of the secondary gamma-ray data. However the verification is still not adequate for applications of the data to real designs of fusion devices.

Recently benchmark experimental data [5-7] related to the secondary gamma-ray for many materials have been accumulated at the two principal D-T neutron source facilities in Japan; FNS in Japan Atomic Energy Research Institute and OKTAVIAN in Osaka University. On the other hand, two cross section libraries for the MCNP code [8], FSXLJ3R2 [9] and FENDL/MC-1 [10], have been available since the summer of 1994. The FSXLJ3R2 library is based on the latest version of the Japanese Evaluated Nuclear Data Library, JENDL-3.2. The FENDL/MC-1 library distributed by IAEA on July 26, 1994 is derived from the FENDL/E-1 evaluated nuclear data library. The FENDL/E-1 library consists of the data selected from three major evaluated nuclear data libraries, JENDL-3.1, ENDF/B-VI and BROND-2. In order to verify secondary gamma-ray data in JENDL-3.2 and FENDL/E-1, analyses of the above benchmark experiments were carried out with MCNP-4A.

2. Brief Review of the Experiment

In the FNS experiment[2,5,7], gamma-ray spectra and gamma-ray heating rates were measured at several positions in cylindrical experimental assemblies made of Fe, Cu and W. The experimental assemblies were thick, i.e., about 5.5 to 8.5 mean free paths of 14 MeV neutrons. There were many low energy neutrons in the assemblies and observed gamma-rays were produced not only threshold reactions caused by D-T neutrons but also radiative neutron capture reactions by low energy neutrons. The gamma-rays were measured in the steady state without any time cut-off. Therefore secondary gamma-ray data for a wide neutron energy range can be verified with the FNS experiments.

As for the OKTAVIAN experiment[3,6], leakage gamma-ray spectra from spherical piles made of LiF, CF_2 (Teflon), Al, Si, Ti, Cr, Mn, Co, Cu, Nb, Mo, W and Pb were measured. Since thicknesses of the piles for most of the materials were not so large, i.e., around one mean free path of 14 MeV neutrons, 14 MeV neutrons were dominant in the spherical piles. The spectra were measured from the time of neutron emission to about 70 ns. Source D-T neutrons from the target did not slow down below about 0.1 MeV within the time range. Because of the above two reasons, most of observed gamma-rays were produced by threshold reactions mainly with 14 MeV neutrons. Thus the OKTAVIAN experiments are suitable to examine secondary gamma-ray data produced by neutrons around 14 MeV.

3. Calculation

The continuous energy Monte Carlo transport code MCNP-4A[8] was used for all the calculations with the FSXLJ3R2[9] and FENDL/MC-1[10] libraries. Original nuclear data libraries taken in FENDL/E-1 are presented in Table 1. Since cross section data of Si and Mo were not included in the FENDL/MC-1 library, FSXLIB-J3[11,12] library based on JENDL-3.1 was used for the two materials instead of FENDL/MC-1. The data adopted in FENDL/E-1 for Mo was the same JENDL-3.1 while that for Si was BROND-2. The MCPLIB1 library was used as the photon transport cross section library.

As regards calculations for the FNS experiments, angle-dependent source neutron spectra were used as a source term. The source spectra were obtained by a Monte Carlo calculation precisely simulating the real target structure. Gamma-ray kerma factors derived from the photon interaction cross section library, DLC-99[13], were adopted to calculate gamma-ray heating rates of each material.

In the OKTAVIAN experiments, the sample materials except lead were filled in containers made of type 304 stainless steel or soft steel.

Table 1 Original nuclear data libraries taken in the FENDL/E-1 library.

Li-6	ENDF-B/VI.1	Mn	ENDF-B/VI
Li-7	ENDF-B/VI	Fe	ENDF-B/VI.1
C	ENDF-B/VI.1	Co	ENDF-B/VI.2
F	ENDF-B/VI	Cu	ENDF-B/VI.2
Al	JENDL-3.1	Nb	BROND-2
Si	(BROND-2)	Mo	JENDL-3 1
Ti	JENDL-3.1	W	ENDF-B/VI
Cr	ENDF-B/VI	Pb	ENDF-B/VI & VI.1

Both the sample material and container were modeled in one-dimensional spherical geometry in the calculations. Measured source neutron spectra[14] were used as an isotropic source term. A spherical surface of 5.8 m in radius, which was the distance between the real target and the detector, was used for a detector surface. A time cut-off about 70 ns was taken in the calculations. The real D-T neutron targets simultaneously emitted gamma-rays along with D-T neutrons. In order to consider the target gamma-rays, another series of calculations with source gamma-rays were made for all the OKTAVIAN calculations. A flagging method [1, 15] was applied to the OKTAVIAN calculations to examine contributions of gamma-rays emitted from the containers and the targets to the measured spectra.

4. Results and Discussions

4.1. FNS Experiments

Calculated to experimental values (C/Es) for gamma-ray heating rate of the iron experiment along the central axis of the experimental assembly are shown in Fig. 1. The heating rates by FENDL agree well with the experiment within the experimental error bands of about ± 10 %. However those by JENDL-3.2 are larger than the experiment by 10 - 70 %, especially near the front surface of the assembly where 14 MeV neutrons are dominant. Since the gamma-ray heating rate means deposited energy to a surrounding medium by gamma-rays, the heating rate has strong correlation with total gamma-ray energy released by gamma-ray production reactions around the measurement point. Hence the discrepancy between JENDL-3.2 and the experiment near the front surface of the assembly implies that energy balance of the gamma-ray production cross sections in JENDL-3.2 are distorted for incident neutron energy around 14 MeV. Excess gamma-ray energies are released by 14 MeV neutron reactions according to JENDL-3.2.

Figure 2 shows C/Es for gamma-ray heating rate of the copper experiment. It is seen in the figure that the FENDL and JENDL-3.2 calculations result in almost the same

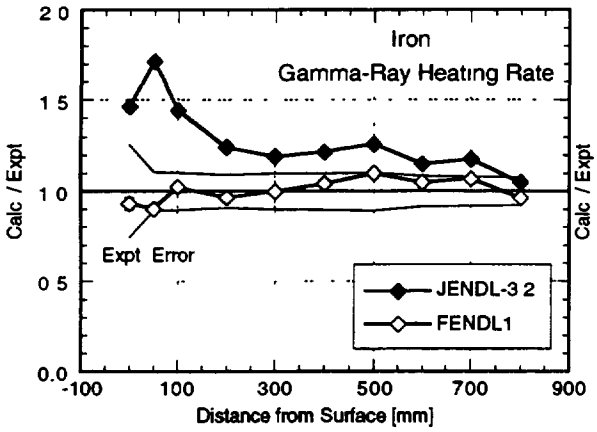

Fig. 1 Calculated to experimental values for gamma-ray heating rate of iron.

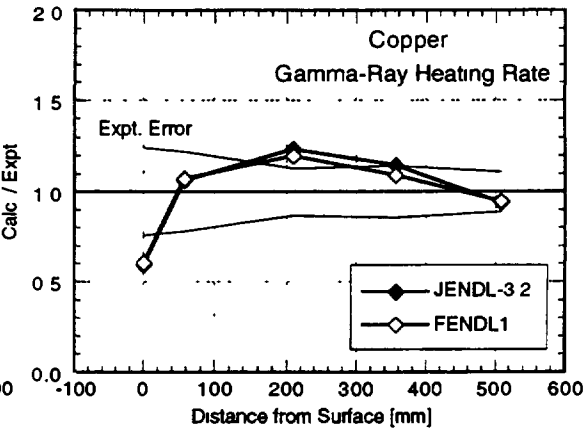

Fig. 2 Calculated to experimental values for gamma-ray heating rate of copper.

heating rate at all the measurement points. Although the C/Es range between 0.6 and 1.25, both calculations agree with the experiment if experimental errors of 10 - 25 % are considered. As it is pointed in the previous works[2, 16], 14 MeV neutrons are dominant near the front surface of the assembly. When one moves to the deeper part of the assembly, a fraction of low energy neutrons below 1 MeV increases with decrease of the 14 MeV neutrons. Therefore it is deduced that secondary gamma-ray data of copper in both JENDL-3.2 and FENDL/E-1 for not only 14 MeV neutrons but also lower energy neutrons are valid.

As for the tungsten experiment, C/Es of gamma-ray heating rate are shown in Fig. 3. The C/Es by JENDL-3.2 are a little closer to unity than those by FENDL, and the C/Es by both calculations have almost the same trend. Calculated heating rates with both libraries are larger than the experimental ones at all the measurement points. The discrepancies between the calculations and the experiment are remarkable, nearly a factor of 2, at shallower measurement positions. This fact suggests that gamma-ray production cross sections of tungsten in both libraries are evaluated larger than the true ones for incident neutron energy around 14 MeV. Figure 4 represents the measured and the calculated gamma-ray spectra at 76 mm position. Both calculated spectra are somewhat softer than the measured one, that is, the calculated spectra are larger and smaller than the measured one in energy ranges of 1 - 3 and 3 - 10 MeV, respectively. Although the calculated spectra differ a little each other, they agree with the experiment as a whole.

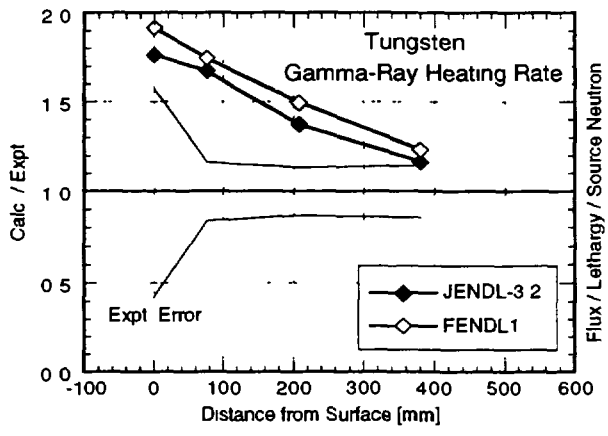

Fig. 3 Calculated to experimental values for gamma-ray heating rate of tungsten.

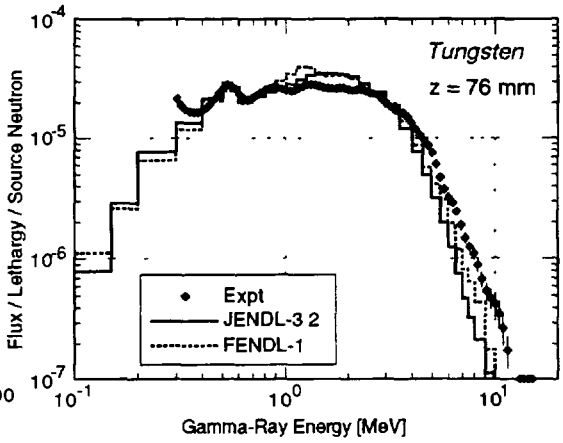

Fig 4 Measured and calculated gamma-ray spectra in the tungsten assembly.

4.2. OKTAVIAN Experiments

The measured gamma-ray spectrum in the OKTAVIAN experiment consists of three components; gamma-rays from the testing material, from the container and from the target. Since only the first component is under consideration, the latter two components are regarded as parasitic. Thus contributions of the parasitic gamma-rays to the spectra are investigated by means of the flagging method. Figures 5 and 6 illustrate the contribution

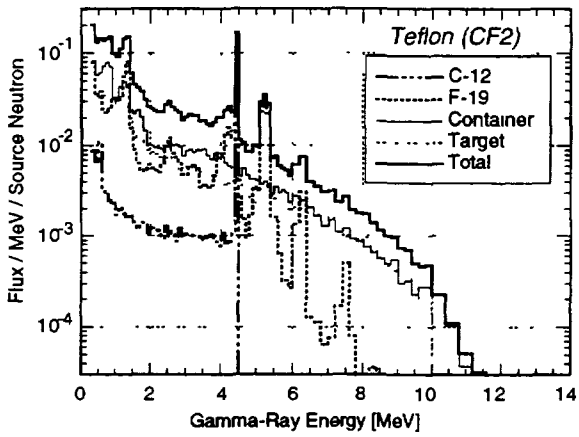

Fig 5 Contribution of parasitic gamma-rays to the total gamma-ray spectrum for CF_2 pile.

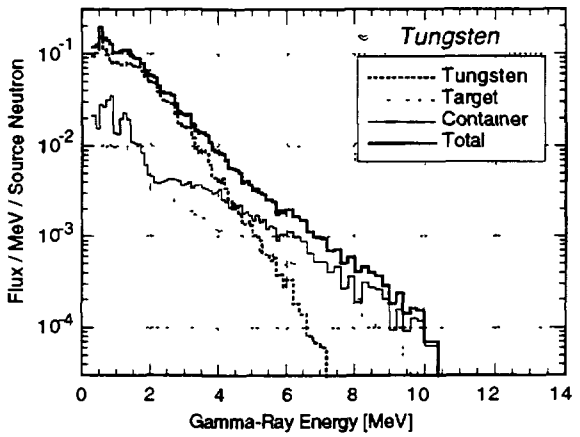

Fig. 6 Contribution of parasitic gamma-rays to the total gamma-ray spectrum for tungsten pile.

of the parasitic gamma-rays to the spectra in the CF_2 and W cases. It is clearly seen from Fig. 5 that the parasitic gamma-rays are comparable or dominant to the gamma-rays from the Teflon over all the energy range. In the spectrum of tungsten, Fig. 6, parasitic gamma-rays are larger than the gamma-rays from the tungsten above 5 MeV. Similarly it is found for most of the materials that the contribution of the parasitic gamma-rays are considerable. Hence it should be noticed that discrepancies found between the measured and the calculated spectra are not always attributed to inadequacy of the cross sections used.

Some examples of the calculated leakage gamma-ray spectra are presented in Figs 7 (a) - (d) with the measured ones for the four materials. As for Al, both JENDL-3.2 and FENDL agree well with the experiment. Good agreements are similarly seen between the calculated with both libraries and the measured spectra for LiF, CF_2, Si, Cu and Mo. In Fig. 7 (b), the calculated spectrum by FENDL is closer to the measured one comparing with JENDL-3.2 for Cr. On the other hand, JENDL-3.2 shows better agreement with the experiment for Co and Nb as seen in Figs. 7 (c) and (d). Discrepancies between the calculated spectra with both libraries and measured ones are observed for Ti, Mn, W and Pb.

All the calculated and measured spectra are integrated above 0.5 MeV except Mn and Nb. The lower limit energy of 0.7 MeV is adopted to Mn and Nb because the measured spectra around 0.5 MeV seem to be distorted. The upper limit energy is changed to 6.5 MeV for LiF and CF_2, and 5.0 MeV for Nb and W, respectively, since contributions of the parasitic gamma-rays are large above the upper limit energies. There are two advantages of the integrated spectrum; the measured and the calculated spectra can be compared quantitatively, and mismatches of energy resolution between the experiments and the calculations can be avoided. The integrations are carried out in two ways; direct integration of the gamma-ray flux and integration of products of gamma-ray flux and energy, that is,

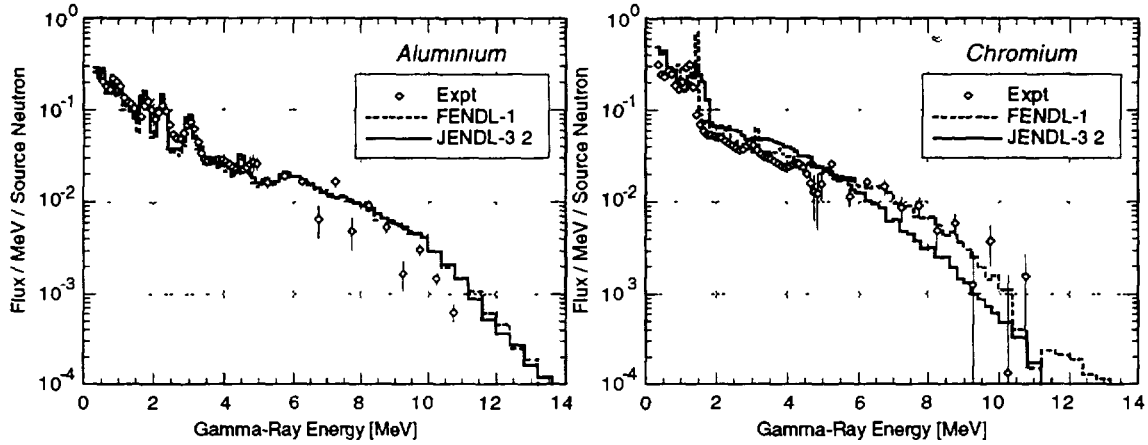

(a) Aluminium. (b) Chromium.

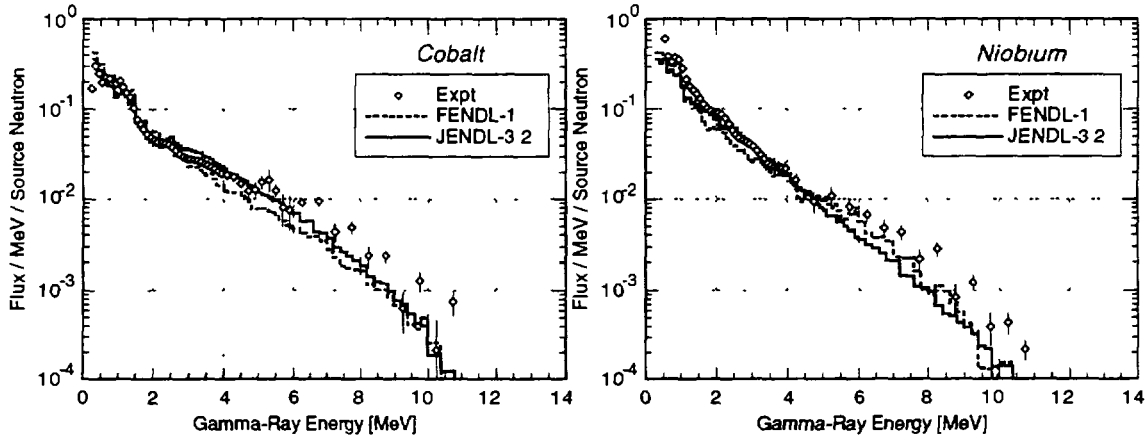

(c) Cobalt. (d) Niobium.

Fig 7 Measured and calculated gamma-ray spectra for OKTAVIAN experiment.

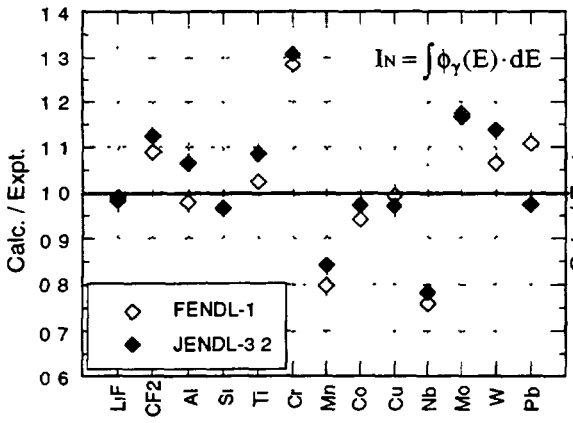

Fig 8 Calculated to experimental values for integrated gamma-ray flux of I_N.

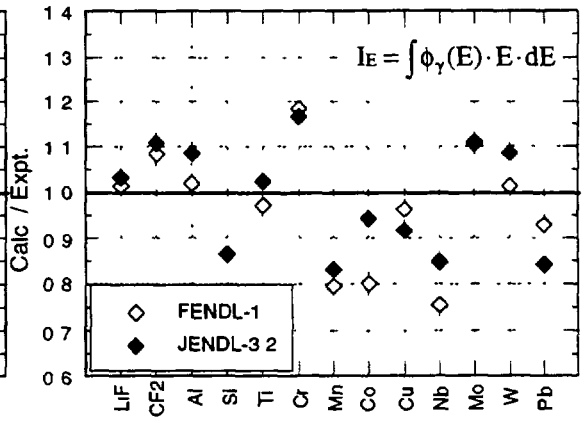

Fig 9 Calculated to experimental values for integrated gamma-ray flux of I_E

$$I_N = \int \phi_\gamma(E) \cdot dE \qquad (1)$$

and

$$I_E = \int \phi_\gamma(E) \cdot E \cdot dE. \qquad (2)$$

The former, I_N, is equivalent to total number of gamma-rays while the latter, I_E, corresponds to total gamma-ray energies. From a viewpoint of engineering, the latter has much meanings because most of design parameters concerning gamma-rays have strong relation to the total gamma-ray energies. Figures 8 and 9 show C/Es of the I_N and I_E for each material.

It is found from the figures that all the calculated I_N and I_E values agree with the experiment within 30 %. The I_N values by FENDL scatter around the unity as similar to the I_E values while as regards JENDL-3.2, the I_E values are more gathered around unity than the I_N values. Differences of all the I_E values between JENDL-3.2 and the experiment are smaller than 17 %. But the I_E values by FENDL/E-1 for four materials, Cr, Mn, Co and Nb, differ more than 18 % from those by experiment. Hence it is pointed out that JENDL-3.2 presents better agreements than FENDL/E-1 for the total gamma-ray energies released by mainly 14 MeV neutron reactions.

5. Concluding Remarks

Present status of the accuracy of the secondary gamma-ray data in JENDL-3.2 and FENDL/E-1 is briefly summarized in Table 2 taking account of both FNS and OKTAVIAN experiments. Through the benchmark test of the secondary gamma-ray data for fourteen elements, validity of the data in both libraries is proved for about half of the element while some problems are pointed out for several elements.

Table 2 Status of accuracy of secondary gamma-ray data in JENDL-3.2 and FENDL-1. Symbols of ◎, ○ and △ indicate excellent, good and poor, respectively

Element	JENDL-3.2	FENDL-1	Element	JENDL-3.2	FENDL-1
C	◎	◎	Fe	△	◎
F	◎	◎	Co	◎	○
Al	◎	◎	Cu	◎	◎
Si	◎	not available	Nb	○	△
Ti	○	○	Mo	◎	◎
Cr	△	○	W	△	△
Mn	○	○	Pb	○	○

6. References

1. F. Maekawa, K. Kosako and Y. Oyama, "Verification of Gamma-Ray Data in JENDL-3.1 through Analysis of OKTAVIAN Experiment," Proc. of International. Conf. on Nucl. Data for Sci. and Technol., May 9-13, 1994, Gatlinburg, Tennessee USA, to be published.
2. F. Maekawa, et al., "Benchmark Experiment on Copper with D-T Neutrons for Verification of Secondary Gamma-Ray Data in JENDL-3.1," Proc. of 3rd International. Symposium on Fusion Nucl. Technol., Jun. 27 - Jul. 1, 1994, Los Angeles, California USA, to be published.
3. J. Yamamoto, et al., "Integral Experiment on Gamma-Ray Production at OKTAVIAN," *JAERI-M 91-62* (1991) 118.
4. E. Goldberg, et al., *Nucl. Sci. Eng.*, **105** (1990) 319.
5. F. Maekawa, et al., "Benchmark Experiment on a Copper Slab Assembly Bombarded by D-T Neutrons," *JAERI-M 94-38* (1994).
6. J. Yamamoto, et al., "Gamma-Ray Energy Spectra Emitted from Spheres with 14 MeV Neutron Source," *JAERI-M 94-14* (1994) 32.
7. F. Maekawa, et al., to be published.
8. J. F. Briesmeister, ed., "MCNP - A General Monte Carlo N-Particle Transport Code, Version 4A," *LA-12625-M* (1993).
9. K. Kosako, et al., to be published.
10. R. MacFarlene, private communication (1994).
11. K. Kosako, Y. Oyama and H. Maekawa, "FSXLIB-J3: MCNP continuous energy cross section library based on JENDL-3," *JAERI-M 91-187* (1991) (in Japanese).
12. K. Kosako, Y. Oyama and H. Maekawa, "MCNP continuous cross section library based on JENDL-3," Proc. of Topical Meeting on New Horizons in Radiation Protection and Shielding, Pasco, Washington USA (1992) 357.
13. R. W. Roussin, J. R. Knight, J. H. Hubbell and R. J. Howerton, "Description of the DLC-99/HUGO package of photon interaction data in ENDF/B-V format," *ORNL/RSIC-46* (1986).
14. C. Ichihara, et al., "Leakage Neutron Spectra from Various Sphere Piles with 14 MeV Neutrons," *JAERI-M 94-14* (1994) 63.
15. F. Maekawa and Y. Oyama, "Techniques of Integral experiment and Methods for Validation of Evaluated Nuclear Data Libraries for Secondary Gamma-Ray Data under D-T Neutron Field," *JAERI-M 94-19* (1994) 369.
16. C. Konno, et al., "Benchmark Experiment on Copper with D-T Neutrons for Verification of Neutron Transport Codes and the Related Nuclear Data of JENDL-3.1," Proc. of 3rd International. Symposium on Fusion Nucl. Technol., Jun. 27 - Jul. 1, 1994, Los Angeles, California USA, to be published.